View metadata, citation and similar papers at core.ac.uk

brought to you by CORE

provided by University of Liverpool Repository

Development and Verification of Semi-Blind Receiver Structures for Broadband Wireless Communication Systems

Thesis submitted in accordance with the requirements of
the University of Liverpool for the degree of Master in Philosophy

by

Teng Ma

February 2015

Declaration

The work in this thesis is based on research carried out at the University of Liverpool. No part of this thesis has been submitted elsewhere for any other degree or qualification and it is all my own work unless referenced to the contrary in the text.

Abstract

The increasingly high demands for high data rate wireless communication services require spectrum- and energy-efficient solutions. In this thesis, a number of energy-efficient semi-blind receiver structures are proposed to perform Doppler spread estimation, channel estimation and equalisation for broadband wireless orthogonal frequency division multiplexing (OFDM) systems. A real-time wireless communication testbed is developed to verify the proposed semi-blind receiver structures.

In the first contribution, a semi-blind Doppler spread estimation and Kalman filtering based channel estimation approach is proposed for wireless OFDM systems. A short sequence of reference data is carefully designed and applied as pilot symbols for Doppler spread estimation and channel estimation initialisation of the Kalman filter. Then the estimates of inter-carrier interference (ICI) caused by Doppler spread are gathered into the equivalent channel model and compensated for through channel equalisation, which dramatically reduces the computational complexity. The simulation results show that the proposed approach outperforms the conventional pilot aided Doppler spread and channel estimation schemes.

In the second contribution, a semi-blind Doppler spread estimation and independent component analysis (ICA) based equalisation scheme aided by non-redundant precoding is proposed for wireless multiple-input multiple-output (MIMO) OFDM systems. A number of reference data sequences are selected from a pool of orthogonal sequences for two purposes. First, the reference data sequences are superimposed in the source data sequences through non-redundant linear precoding to enable the Doppler spread estimation by minimising the sum cross-correlation between the compensated signals and the rest of the orthogonal sequences in the pool. Second, the same reference data

sequences are applied to eliminate the phase and permutation ambiguity in the ICA equalised signals. Simulation results show that the proposed semi-blind MIMO OFDM system can achieve a bit error rate (BER) performance which is close to the ideal case with perfect channel state information (CSI).

In the third contribution, a real-time wireless communication testbed is developed with a vector signal generator, a vector signal analyser and a pair of antennas, to verify the effectiveness of the proposed receiver structures over the air in different environments such as Reverberation chamber and office area. Measurement results show a good match with simulation results. Also, a pilot is employed for three purposes at a semi-blind receiver: time synchronisation, Doppler spread estimation and Kalman filtering initialisation, which is an extension of the work in the first contribution.

Acknowledgement

First, I would like to express my deepest gratitude to Dr. Xu Zhu for teaching me so much about research skills. This work benefits from her patient guidance, constant encouragement and invaluable comments during the period of my study in U.K.. I also appreciate concerns from Prof. Yi Huang for my research. This thesis would not have been completed without loads of support and help from them.

I would like to thank the University of Liverpool, as well as the Department of Electrical Engineering and Electronics, for providing outstanding training and facilities to research students.

I would also like to thank my colleagues in the Wireless communication and Smart Grid Group: Dr. Yufei Jiang for inspiring discussion and sharing research ideas with me, Dr. Linhao Dong for his support and encouragement, Mr. Chao Zhang, Mr. Qinyuan Qian, Mr. Yanghao Wang, Mr. Kainan Zhu, Mr. Yang Li, Mr. Jun Yin, Mr. Chaowei Liu, Mr. Zhongxiang Wei and Mr. Heggo Mohammad for creating a family-like atmosphere in the lab where I have been working. I was a pleasure to share my good times with you.

Finally, my gratitude is dedicated to my parents. I would had no chance to pursue my goals in my life without their support, patience and encouragement.

This thesis is dedicated to them.

Contents

List of Figures

List of Tables

Abbreviations and Acronyms

3G	Third Generation
3GPP	Third Generation Partnership Project
4G	Fourth Generation
5G	Fifth Generation
AWGN	Additive White Gaussian Noise
BER	Bit Error Rate
BSS	Blind Source Separation
CAZAC	Constant Amplitude Zero Auto-Correlation
CDMA	Code-division Multiple Access
CFO	Carrier Frequency Offset
CIR	Channel Impulse Response
CP	Cyclic Prefix
CPI	Cyclic Prefix Insertion
CPR	Cyclic Prefix Removal
CSI	Channel State Information
DL	Downlink
DFT	Discrete Fourier Transform

EDGE	Enhanced Data Rates for GSM Evolution
FDE	Frequency Domain Equalisation
FDM	Frequency Division Multiplexing
FDMA	Frequency Division Multiplexing Access
FFT	Fast Fourier Transform
GSM	Global System Mobile
HOS	High Order Statistics
HSPA	High Speed Packet Access
IBI	Inter-Block Interference
ICI	Inter-Carrier Interference
ICA	Independent Component Analysis
IDFT	Inverse Discrete Fourier Transform
IFFT	Inverse Fast Fourier Transform
i.i.d.	Independent Identically Distributed
I/Q	Inphase/Quadrature
ISI	Inter-Symbol Interference
JADE	Joint Approximate Diagonalisation of Eigenmatrices
LO	Local Oscillators
LOS	Line-of-Sight
LS	Least Square
LTE	Long Term Evolution
MIMO	Multiple-Input Multiple-Output

ML	Maximum Likelihood
MMSE	Minimum Mean Square Error
MSE	Mean Square Error
NMSE	Normalised Mean Square Error
OFDM	Orthogonal Frequency Division Multiplexing
OFDMA	Orthogonal Frequency Division Multiple Access
PAPR	Peak-to-Average Power Ratio
PL	Path Loss
PDF	Probability Density Function
PDP	Power Delay Profile
RMS	Root Mean Square
SC-FDMA	Single-Carrier FDMA
SISO	Single-Input Single-Output
SNR	Signal-to-Noise Ratio
SOS	Second Order Statistics
TDD	Time Division Duplexing
TDMA	Time Division Multiple Access
UL	Uplink
UMTS	Universal Mobile Telecommunications System
WiMAX	Worldwide Interoperability for Microwave Access
ZF	Zero Forcing

Chapter 1

Introduction

1.1 Background

Wireless communications is, by any measure, a dynamic and broad field that has experienced the fastest grouth in the communication industry over the past few decades [1, 2]. The demands for high-data-rate services allow amounts of research activities carried out for promoting a higher system capacity. In order to serve the purpose, a number of wireless communication systems have been proposed and exploited. By utilising multiple transmit and receive antennas, Multiple-input multiple-output (MIMO) systems [3] becomes the dominant wireless communication technology, which can provide considerable channel capacity improvement than the systems with single-input single-output (SISO).

Orthogonal frequency division multiplexing (OFDM) technology was first proposed in 1960 [4]. It is robust against frequency selective fading channels. By dividing the frequency selective fading channel into a number of parallel flat fading sub-channels, the spatial diversity gain can be obtained. Due to the rapid development of digital signal processing, this technology becomes practically possible and attractive to the modern wireless communication systems. So far, OFDM has been employed in a range of modern wireless communication systems. A well known technique, Long Term Evolution-Advanced (LTE-A) [5], is well developed and utilised in fourth generation (4G) technologies.

At the receiver side, the channel equalisation [2, 6] is needed to combat multipath fading effects and transform the received signals back into their original status before

transmitted. The equaliser coefficients are required, which can usually be obtained directly from channel state information (CSI). In wireless communication systems, based on some traditional methods, a number of reference data sequences regarded as training signals are commonly applied to estimate the CSI before equalisation at the receiver. However, the transmission of training signals not only consumes additional transmit power but also reduces the spectral efficiency. In order to recover source signal, blind or semi-blind channel estimation and equalisation techniques [7] was proposed to obtain the CSI. Without consuming extra transmit power and spectral resource, the source data can be recovered by employing the reference data sequences directly from the statistics and structure of the received data sequences. As it requires non or only a little prior information in advance at the receiver, blind or semi-blind equalisation technologies can improve spectral and power efficiency. The aim of this thesis is to develop a real time measurement testbed and verify a number of energy efficient receiver structures in wireless communication systems over frequency selective channels.

In modern wireless communication systems, high mobility between transmit and receive antennas results in Doppler shift, which leads to time variate [8, 9] channel. In mobile OFDM systems, the orthogonality among subcarriers can be destroyed by the time variation, which accompanied with power leakage in OFDM subchannels. This phenomenon is known as inter-channel or inter-carrier interference (ICI) [10, 11, 12]. ICI, if not mitigated, could introduce ignorable system degradation and error floor that will increase while Doppler spread is getting large. Consequently, the estimation of channel and channel parameters, such as Doppler spread, as well as channel equalisation are becoming important aspects while designing a wireless OFDM communication system. In the future wireless communication systems, support of mobility feature is considered as one of the most critical characteristics. In many modern and future wireless communication systems, OFDM aided with the ability that can combat rapid time varying fading channels is deeply needed.

The Kalman filter [13] is known as a linear quadratic estimation technique. It is a group of algorithms that applies a number of measurements and status information obtained over time, including indirect, inaccurate and uncertain observations. It ac-

quires the previous measurement state information from unknown variables and then update the estimates, which is much more precise than that of single measurement and estimation method. Formally, the Kalman filter is regarded as a recursive and optimal estimator which obtain the estimates on streams of input noisy and uncertain signal sequences in order to process and update a statistically optimised estimates. Furthermore, it is considered and employed as an ideal technique in time domain estimation and signal analysis, for instance, signal processing [14]. In order to adaptively track the channel variations of wireless communication, Kalman filtering based channel estimation [15] was proposed for frequency selective fading channels systems. This kind of channel estimation method is an efficient method as it requires only limited number of reference data to obtain the CSI even in time-varying channel.

Among those high order statistics (HOS) based techniques, independent component analysis (ICA) [16] is considered as an high efficient blind source separation (BSS) technology [17]. It can recover the source data by maximising the non-Gaussianity of the observed signals. Compared to the Second order statistics (SOS) based blind approaches [18], ICA potentially reduces the system sensitivity to noise. It is because that the cumulates of the Gaussian noise in fourth or higher order are tending to be zero. The ICA technique is applied to separate and recover the statistical independent components from the received data. So far, ICA has been used in a number of fields, including signal separation in audio applications or brain imaging, analysis of economic data and feature extraction [16]. The advantage of applying ICA is that it requires no CSI while performing blind or semi-blind equalisation. To improve the spectral efficiency, ICA is employed in this thesis to do equalisation in simulation and the real-time OFDM wireless communication systems.

1.2 Research Contributions

The research conducted during the MPhil study has produced the following main contributions:

- A semi-blind Doppler spread tracking and Kalman filtering based channel estima-

tion approach is proposed for single-input single-output (SISO) OFDM systems, where a short sequences of reference data are carefully designed and employed as the pilot for Doppler spread estimation and Kalman filtering channel estimation initialisation. The estimates of inter-carrier interference (ICI) introduced by Doppler spread is gathered into the equivalent system model and mitigated through the equalisation process, which dramatically reduces the system computational complexity. According to the simulation results, it can be demonstrated that the proposed estimation approach can outperform the conventional comb type pilot aided estimation methods in bit error rate (BER).

- A semi-blind receiver structure is proposed for MIMO OFDM systems, with a precoding aided Doppler spread estimation method and ICA based equalisation structure. A number of reference data sequences are superimposed into the source data sequences through a non-redundant linear precoding process without introducing any extra transmit power and spectral overhead. These reference data sequences are carefully designed offline and selected from a pool of orthogonal sequences for two purposes. First, the precoding based Doppler spread estimation is performed by minimising the sum cross-correlation between the ICI compensated signals and the rest of the orthogonal sequences in the pool. Second, the same reference data sequences are employed to eliminate the phase and permutation ambiguity in the ICA equalised signals by maximising the cross-correlation between the reference signals and ICA equalised signals. According to the simulation results, it can be indicated that the semi-blind precoding aided Doppler spread estimation approach achieves a higher accuracy than the existing training based methods. The proposed semi-blind Doppler spread estimation and ICA equalisation for MIMO OFDM system can provide a good performance of BER which is approach to the BER performance of the perfect case while the ideal CSI is known.

- A real-time wireless communication testbed is developed with a vector signal generator, a vector signal analyser and a pair of antennas to verify the effectiveness of

the proposed receiver structures, under various wireless communication environments, such as office area and Reverberation Chamber. The measurement results show a good match with the simulation results. The effects of various parameters on the performance are investigated. In particular, a pilot is employed for three purposes at a semi-blind receiver: time synchronisation, Doppler spread estimation and Kalman filtering initialisation, which is an extension of the work in the first contribution.

1.3 Thesis Organisation

The rest of this thesis is organised as follows.

In Chapter 2, the fundamental characteristics of wireless communication channels are surveyed, and the OFDM systems are introduced with channel estimation and equalisation techniques.

In Chapter 3, a semi-blind Doppler spread tracking and Kalman filtering based channel estimation structure are proposed for OFDM systems, where a short sequence of reference data are employed as the pilot blocks for Doppler spread estimation and channel estimation initialisation based on Kalman filter. The estimates of ICI mitigation can be realised together with channel equalisation, which dramatically reduces the system computational complexity.

In Chapter 4, a semi-blind Doppler spread estimation and ICA based equalisation structure are proposed for MIMO OFDM systems, where a number of reference data sequences are designed offline and superimposed into the source data sequences via a precoding process, for Doppler spread estimation and ambiguity elimination in ICA equalised signals without consuming extra transmit power and spectral resources.

In Chapter 5, the development of the real-time wireless communication testbed is presented, including the system requirement on hardware and software, connection between computer and the instruments and measurement setups. The measurement results are presented and discussed, in comparison with the simulation results in Chapters 3 and 4. The measurement environments of office area and Reverberation chamber are introduced, and some important measurement parameters are given. The proposed two

receiver structures are verified through this real-time wireless communication system platform.

Finally, the findings are summarised and conclusions are drawn in Chapter 6, followed by an outlook towards future work.

1.4 Publications

- Teng Ma, Xu Zhu, Yufei Jiang and Yi Huang, "Validation of a green wireless communication system with ICA based semi-blind equalization", in *Proc. Signal and Information Processing Association Annual Summit and Conference (APSIPA)*, pp. 1-5, Dec. 2012.

- Teng Ma, Xu Zhu, Yufei Jiang, Yi Huang and Eng Gee Lim, "Semi-blind Doppler spread tracking and channel equalisation for green wireless MIMO systems", in *Proc. IEEE International Conference on Consumer Electronics - Taiwan (ICCE-TW)*, Jun. 2015.

- Teng Ma, Xu Zhu, Yufei Jiang and Yi Huang, "Semi-blind MIMO OFDM systems with precoding aided Doppler spread estimation and ICA based equalisation", To be submitted to *IET Electronics Letters*.

Chapter 2

Wireless Communication Channels and Systems

In this chapter, the development of wireless communication systems is first presented. Wireless communication channels are reviewed in the following section. Then several wireless communication systems are presented, including OFDM technology and MIMO OFDM systems. Finally, some equalisation techniques are explained.

2.1 Evolution of Wireless Communication Systems

Since Guglielmo Marconi conducted the first wireless communication experiment in 1897, and the cellular systems were launched in 1980s, the mean of communications between people have changed dramatically. In mid 1990s, the wireless communication industry has explosively developed and expanded. Wireless communication networks [2] have been becoming more precious than anyone could have imagined when the cellular concept was first developed. Most countries through the world started to develop and research on cellular networks which has the increases of 40% or more annually. The fast growth in the world of cellular telephone subscribers has indicated that wireless communications is a viable, robust voice and data transmission technology. With the widespread development and success of cellular networks, besides mobile voice telephone calls, the development of novel wireless communication systems and standards for a lot of different types of telecommunication transportation [2, 19]. In the first generation (1G) cellular communication systems, the technologies mainly depended on analogue FM and FDMA/FDD. It was first introduced in the 1980s and developed

until being taken the place by the second generation of telecommunication systems. The 1G is different from the following generations because that the radio signals used by the network are analogue, while others are digital.

In the 1990s, the second generation (2G) mobile phone systems started to lead the major communication standards, which primarily utilizing the Global System Mobile (GSM) [20] standards. In most part of the world, GSM has been employed widely in cellular communication networks by the providers. It is able to support users with each channel of 200 kHz. Another two popular mobile phone systems standards are IS-136(TDMA) and IS-95(CDMA). General packet radio services (GPRS) is a wireless communication standard based on packet. It is mainly developed on the existing standards, such as GSM. By applying the existing cellular techniques and TDMA frame structures, the standard of EDGE is developed on GSM technology [2, 19]. Unlike the previous generation, it applies the usage of digital transmission instead of analogue transmission, and it also introduced the advanced and fast phone-to-network signalling. The rise in mobile phone usage as a result of 2G was explosive and this era also saw the advent of prepaid mobile phones. 2G helps mobile batteries to last long because of digital signals consuming less battery power.

The third generation (3G) mobile technology broadened the data and information transmission capacity of 2G. It is considered as a milestone for enlarging the existing SMS messaging to a multiple media communication including Television, mobile video and internet. The capacity of 3G [2, 19] was developed with a wide range of standards, and the data transmission speed is increased with each new standard, which dominantly enhanced the data access capacity in mobile communication with mobile phones. Most 3G standards can provide not only SMS messages but also voice transmissions. Companies developing 3G equipment envision users having the ability to receive live music, conduct interactive web sessions and have simultaneous voice and data access. Universal mobile telecommunications service (UMTS) can provide a multiple media communication at a data rate up to 2 $Mbps$ to users with mobile equipments [19]. Wideband code-division multiple access (WCDMA) is an ITU standard derived from CDMA, officially known as IMT-2000 direct spread. It can provide services including

video, image, data and voice.

From the beginning of the 21st century, demands for data services have been increasing dramatically. Hence, evolution-data optimized (EV-DO) [21] and high speed packet access (HSPA) [22], which are regarded as 3G transitional (3.5G) systems, were respectively operated in 2003 and 2005, to provide mobile broadband over cellular networks. The maximum download speeds for HSPA and EV-DO are 14.4 $Mbps$ and $4.9 \times N$ $Mbps$, respectively, and their maximum upload speeds are 5.76 $Mbps$ and $1.9 \times N$ $Mbps$, respectively, where N is the number of 1.25 MHz spectrum chunks used in EV-DO systems. The evolution of HSPA, which is referred to as HSPA+, was proposed to enhance the system capacity of HSPA.

The following stage is called pre-4G [23]. LTE and WiMAX are the major standards during this period, which is considered as a transition span from 3G to 4G. WiMAX is a novel technique based on the IEEE 802.16 standards. Both WiMAX and LTE can provide broadband access with high data rates.

The fourth generation (4G) [23] mobile technology has been established and developed for full broadband mobile communication. This promising generation employed lots of novel technologies, some of which are still being researched now. Since the previous mobile generations are too complicated for users to access, the basic goal of the 4G wireless network are to develop a transparent system architecture for users, which is out off restriction from wireless access technology. Wireless-Man-Advanced (WiMAX 2) and LTE-Advanced are the two standards that can be fully satisfied the 4G classification. All the aforementioned wireless communication techniques are summarised in Table 2.1.

2.2 Wireless Communication Channels

Wireless channels are the physical transmission medium used to convey a signal from transmitter to receiver. In this section, a number of based propagation mechanisms are presented, followed by the introduction of large-scale and small-scale radio propagations.

Table 2.1: Evolution of Mobile Telephony Standards and Technologies

Generation	Family	Standard	Technology	Peak Data Rates (bps)
2G	3GPP	GSM	TDMA FDMA	43k (DL) 14k (UL)
	3GPP2	CDMA One (IS-95)	CDMA	154k (DL) 115k (UL)
2G Traditional (2.5G, 2.75G)	3GPP	GPRS	TDMA	114k (DL) 20k (UL)
		EDGE	WCDMA	384k (DL) 60k (UL)
3G	3GPP	UMTS	WCDMA	384k (DL) 64k (UL)
		WCDMA (IMT-2000)	WCDMA	2M (DL) 153k (UL)
	3GPP2	CDMA2000 (IS-2000)	CDMA	3.1M (DL) 1.8M (UL)
3G Traditional (3.5G, 3.75G)	3GPP	HSPA	WCDMA	14.4M (DL) 5.76M (UL)
		HSPA+	WCDMA	56M (DL) 22M (UL)
Pre 4G (3.9G)	3GPP	LTE	OFDMA (DL) SC-FDMA (UL)	100M (DL) 50M (UL)
	IEEE	WiMAX (IEEE 802.16e)	SOFDMA	6M (DL) 1M (UL)
4G	3GPP	LTE-Advanced	OFDMA	1G (DL) 500M (UL)
	IEEE	WiMAX 2 (IEEE 802.16m)	SOFDMA	1G (DL) 500M (UL)

2.2.1 Propagation Mechanisms

The behaviour of radio waves is referred as the radio propagation [2] through wireless communication channels from transmitter to receiver. Basically, there are three different propagation mechanisms which have impact on the radio propagation: reflection, diffraction and scattering. These physical propagation mechanism can be described as follows:

- Reflection —Radio waves can be reflected back off the surfaces of objects with dimensions which are large in comparison to radio wavelength, for example, the surfaces of buildings and the earth. The amount of reflection depends on incident angle, materials and so on.
- Diffraction —Radio waves are propagated around the sharp edge of surfaces, for example, street corners.
- Scattering —Radio waves travel through multiple objects with smaller dimensions compared to their wavelength, for example, rain drops and lamp posts.

2.2.2 Additive White Gaussian Noise Channel

The propagation effects and other signal impairments are often collected and categorically referred to as the channel. The wireless communication channels suffers from a variety of impairments that contribute to errors. Noise, a critical component in the analysis of the performance of communication systems, are the unwanted signals that affect the fidelity of the desired signal. In wireless communication systems, there are numerous of noise: thermal noise that exists in all matter, artificial noise from other electrical machinery and impulse noise from radiation emitting devices [24]. The Additive white Gaussian noise (AWGN) channel often provides a reasonably good model in the situation of direct line-of-sight path between transmitter and receiver. The zero-mean noise having a Gaussian distribution is added to the signal. The noise is always assumed to be white which means that all frequency components appear with equal power. This channel model can be mathematically described by

$$r(t) = s(t) + n(t), \tag{2.1}$$

Table 2.2: Path Loss Exponent Values in Different Environments

Environment	Path Loss Exponent τ
In building line-of-sight	1.6 to 1.8
Free space	2
Obstructed in factories	2 to 3
Urban area cellular	2.7 to 3.5
Shadowed urban cellular	3 to 5
Obstructed in building	4 to 6

where $s(t)$ is the transmitted time domain signal; $n(t)$ is a sample waveform of a zero-mean white Gaussian noise process with power spectral density of $N_0/2$; and $r(t)$ is the received waveform. There are a great number of ways to combat AWGN, the easiest one of them is making the transmitting power much higher than that of the noise.

2.2.3 Large Scale Propagation

Based on the general 3-level model of mobile radio propagation, Path loss and Shadowing are the main cause of large-scale fading in wireless communication. The exact propagation characteristic is hard to obtain and depends highly on the location, environment, etc. The large-scale fading is multiplicative, not additive which is like AWGN [1, 2, 8]. Path loss model is applied for system planning, cell coverage and link budget. Shadowing is employed for power control design and second order interference and transmit power analysis.

Path Loss

Path loss is caused by the distance between the transmit-receive antennas and the loss that is due to obstacles and blockages. It leads to steady decreases in the long-term average of signal power as a function of the distance between the transmit-receive antennas. Denoting a transmitter of power as P_t Watts. When the transmit antenna gain is G_t and the receive antenna gain is G_r, the received power $P_r(d)$ can be described as a function of d [1]

$$P_r = \frac{P_t G_t G_r \lambda^2}{(4\pi)^2 d^\tau L} \tag{2.2}$$

where λ is the wavelength of the operation frequency, d is the T-R separation distance in meters, and L is the system loss factor not related to propagation ($L \geq 1$). A value

$L = 1$ indicates no loss in the system hardware. The path los exponent τ can vary from 1.6 to 6 according to various propagation environments, which can be shown in Table 2.2 [2]. Generally, the value of τ increases with the number of obstructions. $\tau = 2$ corresponds to the line-of-sight (LOS) free space path loss.

The path loss is defined as the difference between the received signal power and the effective transmitted power. It regards signal attenuation as a positive measurement in dB. For the free space model, the path loss, while antenna gains are included, can be expressed as [2]

$$PL(dB) = 10 \log \frac{P_t}{P_r} = -10 \log \left[\frac{G_t G_r \lambda^2}{(4\pi)^2 d^\tau L} \right]. \tag{2.3}$$

It can be seen from (2.3) that pass loss can be also written as

$$PL(dB) = C + 10n \log d, \tag{2.4}$$

with $C = 10 \log \left[\frac{(4\pi)^2 L}{G_t G_r \lambda^2} \right]$. $PL(dB)$ is a major component in the analysis and planning of a wireless communication system. In order to compensate for the effect of path loss, the transmitting power of the signal is increased, within acceptable bounds. Unfortunately, this will not always solve the shadowing problem, because shadowing is randomly existing.

Shadowing

Shadowing is caused by the changes of radio propagation in the terrain or obstacles, for instances, rural areas with large open spaces, urban areas with tall buildings and suburban areas with low rises. This effect leads to variation in the short-term average of signal power or shadow fading. A signal might undergo multiple reflections, which will encounter different power attenuations. Normally, shadowing is associated with the long-normal distribution [1, 2]. Incorporating the effect of free space path loss, the long-normal shadowing model $PL(d)$ at a distance d can be expressed as [2]

$$PL(d) = PL_F(d_0) + 10n \log(\frac{d}{d_0}) + X_\sigma, \tag{2.5}$$

where d_0 is a reference distance, and X_σ represents the shadowing factor with Gaussian random variables of a zero mean and a standard deviation of σ, where the value of X_σ ranges from 5 dB to 10 dB [1].

2.2.4 Small Scale Propagation

Small scale fading, mostly simplified by fading, is referred as the rapid fluctuation of the multipath delays, amplitudes or phases of a wireless signal over travel distance or a short period of time, where the large scale path loss effects can be ignored. In small scale propagation, such as multipath, the transmitted signal may arrive at the receiver with slightly delays. These delays can lead to fluctuations which are caused by the interference between those different versions of transmitted signals [1, 2, 8]. Fading is common in urban areas where transmitters and receivers are surrounded by structures, trees, moving vehicles and pedestrians, which lead to reflection, diffraction and scattering of the transmitted signals. Unlike large scale pass loss, the effects of small scale fading are realised over very small distances (a few wavelengths) and are time dependent. Therefore, the signal with their unique waveforms generated by different paths have randomly distributed amplitudes, phases and delays. The receiver combines all of these waveforms, which causes the signal distortion and fading.

Root Mean Square Delay Spread

A number of the same copies of the transmitted signal travel through various paths, and received at different arrivals of times. Some paths give rise to a loss of signal power, while some paths with less obstacles have larger signal power. The span of path delay in time domain is referred to as delay spread. Generally, a number of multipath channel parameters are obtained from the power delay profile (PDP), such as mean excess delay, root mean square (RMS) delay spread and excess delay spread. The mean excess delay $\bar{\tau}$ is the first moment of the PDP, which can be defined as [2]

$$\bar{\tau} = \frac{\sum_i \alpha_i^2 \tau_i}{\sum_i \alpha_i^2}, \tag{2.6}$$

where α_i and τ_i denote the path gain and delay for the i-th path, respectively. The RMS delay spread is the square root of the second central moment of the PDP and can be expressed as

$$\sigma = \sqrt{\bar{\tau^2} - (\bar{\tau})^2}, \tag{2.7}$$

where the second central moment of the PDP can be defined as

$$\bar{\tau^2} = \frac{\sum_i \alpha_i^2 \tau_i^2}{\sum_i \alpha_i^2}. \tag{2.8}$$

These delays are measured relative to the first detectable signal arriving at the receiver at $\tau_0 = 0$. If there is only one path $i = 1$, the RMS delay spread is equal to zero. The normalised mean excess delay and the RMS delay spread are obtained from a single PDP. This single PDP is the spatial average of consecutive impulse response measurements which are averaged and collected through a local area.

Coherence Bandwidth

In general, the coherence bandwidth, denoted as B_c, can be considered as a relation derived from the RMS delay spread [2]. More simply, it can be regarded as inversely proportional to the RMS delay spread. It is a statistical measure of the range of frequencies over which the channel can be considered "flat", that means a channel passing all spectral components with approximately equal gain and linear phase. In other words, coherence bandwidth is the range of frequencies over which two frequency components have a strong potential for amplitude correlation. The relation between the coherence bandwidth and the RMS delay spread varies with its definition. In the case where the frequency correlation function of the bandwidth is 0.5 or above [2], the coherence bandwidth can be approximately expressed as

$$B_c \approx \frac{1}{5\sigma}. \tag{2.9}$$

It is obvious that coherence bandwidth is totally depending on the RMS delay spread. The increasing of RMS delay spread leads to decreasing of the coherence bandwidth. A channel with a large RMS delay spread is highly frequency dispersive.

Doppler Spread

Doppler spread [1], denoted as B_d, can be defined as a range of frequencies. In other words, Doppler spread is the measurement of spectral broadening caused by time changing with the rate of the mobile radio channel. Within this spectrum, the received

Doppler spectrum is essentially non zero. Between the transmitter and receiver antennas, relative movements of mobiles or objects causes Doppler spread. The Doppler shift f_d, or named Doppler frequency, is given by [2]

$$f_d = \frac{\nu}{\lambda}\cos\theta = \frac{\nu}{c} f_c \cos\theta, \tag{2.10}$$

where ν is the relative velocity between transmitter and receiver or other movement of objectives between them, λ is the wavelength of the carrier frequency and θ is the angle between the direction of the received signal wave and the direction of the mobile user's motion. $f_{max} = \frac{\nu}{\lambda}$ is defined as the maximum Doppler shift while the angle θ is zero. Doppler spread B_d of a channel is equal to the maximum Doppler shift.

Coherence Time

Coherence time, denoted as T_c [2], is the time duration that the fading parameters, such as channel impulse response, remain fairly constant. In other words, two received signal sequences have a strong correlation in amplitude within a time duration which can be named as coherence time. In general, coherence time is usually employed in the time domain to characterise the nature of time varying for the frequency dispersiveness of the channel. If the time correlation function is above 0.5, based on the Clarke's Model, the coherence time T_c is given by [9]

$$T_c \approx \frac{9}{16\pi f_{max}}, \tag{2.11}$$

where f_{max} is the maximum Doppler shift. Sometimes the Doppler spread and coherence time are inversely proportional to one another. That is given by

$$T_c \approx \frac{1}{f_{max}}. \tag{2.12}$$

A popular rule of thumb for modern digital communications is to define the coherence time as the geometric mean of Equation (2.11) and (2.12), which can be defined as [2, 24, 9]

$$T_c = \sqrt{\frac{9}{16\pi f_{max}^2}} = \frac{0.423}{f_{max}}. \tag{2.13}$$

The definition of coherence time implies that two signals arriving with a time separation greater than T_c in (2.11) are affected differently by the channel.

Types of Fading

Based on the characteristics of the transmitted signal (such as bandwidth, symbol period) and the parameters of multipath channel (such as Doppler spread and RMS delay spread), four types of fading effects are given to describe the fading features [2], which are flat fading and frequency selective fading caused by multipath delay spread, and fast fading and slow fading due to Doppler spread. These fading effects and conditions are shown in Table 2.3.

- **Flat Fading**

  The channel is regarded as flat fading [1] if the signal bandwidth B_s is much smaller than the channel coherence bandwidth B_c and the symbol duration T_s is much greater than the RMS delay spread σ. The mobile radio channel will have constant gain and linear phase response over the transmission bandwidth. In flat fading, the transmitted signal spectral features are preserved at the receiver side, and so as the multipath structure of the channel. However, the features of the received signal changes with time according to different distributions such as Rayleigh fading, Rician fading and Nakagami fading [2]. Furthermore, from Equation (2.9), the coherence bandwidth will be infinite while the RMS delay spread is zero, meaning the channel is frequency flat over all ranges of frequencies.

- **Frequency Selective Fading**

  The channel is regarded as frequency selective fading [1] if the signal bandwidth B_s is greater than the channel coherence bandwidth B_c and the symbol duration T_s is smaller than the RMS delay spread σ. Under this circumstance in the time domain, the received signal is distorted, since the received signal is a mixture of multiple versions of the transmitted signals with fading and time delay. Within the channel, time dispersion of the transmitted waveforms results in frequency selective fading. Therefore, the overlapped received signals lead to inter-symbol interference (ISI) [2]. In the received signal spectrum, certain frequency components have greater gains than the others in the frequency domain.

Table 2.3: Fading Types

Flat Fading	Signal Bandwidth < Coherence Bandwidth
Frequency Selective Fading	Signal Bandwidth > Coherence Bandwidth
Fast Fading	Coherence Time < Symbol Duration
Slow Fading	Coherence Time ≫ Symbol Duration

- **Fast Fading**

  The channel is regarded as fast fading if the signal symbol duration T_s is larger than the channel coherence time T_c and the signal bandwidth B_s is smaller than the Doppler spread B_d. Which is to say, the channel impulse response changes rapidly within the symbol duration. This leads to frequency dispersion (or time selective fading) due to Doppler spread, which causes signal distortion. According to Equation (2.10) and (2.11), in frequency domain, the signal distortion due to fast fading increases with increasing the mobile speed, because the coherence time decreases with an increase in Doppler spread.

- **Slow Fading**

  The channel is regarded as slow fading if the signal symbol duration T_s is much smaller than the channel coherence time T_c and the signal bandwidth B_s is much greater than the Doppler spread B_d. In this case, the channel may be assumed to be static over one or several continuous symbol periods.

Flat and frequency selective fading determine the frequency diversity of the channel while the fast and slow fading determine the time diversity of the channel. It is not specifying that in the nature of the channel is frequency selective or flat fading while a channel is specified as a slow fading or a fast fading channel. Fast fading is only employed while dealing with the variation rate of the channel due to mobility. For flat fading channels, it can be approximated that there is no time delay in the impulse response. Figure 2.1 summarised the relationship between the types of fading experienced by the signal and various multipath parameters [2].

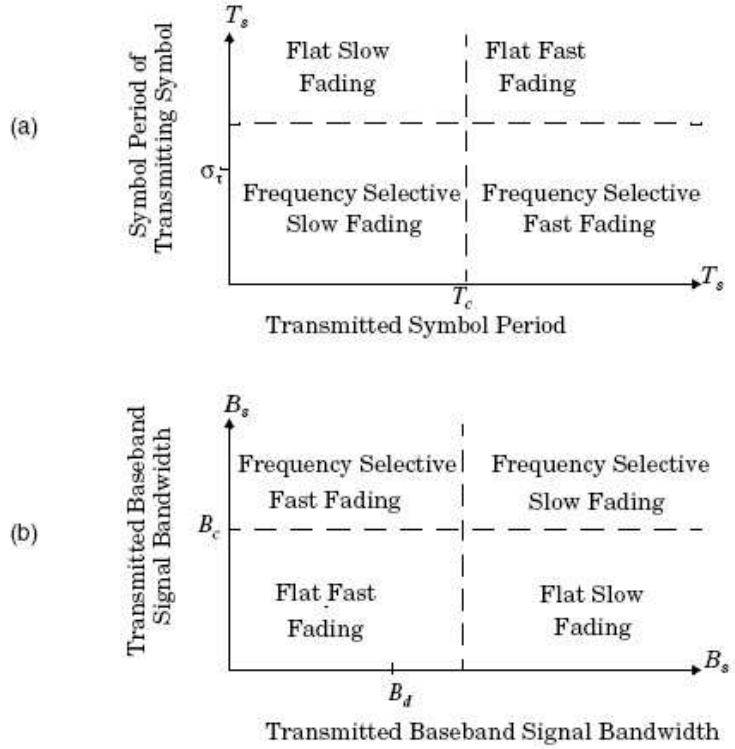

Figure 2.1: Fading channel types

Channel Models

The small-scale multipath channel model is introduced here. It is assumed that each symbol is transmitted through signal bandwidth B_s during symbol period T_s. Supposing the number of the multipath between transmitter and receiver is L_{ch}, the time domain channel impulse response (CIR) $h(t)$ can be given as [2]

$$h(t) = \sum_{i=0}^{L_{ch}-1} \alpha_i \delta(t - \tau_i), \tag{2.14}$$

where α_i and τ_i are the path gain and delay for the ith path, respectively. Note that the channel reduces to flat fading when $L_{ch} = 1$.

Assuming that with different delay and different spatial diversity branches are independent, α_i is an independent zero mean complex Gaussian random variable, with a variance following the discrete exponential power delay profile:

$$E\left|\alpha_i\right|^2 = d \cdot e^{-\frac{\tau_i}{\sigma}}, \tag{2.15}$$

where d is the normalising factor, and σ is the RMS delay spread.

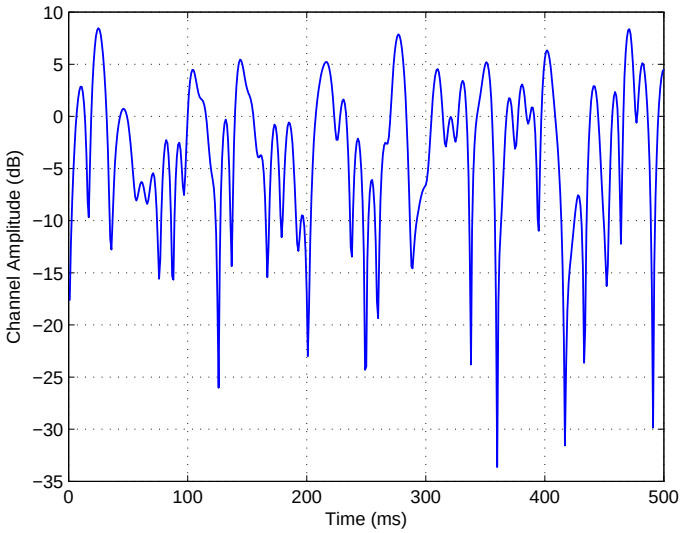

Figure 2.2: A typical Rayleigh fading channel impulse response

In mobile radio channels, the channels distortion [1, 2] can be modelled as a sequence of complex numbers in the baseband by projecting the RF channel impulse response onto the signal space in two-dimension. The real and imaginary parts of the response are usually modelled by independent and identically distributed zero-mean Gaussian random processes. The envelop amplitude of the complex channel response follows the Rayleigh distribution, and its phase follows the uniform distribution. In another words, each path gain is a complex random variable, of which both real part and imaginary part of the path gain are independent zero mean Gaussian with variance σ_r^2. A typical Rayleigh fading channel impulse response is illustrated in Figure 2.2. The Rayleigh distribution has a probability density function (PDF) which can be expressed as

$$P(|\alpha_i|) = \frac{|\alpha_i|}{\eta^2} e^{-\frac{|\alpha_i|^2}{2\eta^2}} \qquad 0 \leq |\alpha_i| \leq \infty, \tag{2.16}$$

where η is the RMS value of the received voltage signal before evelope detection, and η^2 is the time-average power of the received signal before envelope detection.

Clark's channel model [1, 2, 24], confirmed by measurement in urban area, has been widely applied in lots of literature. It is also employed in this thesis.

2.3 OFDM Systems

For multi-carrier modulation [1, 2], the basic concept is dividing the serial bit stream into a lot of different parallel sub-streams while transmitting them through the parallel sub-channels. Under ideal cases of the propagation conditions, the sub-channels are orthogonal to each other in typical. Each sub-channel has a data rate which is much less than that of the total data rate. Consequently, the bandwidth of the corresponding sub-channel is much less than the whole system bandwidth. In order to make sure that each sub-channel has a bandwidth which is less than the coherence bandwidth, the number of sub-streams is carefully chosen, by which each sub-channel experiences relatively flat fading. Therefore, the inter-symbol interference (ISI) on each sub-channel is small.

2.3.1 OFDM Technology

A high efficient and promising technology, named orthogonal frequency division multiplexing (OFDM) [2], is proposed to combat frequency selective fading channels. By employing cyclic prefix, the ISI can be completely eliminated. OFDM [25, 26] is one of the effective solutions to frequency selective fading. Compared to previous techniques, OFDM requires less complex equalisation filters. It has been selected as one of the key techniques for wireless local area networks IEEE 802.11 standards [27], and has been adopted by LTE-A [5, 28]. Also, it has been chosen as a strong candidate for the WiGig [29] and the Fifth Generation (5G) wireless communication standards [30, 31] in the future.

In Figure 2.3, the OFDM implementation of multi-carrier modulation is demonstrated. The input data stream is modulated by a PSK modulator, resulting in a complex stream with N OFDM symbols as $\{S[0], S[1], ..., S[N-1]\}$. Then the symbols are converted into time samples by performing an inverse Discrete Fourier Transform (IDFT), which is efficiently implemented using the Inverse Fast Fourier Transform (IFFT) algorithm. The IFFT yields the OFDM symbol consisting of the sequence $x[n]$

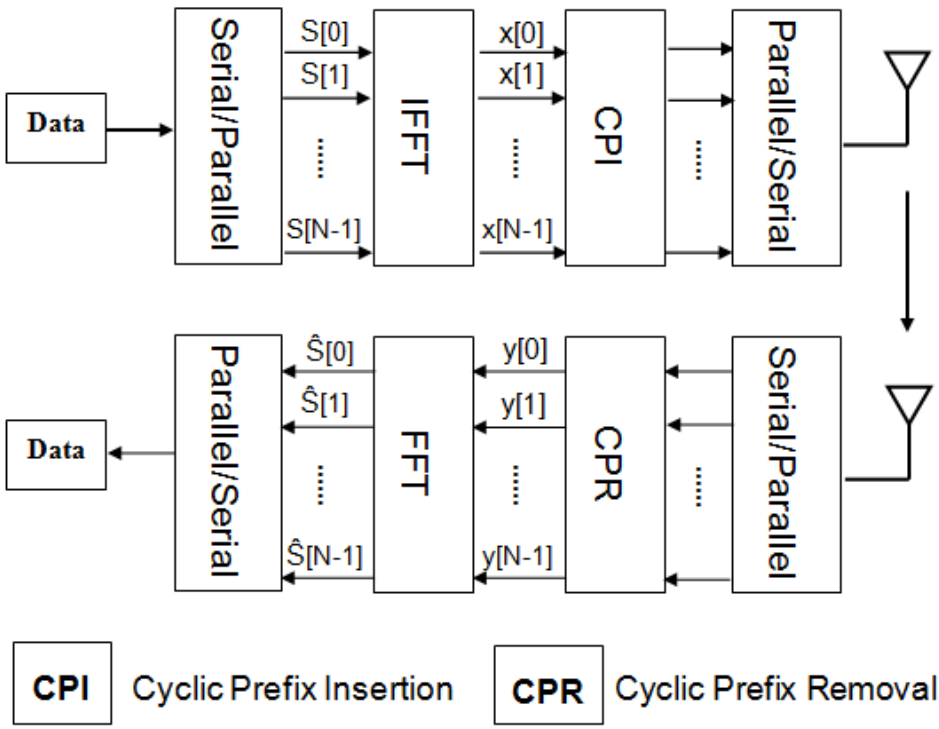

Figure 2.3: Wireless OFDM system model block diagram

of length N can be presented as

$$x[n] = \sum_{m=0}^{N-1} S[m] e^{j2\pi nm/N}, \qquad 0 \leq n \leq N-1. \tag{2.17}$$

Then the cyclic prefix is prepended to each OFDM symbol. Accordingly, the sequences are ordered with passing through parallel-to-serial converter.

It can be considered that the transmitted waveform passes through the filter of channel impulse response [2], and then added with the noise (AWGN), which lead to the received signal in time domain. The received signal is then down-converted to baseband, by which the high-frequency components can be filtered out. After serial-to-parallel convert and CP removal, the received signal sequences $y[n]$ can be given as

$$y[n] = \sum_{l=0}^{L-1} h[l] * x[n-l] + z[n] \quad 0 \leq n \leq N-1, \tag{2.18}$$

where $h[n]$ and $z[n]$ are the discrete-time equivalent lowpass CIR and AWGN, respectively. These time domain samples are serial-to-parallel converted and passed through an DFT operator as $\mathbf{F}$. This results, shown as (2.19), in scaled versions of the original

symbols, where H_n and $Z[n]$ are the CIR and noise associated with the n-th subchannel in frequency domain. The DFT output is parallel-to-serial converted and passed through PSK demodulator to recover the original data.

$$\begin{aligned}\hat{S}[m] &= \sum_{n=0}^{N-1} y[n]e^{-j2\pi nm/N} \qquad 0 \leq n \leq N-1 \\ &= H_m S[m] + Z[m]. \end{aligned} \tag{2.19}$$

It can be derived from (2.17) that each transmission data sequence consists of information from N symbols, and the information of one symbol has been spread across N transmission data. Therefore, the symbol period in OFDM systems becomes NT_s, leading to a mitigated ISI. In the frequency domain, the frequency range for each symbol is narrowed to B_s/N so that each transmission data carried on one subcarrier undergoes flat fading.

There are several benefits while utilizing OFDM technique in wireless communication. First of all, in OFDM systems, each subcarrier suffers from flat fading so the ISI effect in multipath phenomenon can be eliminated. Secondly, each subcarrier has a narrow bandwidth, which means that not all of the subcarriers suffer fading in a multipath channel. Thirdly, each subcarrier can be modulated independently in OFDM systems, which achieving a higher spectral efficiency than conventional single-carrier systems under frequency selective fading channel. Furthermore, OFDM leads to a higher efficiency in spectrum than the conventional frequency division multiplexing (FDM), where the frequency bands are not overlapped, and there is a guard band between two adjacent carriers. In OFDM systems, all the subcarriers are orthogonal overlapped, in which one subcarrier achieves its peak attenuation when others are zeros. This is because of the function of IFFT. Therefore, OFDM system can obtain a higher spectral efficiency than FDM systems due to the removal of the guard bands.

Therefore, the frequency selective fading channel can be divided into a number of frequency flat fading channels. Thanks to the CP insertion, the ISI can be avoided. OFDM systems require equalisation with lower complexity than that employed in some traditional approaches as in [32, 33, 34].

2.3.2 MIMO OFDM Systems

In order to improve the system capacity, multiple transmit and receive antennas are employed to establish multiple spatial branches, referred to as MIMO systems [35]. Compared to the traditional SISO systems, MIMO systems can enhance bandwidth efficiency, as multiple transmit and receive antennas operate on the same frequency band for the signal transmission. OFDM is well suited and employed in MIMO systems to combat the frequency selective fading. Also, equalisation can be simplified in the frequency domain for OFDM based systems. Therefore, MIMO OFDM systems have been adopted by the wireless local area network standards (IEEE 802.11) [27] and LTE Advanced, respectively [27, 36, 37].

A MIMO OFDM system is always considered with K transmit and M receive antennas in the frequency selective fading environment. The incoming serial data at the transmitter is divided into parallel first. Then the IDFT/DFT pair enables the signal to be transferred in between the frequency domain and the time domain. Let $s_k(n,i)$ denote the symbol on the n-th subcarrier ($0 \leq n \leq N-1$) in the i-th block ($0 \leq i \leq P-1$) transmitted by the k-th transmit antenna ($0 \leq k \leq K-1$). Define $\mathbf{s}_k(i) = [s_k(0,i), s_k(1,i), ..., s_k(P-1,i)]^T$ as the signal vector in the i-th block for the k-th transmit antenna.

At the transmitter, the signal in the i-th OFDM block is first transformed to the time domain as $\tilde{\mathbf{s}}_k(i)$ by IDFT as

$$\tilde{\mathbf{s}}_k(i) = \mathbf{F}^H \mathbf{s}_k(i), \tag{2.20}$$

where $\mathbf{F}$ is an $N \times N$ DFT matrix, with the entry given by $\mathbf{F}(a,b) = \frac{1}{\sqrt{N}} e^{-j2\pi ab/N}$, $(a,b = 0, ..., N-1)$, and $\mathbf{F}^H$ is an IDFT matrix, with $\mathbf{F}^H = \mathbf{F}^{-1}$ since $\mathbf{F}$ is a unitary matrix [38]. The computationally efficient IFFT/FFT pair may also be employed.

The total number of channel path is assumed as L, a CP of length L_{CP}, at least $L_{CP} \geq L-1$, is prepended to each OFDM block $\tilde{\mathbf{s}}_k(i)$. The guard symbols consist of a copy of the last L_{CP} entries of each OFDM block. The insertion of a CP is aimed to avoid IBI and circular convolution between time-domain signal and CIR. With the CP insertion, the transmitted signal vector can be written as $\bar{\mathbf{s}}_k(i)$.

The signal is then transmitted through the frequency selective fading channel, which is assumed to be constant for the duration of a frame which consists of a total number of P OFDM blocks. This is a convolution process in time domain. The received signal vector $\bar{\mathbf{y}}_m(i) = [\bar{y}_m(0,i), \bar{y}_m(1,i), ..., \bar{y}_m(N-1,i)]^T$ at the m-th receive antenna $(0 \leq m \leq M-1)$ in the time domain can be given as

$$\bar{\mathbf{y}}_m(i) = \sum_{k=0}^{K-1} \bar{\mathbf{H}}_{m,k} \bar{\mathbf{s}}_k(i) + \bar{\mathbf{z}}_m(i), \tag{2.21}$$

where $\bar{\mathbf{H}}_{m,k}$ is the convolution chanel matrix with size of $(L_{CP}+N)\times(L_{CP}+N)$ between the m-th receive antenna and the k-th transmit antenna, which can be expressed as

$$\bar{\mathbf{H}}_{m,k} = \begin{bmatrix} h_{m,k}(0) & 0 & \cdots & \cdots & 0 \\ \vdots & h_{m,k}(0) & 0 & \cdots & 0 \\ h_{m,k}(L-1) & & \ddots & & \vdots \\ \vdots & \ddots & & \ddots & 0 \\ 0 & \cdots & h_{m,k}(L-1) & \cdots & h_{m,k}(0) \end{bmatrix}, \tag{2.22}$$

where $h_{m,k}(l)$ is the l-th $(0 \leq l \leq L-1)$ channel path between the m-th receive antenna and the k-th transmit antenna, and $\bar{\mathbf{z}}_m(i)$ is the AWGN vector whose entries are i.i.d. complex Gaussian random variable with a zero mean and variance of N_0 [35].

After the CP removal, the received signal can be written as $\tilde{\mathbf{y}}_m(i)$ which then is transformed to the frequency domain by applying the $N \times N$ DFT matrix as

$$\mathbf{y}_m(i) = \mathbf{F}\tilde{\mathbf{y}}_m(i). \tag{2.23}$$

The time domain circular convolution can be transformed to a linear multiplication in the frequency domain by applying the IDFT/DFT operator pair, leading to simple equalisation for the frequency selective fading environment [39]. The resulting transceiver signal model in the frequency domain can be given as

$$\mathbf{y}_m(i) = \sum_{k=0}^{K-1} \mathbf{H}_{m,k} \mathbf{s}_k(i) + \mathbf{z}_m(i), \tag{2.24}$$

where $\mathbf{H}_{m,k} = \mathbf{F}\tilde{\mathbf{H}}_{m,k}\mathbf{F}^H$ is the diagonal frequency domain channel matrix. The entry (n,n) in $\mathbf{H}_{m,k}$ can be written as $H_{m,k}(n,n) = \sum_{l=0}^{L-1} h_{m,k}(l) e^{-j2\pi nl/N}$, and $\mathbf{z}_m(i)$ is the frequency domain noise vector. Note that the distribution statistics of the channel

can be preserved by the DFT [35], if the CIR $h_{m,k}(l)$ is assumed to have the Rayleigh distributed magnitude and uniformly distributed phase. Also, the distribution of the white Gaussian noise samples can be preserved by the DFT.

Finally, the Frequency Domain Equalisation (FDE) can be performed on each subcarrier in MIMO OFDM systems, since the frequency selective fading channel is divided into a number of flat fading channels. let $\mathbf{s}(n,i) = [s_0(n,i), s_1(n,i), ..., s_{K-1}(n,i),]^T$ denote as the signal vector from K transmit antennas on the n-th subcarrier in the i-th block. The received signal vector $\mathbf{y}(n,i) = [y_0(n,i), y_1(n,i), ..., y_{M-1}(n,i),]^T$ in the frequency domain on the n-th subcarrier, which can be given as

$$\mathbf{y}(n,i) = \mathbf{H}(n)\mathbf{s}(n,i) + \mathbf{z}(n), \tag{2.25}$$

where $\mathbf{H}(n)$ is the $M \times K$ channel frequency response matrix on the n-th subcarrier, with $H_{m,k}(n)$ denoting the entry (m,k) in $\mathbf{H}(n)$, the channel frequency response between the m-th receive antenna and the k-th transmit antenna, and $\mathbf{z}(n)$ is the noise vector. The estimate $\hat{\mathbf{s}}(n,i)$ of the source data can be performed by either Zero Forcing (ZF) or Minimum Mean Square Error (MMSE) based equalisation on the received signal on the n-th subcarrier as

$$\hat{\mathbf{s}}(n,i) = \mathbf{W}(n,i)\mathbf{y}(n,i), \tag{2.26}$$

where $\mathbf{W}(n,i)$ is the weighting matrix detected by the ZF or MMSE equalisation criterion.

2.3.3 Drawbacks of OFDM Systems

Although OFDM systems can combat frequency selective fading, there are some drawbacks which may degrade the system performance, such as ICI, carrier frequency offset (CFO), Inphase/Quadrature (I/Q) imbalance and Peak-to-Average Power Ratio (PAPR).

ICI

In high mobile fading channel, the time variation of the channel over an OFDM symbol period results in a loss of subchannel orthogonality which leads to ICI [12, 40] due to power leakage among OFDM subcarriers, resulting in an error floor that increases with

the Doppler spread. The performance degradation becomes significant as the carrier frequency, block size and vehicle velocity increase [41].

CFO

CFO is another typical radio frequency imperfect [42], and is introduced by frequency discrepancy between the carrier and the local oscillators. The CFO not only causes interference between frequency bins for frequency domain equalisation, but also degrades performance accumulatively with the increase of the block length for block-wise transmission method [43].

I/Q Imbalance

Due to the drive of low cost and low power consumption, Direct Conversion Architecture (DCA) has become a trend for the front-end design, particularly in OFDM based wireless communication systems [44]. However, I/Q imbalance is introduced by the DCA, including frequency independent and frequency dependent I/Q imbalance, at the transmitter and receiver [45, 46]. Frequency dependent I/Q imbalance is caused by the component mismatching in I and Q branches, and it is frequency selective. On the other side, frequency independent I/Q imbalance is due to the non-ideal local oscillators and is constant over the signal bandwidth. I/Q imbalance, if not compensated for, will introduce an ignorable error floor which can degrade the system performance severely in MIMO OFDM systems.

PAPR

The transmit signals in an OFDM system can have high peak values in the time domain since many subcarrier components are added via an IFFT operation. Therefore, OFDM systems are known to have a high PAPR [47], compared with single-carrier systems. The high PAPR is one of the most detrimental aspects in the OFDM systems, as it decreases the signal to noise ratio of analogue to digital converter and digital to analogue converter while degrading the efficiency of the power amplifier in the transmitter. the PAPR problem is more important in the uplink since the efficiency of power amplifier is critical due to the limited battery power in a mobile terminal.

2.4 Channel Estimation and Equalisation

After receiving the wireless transmitted signal sequence, the major challenge faced in OFDM systems is how to obtain the wireless CSI or CIR accurately. With the estimated CIR, a prompt channel equalisation technology can be utilized to recover the original signal sequence. Channel estimation and equalisation can be classified into the following types: training based, blind or semi-blind based approaches, respectively. For training based channel estimation and equalisation, a large number of symbol sequences are needed, while semi-blind or blind approaches require non of the training symbols. Therefore, semi-blind or blind channel estimation and equalisation have higher spectral efficiency than that of training based approach.

2.4.1 Training Based Channel Estimation and Equalisation

Training Based Channel Estimation

In training based channel estimation approach, the training symbol sequences are known as a priori at the receiver. In order to estimate the source signals, training symbols are first transmitted for channel estimation. Then, the estimated CSI can be applied to equalise the source data. This approach is easily applied to any wireless communication systems, and it is the most popular method used today because of its low computational complexity. However, it has a major drawback that it is wasteful of the information bandwidth.

Three widely used channel estimation schemes are discussed in this section: least squares (LS) based channel estimation, minimum mean square error (MMSE) based channel estimation [48, 49] and linear channel interpolation approach [50].

LS based Channel Estimation

The LS based method has been widely applied for wireless channel estimation for its low complexity. Let $\mathbf{h} = [h_0, ..., h_{L-1}, h_L, ..., h_{N-1}]^T$ denote the channel vector, of which elements are assumed to be Gaussian variables and independent to each other. If there are a total number of L channel paths, then $h_L = \cdots = h_{N-1} = 0$. The channel response energy is normalised to unity as $\sum_{l=0}^{N-1} \mathbf{E}\{h_l^2\} = 1$. In SISO systems, the

received signal vector $\mathbf{y}(i) = [y(0,i), y(1,i), ..., y(N-1,i)]^T$ in the i-th block can be written as

$$\mathbf{y}(i) = \mathbf{X}(i)\mathbf{H} + \mathbf{z}(i), \tag{2.27}$$

where $\mathbf{X}(i) = diag\{[x(0,i), x(1,i), ..., x(N-1,i)]^T\}$ is the $N \times N$ diagonal training matrix, $\mathbf{H} = \sqrt{N}\mathbf{F}\mathbf{h}$ is the channel frequency response vector on N subcarriers, and $\mathbf{z}(i)$ is the noise vector.

Assuming the training blocks is a length with a total number of P, the LS based channel estimation can be performed as

$$\hat{\mathbf{H}}_{LS} = \frac{1}{P}\sum_{i=0}^{P-1}[\mathbf{H} + \mathbf{X}^{-1}\mathbf{z}(i)]. \tag{2.28}$$

However, the term $\mathbf{X}^{-1}\mathbf{z}(i)$ may be subject to noise enhancement, especially when the channel is in a deep null.

For MIMO OFDM systems, the channel estimation can be divided into a number of independent SISO OFDM channel estimations, if the training symbols of transmit antennas are orthogonal to each other [51]. It means that a different subset of subcarriers is applied by each transmit antenna for the training symbols transmission.

MMSE Based Channel Estimation

If the CSI and noise distribution are known, then this priori information can be exploited to decrease the estimation error for Rayleigh fading channels. This technique usually outperform LS while doing channel estimation, since it can suppress the noise enhancement for known channel characteristics [52]. The MMSE based channel estimate $\hat{\mathbf{H}}_{MMSE}$ is obtained by minimizing the mean square error, which can be expressed as

$$\min E\{\|\hat{\mathbf{H}}_{MMSE} - \mathbf{H}\|^2\}. \tag{2.29}$$

By substituting the estimated channel vector with LS into Equation (2.29), the MMSE based channel estimation method can be written as [53]

$$\hat{\mathbf{H}}_{MMSE} = \mathbf{R}_{HH}(\mathbf{R}_{HH} + \sigma_z^2\mathbf{I}_N)^{-1}\hat{\mathbf{H}}_{LS}, \tag{2.30}$$

where $\mathbf{R}_{HH} = E\{\mathbf{H}\mathbf{H}^H\}$ is the auto-correlation of channel frequency response. MMSE estimation can both decrease the estimation error and shorten the required training sequence. It requires additionally the knowledge of the channel correlation matrix $\mathbf{R}_{HH}$ and noise correlation matrix $\sigma_z^2\mathbf{I}_N$.

Channel Interpolation

Channel interpolation [50] can be employed refine the channel estimation performance by the LS based technique. The correlation between adjacent subcarriers is used to correct some incorrect channel estimates for a few subcarriers. By applying the LS based channel estimation as shown in Equation (2.28), $\hat{\mathbf{H}}_{LS}$ can be expressed as in time-domain channel estimation $\tilde{\mathbf{h}}$ as

$$\tilde{\mathbf{h}} = \frac{1}{\sqrt{N}}\mathbf{F}^{+}_{N\times L}\hat{\mathbf{H}}_{LS}, \tag{2.31}$$

where $(\cdot)^+$ denotes the pseudo-inverse, $\mathbf{F}_{N\times L}$ is the $N \times L$ DFT matrix with its entry (a, b) given by $\mathbf{F}_{N\times L}(a, b) = \frac{1}{\sqrt{N}}e^{-j2\pi ab/N}$ where $(0 \leq a \leq N-1; 0 \leq b \leq L-1)$. The channel information for all subcarriers can be employed so that $\tilde{\mathbf{h}}$ is not influenced by a few errors on some subcarriers.

Training Based Channel Equalisation

With the estimated CSI, channel equalisation is applied to recover the transmitted signal on each subcarrier in the OFDM wireless communication systems. A number of equalisation techniques are discussed here in this subsection: zero forcing (ZF), MMSE and maximum likelihood (ML) based channel equalisation approaches.

ZF based Channel Equalisation

In order to avoid the issues of ISI in OFDM wireless communication systems, the ZF based equalisation method employs the inverse of the channel frequency response to the received signal in the frequency domain. This technique has been widely used in wireless communication systems since its simplicity. However, it may lead to considerable noise power enhancement after the process especially when the subcarriers are in deep fading. The received signal energy might be weaken at some frequencies under this consequence.

According to the Equation (2.26), the ZF based equalisation method can be performed on the n-th subcarrier as

$$\hat{\mathbf{s}}(n,i) = \mathbf{W}_{ZF}(n)\mathbf{y}(n), \tag{2.32}$$

where $\mathbf{W}_{ZF}(n)$ is the ZF equaliser weight on the n-th subcarrier, which can be given by

$$\mathbf{W}_{ZF}(n) = [\mathbf{H}(n)\mathbf{H}^H(n)]^{-1}\mathbf{H}^H(n). \tag{2.33}$$

MMSE based Channel Equalisation

The MMSE channel equalisation technique minimises the expected MSE between the symbol detected at the equaliser output and the transmitted symbols, thereby providing an optimised balance between noise enhancement and ISI mitigation. Since this balance is favourable in equalisation technology, MMSE equalisers tend to obtain better BER performance than those equalisers utilising the ZF algorithm. The MMSE based equalisation method is to optimise the MSE as

$$\mathbf{W}_{MMSE}(n) = \arg\min E\{\|\hat{\mathbf{s}}(n,i) - \mathbf{s}(n,i)\|^2\}. \tag{2.34}$$

Then the MMSE equalisation weight can be obtained by minimising the Equation (2.34) as

$$\mathbf{W}_{MMSE}(n) = \mathbf{H}^H(n)[\mathbf{H}(n)\mathbf{H}^H(n) + \sigma_z^2\mathbf{I}_M]^{-1}. \tag{2.35}$$

The source data sequences have a unit variance and are spatially uncorrelated as $\mathbf{R}_{ss} = E\{\mathbf{s}(n,i)\mathbf{s}^H(n,i)\} = \mathbf{I}_M$, and the noise is also spatially uncorrelated with variance σ_z^2 as $\mathbf{R}_{nn} = E\{\mathbf{z}(n,i)\mathbf{z}^H(n,i)\} = \sigma_z^2\mathbf{I}_M$.

ML based Channel Equalisation

Maximum-likelihood channel equalisation technique [52] avoids the problem of noise enhancement because it estimates the sequence of possible transmitted symbols. The ML based equalised signal $\hat{\mathbf{s}}(n,i)$ on the n-th subcarrier in the i-th block for OFDM wireless communication systems can be given as

$$\hat{\mathbf{s}}(n,i) = \arg\min\{\|\mathbf{x}(n,i) - \mathbf{H}(n)\tilde{\mathbf{s}}(n,i)\|_F^2\}, \tag{2.36}$$

where $\mathbf{x}(n,i)$ and $\tilde{\mathbf{s}}(n,i)$ are the received signal vector and the trial transmitted signal vector, respectively, $\mathbf{H}(n)$ is the channel frequency response matrix on the n-th subcarrier. The ML based equalisation method may need a number of searches, which results in very high complexity.

2.4.2 Semi-Blind and Blind Channel Equalisation

Unlike training based channel equalisation method, only little information is needed in the semi-blind equalisation, and non CIR information is required by blind scheme. This highly increases the spectral efficiency. Basically, semi-blind or blind equalisation techniques exploit the statistics or structure of the received signals and channel characteristics to recover the transmitted signals [7]. Based on the statistics order of the scheme, the equalisation method can be defined as second order statistics (SOS) and high order statistics (HOS).

SOS based Blind Channel Equalisation

The SOS based blind channel equalisation technique is only feasible for non-minimum phase channels which are linear and time-invariant, by utilising cyclostationary signals with the periodic correlation [17, 47]. Channels that are invariant and causal whose inverse or transfer function are known as non-minimum phase channels [47]. It can provide a greater phase response than the minimum phase channels with equivalent magnitude response.

The SOS based channel identification technique was first proposed in [17] for single-input multiple-output (SIMO) systems, where the non-minimum phase channel is estimated from the auto-correlation of the received signal.

A non-redundant linear precoding was first proposed in [54, 55], where the specific precoding structure is explored for semi-blind channel estimation at the receiver. A general precoding scheme was designed for channel estimation in [56] by exploiting the information contained in the signal covariance matrix. It was extended to MIMO wireless communication systems in [57].

HOS based Blind Channel Equalisation

Compared to the SOS, HOS based blind channel equalisation technique are more robust against the Gaussian noise, as the fourth or higher cumulates of the Gaussian noise are equal to zero [58]. Constant modulus algorithm (CMA) [59] and finite alphabet (FA) [60, 61] based equalisation methods are first generally discussed. Then the rest of this subsection will mainly focus on ICA and its application in OFDM wireless communication systems.

CMA is one of the earliest blind channel equalisation method by using the magnitude of a signal while ignoring the phase information of the symbols. It was proposed in [59] for SISO systems with frequency selective fading channels, and extended to MIMO systems with flat fading channels in [62]. The FA based blind equalisation method exploits knowledge of the modulation of a signal. This technique was employed for a number of wireless communication systems, such as SISO OFDM systems in [60] and MIMO systems with frequency selective fading channels in [61].

Independent Component Analysis In order to separate the multivariate signal into additive sub-components, ICA is employed as a HOS computational approach. By assuming that the sub-components are statistically independent with each other and non-Gaussian signals, the separation process of ICA can be realised. ICA is a special case of blind source separation technique [16]. As an efficient HOS based BSS technique, the theory of ICA is applying some received information from the statistics of the observed signals in order to estimating the source signals [63].

Denote $\mathbf{s} = [s_0, s_1, ..., s_{K-1}]^T$ and $\mathbf{y} = [y_0, y_1, ..., y_{M-1}]_T$ as the $K \times 1$ source variables vector and the $M \times 1$ observed variables vector, respectively. Each observed variable is modelled as a linear combination of the source variable. Therefore the general model of ICA can be given as

$$\mathbf{y} = \mathbf{H}\mathbf{s} + \mathbf{z}, \tag{2.37}$$

where $\mathbf{H}$ denotes the $M \times K$ mixing coefficient matrix from all of the K source variables to all of the M observed variables. Z denotes the noise vector. The independent source variable can be estimated by ICA without the knowledge of the mixing coefficient

matrix.

Whitening In order to apply ICA to do equalisation, the received signal should be statistically independent. However, the transmitted signal sequences are not usually completely uncorrelated. The process which is transforming the received components into uncorrelated variables is called whitening [63]. As a standard ICA preprocessing step, the received signal should firstly be whitened [58] by principal component analysis (PCA) to obtain spatially uncorrelated signals on each subcarrier.

First, the auto-correlation of the observed derived. Then a whitening matrix can be obtained from the eigenvalue decomposition (EVD) of the auto-correlation. Assuming that the observed variables have a zero mean, i.e., $E\{\mathbf{x}\} = 0$. Let $\mathbf{R}_{xx} = E\{\mathbf{x}\mathbf{x}^H\}$ denote the auto-correlation of the observed variables. The EVD of the auto-correlation $\mathbf{R}_{xx}$ could also be expressed as [16]

$$\mathbf{R}_{xx} = \mathbf{U}\Lambda\mathbf{U}^H, \tag{2.38}$$

where the colums of $\mathbf{U}$ include the eigenvectors of $\mathbf{R}_{xx}$, and $\Lambda = diag\{[\lambda_0, \lambda_1, ..., \lambda_{M-1}]\}$ is a diagonal matrix, with λ_m denoting the associated eigenvalues.

The $K \times M$ whitening matrix $\mathbf{W}$ can be obtained via the EVD of the auto-correlation $\mathbf{R}_{xx}$, which can be written as

$$\mathbf{W} = \Lambda^{-\frac{1}{2}}\mathbf{U}^H. \tag{2.39}$$

The whitening matrix is designed such that

$$\mathbf{W}E\{\mathbf{x}\mathbf{x}^H\}\mathbf{W}^H = \mathbf{I}_K. \tag{2.40}$$

The noise compensated whitening matrix $\mathbf{W}_z$ can be given as

$$\mathbf{W}_z = (\Lambda - \sigma_z^2\mathbf{I}_K)^{-\frac{1}{2}}\mathbf{U}^H, \tag{2.41}$$

where σ_z denoting the noise variance.

JADE The objective of whitening is make sure that the received signals are uncorrelated with each other. However, whitening is insufficient for a completely separation to

all of the received components. The desired independent components can be obtained by the HOS based ICA [16].

Some well known algorithms for ICA haven been proposed and utilized during the past decade. The Bell-Sejnowske algorithm applies the ML based technique [64]. The Fast ICA technique [65] maximizes the non-Gaussianity of the received components and the Joint Approximate Diagonalisation of Eigenmatrices (JADE) algorithm [66] employs the higher order based decorrelation.

Among these techniques, JADE algorithm has been chosen to the wireless communication equalisation method in the project of this thesis, as it requires shorter data sequences than other ICA methods. JADE is a well established batch algorithm which is based on joint diagonalisation of the cumulate matrices of the received components. The 4-th order statistics are applied in the JADE algorithm, resulting in the 4-th order cross-cumulate. The desired independent components can be estimated from the whitened variables by minimizing the 4-th order cross-cumulate [67].

By imposing the higher order decorrelation matrix V on the whitened signals, the estimate $\hat{\mathbf{s}} = [\hat{s}_0, \hat{s}_1, ..., \hat{s}_{K-1}]^T$ with length of K can be expressed as

$$\hat{\mathbf{s}} = \mathbf{V}^H \mathbf{W} \mathbf{x}. \tag{2.42}$$

The unitary matrix $\mathbf{V}$ is the minimisation of the 4-th order cross-cumulate, which can be given as

$$\mathbf{V} = \arg\min \sum_{jkl=0}^{K-1} |cum[\hat{s}_j, \hat{s}_j^*, \hat{s}_k, \hat{s}_l^*]|^2, \tag{2.43}$$

where $cum[\hat{s}_j, \hat{s}_j^*, \hat{s}_k, \hat{s}_l^*]$ is the 4-th order cross-cumulate which can be proved by [16]

$$\begin{aligned} cum[\hat{s}_j, \hat{s}_j^*, \hat{s}_k, \hat{s}_l^*] =& E\{\hat{s}_j \hat{s}_j^* \hat{s}_k \hat{s}_l^*\} - E\{\hat{s}_j \hat{s}_j^*\} E\{\hat{s}_k \hat{s}_l^*\} \\ & - E\{\hat{s}_j \hat{s}_k\} E\{\hat{s}_j^* \hat{s}_l^*\} - E\{\hat{s}_j \hat{s}_l^*\} E\{\hat{s}_j^* \hat{s}_k\}. \end{aligned} \tag{2.44}$$

Constraints of ICA Although ICA technique is well established and widely utilised now in the blind or semi-blind equalisation, it is not perfect as there are several restrictions [67].

- Source components have non-Gaussian distribution.

  The HOS based ICA technique can only be realised while dealing with the case of

non-Gaussian distribution, as HOS based Gaussian variables vanish [16]. Therefore, ICA is essentially applicable for observed variables with the non-Gaussian distribution.

- The source components should be statistically independent.

  This is the principle that can successfully employ ICA, which means there is no relationship between source components. Although whitening can realise uncorrelated among the received components, it may not be utilised effectively while existing correlated components.

- The unknown mixing coefficient matrix is invertible.

  The number of independent source components is equal to or less than that of the observed components.

There will be two circumstances based on Gaussian and non-Gaussian distribution. If the source signal sequences are Gaussian variables, the distribution of observed components at the receiver is identical to that of source components. Thus, ICA is not fitful for realisation. If the source signal sequences are mixture of Gaussian and non-Gaussian components, only the non-Gaussian components of the mixture can be estimated by ICA but the Gaussian components will vanish.

Ambiguity ICA introduces indeterminacy in the equalised signals in terms of permutation and phase ambiguities, which is similar to other blind channel equalisation techniques. The permutation ambiguity implies the order of the equalised signals is different from that of the source signals, while the phase ambiguity is the scaling and phase shifting. The relationship between the ICA equalised signals vector $\hat{\mathbf{s}}$ and the source signals vector $\mathbf{s}$ can be given as

$$\hat{\mathbf{s}} = \mathbf{PGs}, \tag{2.45}$$

where $\mathbf{P}$ and $\mathbf{G}$ denote the permutation ambiguity and the phase ambiguity, respectively. These ambiguities can be eliminated by applying some additional processes [16].

ICA based OFDM Wireless Communication Systems In the wireless communication environment, the wireless channel between transmitter and receiver is normally either flat or frequency selective fading. For flat fading channel scenario, ICA technique can be directly exploited onto the received signals, as the received signals are linear combination of the transmitted signals. For frequency selective fading channel, the channel is convolutive. Under this condition, the ICA technique can not be directly applied. However, by applying OFDM technology added with CP, the frequency selective fading channel can be divided into a number of flat fading subchannels. In other words, the received signal sequences in OFDM systems can be transformed to be a number of linear instantaneous mixtures. The general OFDM based received signal in frequency domain can be given as in Equation (2.19). It is identical to the linear instantaneous mixture ICA model in Equation (2.37). Thus, the ICA technique can be directly applied to the received signals $\mathbf{y}(n, i)$, in order to separate the mixture and recover the transmitted signals on each subcarrier. The spectral efficiency is improved in ICA based OFDM systems while the CSI is not needed any more.

As it described in the previous section, the drawbacks of ICA model may lead to a possibly different order and phase in the ICA equalised signals on each subcarrier. Then further processing is required to resolve these problems. In [68], ICA was applied onto all of the subcarriers. The correlation between adjacent subcarriers is used to resolve the frequency dependent permutation problem. However, this approach introduces bit errors and ambiguity error propagation across subcarriers, which could not be solved. In order to avoid this error propagation, a blind receiver structure was proposed in [50], where the correlation between the reference subcarriers and other subcarriers is explored to allow more robust reordering and scaling at the receiver. These existing a significant performance gap between the higher order modulation scheme and the case with perfect CSI. In [69], a precoding method was applied at the transmitter. Before the signals were transmitted, the reference data sequences were superimposing onto the source data sequences. At the receiver side, the permutation and phase ambiguities is eliminated by utilising the correlation between reference symbol sequences and the equalised signals. It can be realised without consuming extra bandwidth. However, the precoding based

ambiguity elimination technique is sensitive to the precoding constant and the symbol frame length. A good BER performance can be obtained while the transmitted signal frame size is large. Also, this method high computational complexity, especially for a large number of transmit and receive antennas.

In this thesis, ICA is discussed for OFDM based wireless communication systems. In Chapter 4, ICA is applied in a semi-blind MIMO OFDM systems. A number of reference data sequences are carefully designed, and superimposed into the source data sequences without introducing training overhead or consuming extra transmission power. This precoding process is employed for Doppler spread estimation and ambiguity elimination in the ICA equalised signals. Then ICA based equalisation method is validated through the real-time wireless communication test-bed with signal generator and signal analyser connected with a pair of antennas at 2.4 GHz.

Chapter 3

Pilot Aided Semi-Blind Doppler Spread Estimation and Kalman Filtering Based Channel Estimation for OFDM Systems

3.1 Introduction

Single-carrier frequency-domain equalisation (SC-FDE) [70] is a promising technique to provide broadband data services for future wireless communication systems. Compared to traditional time-domain equalisation approaches, SC-FDE has a much lower complexity to achieve the same performance.

In OFDM wireless communication systems over time-varying channel, Doppler shift can destroy the orthogonality among subcarriers resulting in an intercarrier interference (ICI) [12, 40]. The ICI will introduce an ignorable error floor which is dramatically increased with higher Doppler spread. If the Doppler spread and CIR can be estimated accurately, the ICI can be mitigated from the received signal.

A lot of approaches have been proposed and applied to combat ICI. In [41], a frequency domian equaliser was proposed in order to compensate for the effects of channel variation. Its equalisation technique which is applied on the received OFDM signals is achieved by assuming that the CIR varies in a linear fashion during one transmitted period. However, this assumption is developed on that the multipath fading channel is in slow-time varying. In this case, the time variation of the CIR, for all of the paths, can be approximated by straight lines with low slopes during one block

period. Besides, it also assumes that most energy of the straight line with a low slope is concentrated in the neighbourhood of the dc component in the frequency domain, and then the ICI terms which do not significantly affect the signal can be ignored. But in real-time multipath fading channel, e.g., room or Reverberation chamber environment, the variation of the multipath fading channel is always fast, which means that the CIR during one OFDM block period no longer hold and gives rise to an error floor.

In order to compensate for the ICI effects without increasing the spectrum overhead, blind channel estimation schemes were proposed. In [54], a statistical channel estimation approach was proposed. A linear transformation is applied to the OFDM symbol blocks before transmitted, which could realise the blind channel estimation at the receiver through correlation function to the received OFDM blocks. This precoding approach with high spectral efficiency is so popular that many channel estimators utilise it. However, the complexity of the system should be taken as an consideration.

The previous ICI cancellation methods are able to dramatically reduce the ICI, but they are much sensitive to the phase ambiguity, multipath fading and local frequency drift. Then some robust ICI cancellation schemes with pilot-aided that can estimate time varying channel information. In [71], a channel estimation algorithm was proposed for OFDM mobile communication systems aided with pilot sequence. The channel estimator is derived based on a parametric channel model, of which the channel frequency response is modelled as the Fourier transform of a multipath finite impulse response (FIR). By applying the channel estimator, the channel parameters, including multipath delays, paths gains and phases, are estimated. Then the estimated channel parameters are utilised through rotational invariance techniques in order to estimate the initial multipath time delays. Finally, a MMSE estimator is exploited with the estimated multipath delay information, aiming at estimating channel frequency response. From technical version in frequency domain, a sequence of pilot subcarriers are inserted with a certain interval into the information subcarriers before transmit, then from the version of time domain, the pilots can be thought at as inserting through the whole frame length. The coherence time of the channel is assumed to be long enough for reliable correlation matrix estimates, which is not fitful for real-time wireless systems. Even

with a reasonable simulation results, an extremely high overhead (25%) can not be ignored at all.

In [72], a dynamic phase estimation method was proposed. The amplitude gain of the decoded signal at the ICI cancellation receiver is variable according to the real channel over time. However, it requires the channel to be constant through a long blocks duration that may not suitable to the real time wireless channel. Then the authors [73] proposed a semi-blind ICI equalisation scheme based on JADE algorithm which is more flexible than the previous method. Also aided with the pilot sequences, the semi-blind ICI cancellation scheme can obtain a reasonable performance and results. However, the complexity appears as an issue that cannot be ignorable.

The Kalman filter [13, 14] is known as a mathematical power tool that is playing an increasingly important role in signal estimation. The Kalman filter is a recursive and optimal estimator that can obtain the estimates from indirect, inaccurate and uncertain observations. With a few conceptual tools, the Kalman filter is actually very easy to use. If all noise is Gaussian, the Kalman filter minimises the mean square error of the estimated parameters. The Kalman filter [74] linear estimation scheme is employed in this thesis for the following reasons: first, applying Kalman filtering chanel estimation approach can lead to good results in simulation due to its optimality and structure. Secondly, the form of Kalman filter is convenient for real time processing, which can be demonstrated in Chapter 5. Thirdly, it is easy to formulate and implement given a basic understanding. Finally, the measurement equations in Kalman filtering algorithms need not be inverted.

In this chapter, a low-complexity semi-blind Doppler spread tracking and Kalman filtering based channel estimation scheme is proposed, where a short pilot for each transmit frame is designed carefully for multiple utilisation. The work in this chapter is different in the following aspects:

- First, a set of pilot data sequences is carefully designed as the prefix of the transmitting signal for the following use: it is exploited to estimate the Doppler spread, then the ICI in the received signal can be obtained. After Doppler spread

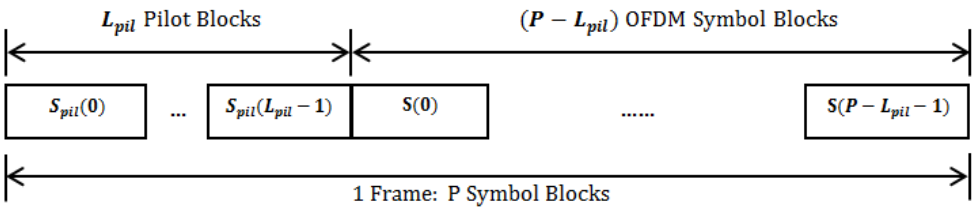

Figure 3.1: Proposed Kalman Filtering based Frame Structure

estimation and ICI mitigation, the same pilot sequence is used by Kalman filter for initialisation of the wireless channel estimation.

- The estimated ICI caused by Doppler spread is gathered into the equivalent channel model and compensated together with the channel equalisation, which leads to a low complexity of the system.

- Simulation results show that, the proposed semi-blind Doppler spread tracking and Kalman filtering channel estimation system can provide a BER performance close to the ideal case with perfect CSI. The proposed approach can outperform the referenced Doppler spread estimation and ICI cancellation schemes in terms of BER and normalised mean square error (NMSE) estimation performance.

The system model is presented in Section 3.2 and the pilot design is presented in Section 3.3. The proposed semi-blind Doppler spread estimation approach is given in Section 3.4. Then the Kalman filtering channel estimation and MMSE based channel equalisation are described in Section 3.5. Section 3.6 presents the simulation results. Finally, Section 3.7 provides the summary of this chapter.

framestructureKFF.eps

3.2 System Model

An OFDM spatial multiplexing system is considered in this chapter. The frame structure can be found in Figure 3.1. Each transmit frame consists of P OFDM blocks with each block of N subcarriers. Before transmission, a CP with length L_{CP} is prepended to the beginning of each OFDM block, which will be removed at the receiver in order to avoid the ISI. Let $s(n, i)$ denote the symbol on the n-th $(0 \leq n \leq N-1)$ subcarrier

in the i-th ($0 \leq i \leq P-1$) OFDM block. Correspondingly, the signal vector in the i-th OFDM block can be denoted as $\mathbf{s}(i) = [s(0,i), s(1,i), ..., s(N-1,i)]^T$. Define an ICI matrix of size $N \times N$ as $\mathbf{C}(\phi_i)$ with the entries of $e^{j2\pi\phi_i(q^{'}-q)/N}$ and the normalized Doppler spread of the i-th block $\phi_i = \Delta f_i T_s$. The channel frequency response matrix is denoted as $\mathbf{H} = diag\{H(0), H(1), ..., H(N-1)\}$, where the entry $H(n)$ represents the channel frequency response element on the n-th subcarrier between the transmit antenna and the receive antenna. Consequently, the received signal vector $\mathbf{y}(i) = [y(0,i), y(1,i), ..., y(N-1,i)]^T$ in the i-th OFDM block at the receive antenna in the frequency domain after CP removal, including ICI, can be given as

$$\mathbf{y}(i) = \mathbf{C}(\phi_i)\mathbf{H}\mathbf{s}(i) + \mathbf{z}(i) \tag{3.1}$$

where $\mathbf{z}(i)$ is the AWGN vector whose entries are i.i.d. complex Gaussian random variables with zero mean and variance.

3.3 Pilot Design

A pilot matrix is designed for each user. Let $\mathbf{S}_{pil} = [\mathbf{s}_{pil}(0), \mathbf{s}_{pil}(1), ..., \mathbf{s}_{pil}(N-1)]$ denote the $N \times N$ pilot matrix. In the initial stage of data transmission, the pilots take the first L_{pil} blocks of the data frame of P blocks for Doppler spread estimation and then for initialisation of the Kalman filtering channel estimation. Denoting $\mathbf{S}_{pil} = [\mathbf{s}_{pil}(0), \mathbf{s}_{pil}(1), ..., \mathbf{s}_{pil}(L_{pli}-1)]$ as the $N \times L_{pil}$ pilot blocks of the transmit data frame. The semi-blind Doppler spread estimation can be obtained by maximising the cross-correlation between the pilot signal with ICI in the received signal frame and the projection operator $\mathbf{Q} = \mathbf{S}_{pil}^H$. Therefore, the optimal reference data design is to maximising the cost function, which can be written as

$$\boldsymbol{J} = \frac{1}{N}\left(\|\mathbf{Q}(l_{pil})\mathbf{s}_{pil}(l_{pil})\|_F^2\right). \tag{3.2}$$

The optimal solution to minimise Equation (3.2) is a set of pilots that are not orthogonal to each other in the frequency domain, which means $\boldsymbol{J} = 1$. A Hadamard matrix M_{had} [75, 76] can provide a solution to Equation (3.2), in which the same pilot data sequences will be applied at the receiver for Doppler estimation. Each L_{pil}

columns will be chosen as the pilot blocks for the transmit data frame of the k-th transmit antenna.

3.4 Semi-Blind Doppler Spread Estimation

A semi-blind pilot aided Doppler spread estimation scheme is proposed for the OFDM systems, where a number of carefully designed pilot data sequences are prefixed to each transmit frame. The Doppler spread estimation is realised by applying the cross-correlation between the trial values of normalised Doppler spread compensated received signals and the projection operator.

With a normalised Doppler spread ϕ_i, the signal vector $\mathbf{s}^{\phi_i}(i)$ with the ICI in the i-th OFDM block can expressed as

$$\mathbf{s}^{\phi_i}(i) = \mathbf{C}(\phi_i)\mathbf{s}(i). \tag{3.3}$$

In order to tracking the Doppler spread, a trial value $\tilde{\phi}_i$ of normalised Doppler spread is given. Based on the Equation (3.1) and (3.3), the received signal vector $\tilde{\mathbf{y}}i$ can be also given as

$$\tilde{\mathbf{y}}(i) = \mathbf{H}\mathbf{s}^{(\phi_i - \tilde{\phi}_i)}(i) + \mathbf{z}(i). \tag{3.4}$$

Let $\boldsymbol{\beta}(i)$ denote as the cross-correlation between the projection operator $\mathbf{Q}$ and the received signal vector $\tilde{\mathbf{y}}(i)$ with ICI at the receive antenna. It can be expressed as

$$\boldsymbol{\beta}(i) = \mathbf{Q}(i)\tilde{\mathbf{y}}(i), \tag{3.5}$$

where the i-th vector of matrix $\mathbf{Q}(i)$ is orthogonal to the reference data sequences in the received data. If the Doppler spread trial value is correctly estimated, the correlation function between the projection operator and the reference data sequences is a matrix with maximum value. Therefore, the correlation $\boldsymbol{\beta}(i)$ between the projection operator and received signals are expressed as

$$\boldsymbol{\beta}(i) = \mathbf{H}\left[\mathbf{Q}(i)\mathbf{s}^{(\phi_i - \tilde{\phi}_i)}(i)\right] + \mathbf{Q}(i)\mathbf{z}(i). \tag{3.6}$$

It can be obtained that the correct normalised Doppler spread can result in a $\boldsymbol{\beta}(i)$ with the maximum energy while the pilot data are matched. The high accuracy of the

Doppler spread estimation can be performed by maximising the sum cross-correlations from all of the i-th block in the received frame. It can be derived that the correctly estimated $\hat{\phi}_i$ can be obtained by

$$\hat{\phi}_i = \underset{\widetilde{\phi}_i \in [0,0.1]}{\arg\max} \left\| \boldsymbol{\beta}(i) \right\|_F^2 , \tag{3.7}$$

where $\|\cdot\|_F^2$ denotes the Frobenius norm.

The NMSE between the estimates of Doppler spread and the true values can be defined as

$$NMSE = \frac{1}{P} E \left\{ \sum_{i=1}^{P} \frac{\left\| \hat{\phi}_i - \phi_i \right\|^2}{\left\| \phi_i \right\|^2} \right\}, \tag{3.8}$$

where $E\{\cdot\}$ denotes the expectation.

3.5 Kalman Filtering Based Channel Estimation and MMSE Based Channel Equalisation

The Kalman Filter [74] is an algorithm that utilises a series of measurements observed over time, containing noise and other inaccuracies, and produces estimates of unknown variables that tend to be more precise than those based on a single measurement alone. It is also known as a linear quadratic estimation scheme. More formally, the Kalman Filter operates recursively on streams of input data with noise in order to produce a statically optimal estimate of the underlying systems state.

The process of the Kalman filter algorithms can be divided into two steps which are prediction and update. In prediction step [74], the Kalman filter can produce estimates of the current state variables, along with their uncertainties. Once the outcome of the next measurement is observed, these estimates are updated by applying a weighted average, with more weights being given to estimates with higher certainty. Based on the recursive nature of the algorithms, Kalman filter is able to be run with only the present input signals and the previously calculated state and its uncertainty matrix. Besides, no additional past information is required.

After Doppler spread estimation, the equivalent channel model in noiseless case can

be given as

$$r(k,i) = \left[\sum_{l=0}^{L_{ch}-1} h(k,l)s(k-l,i) \right] e^{j2\pi\hat{\phi}_i k/N}, \tag{3.9}$$

where $h(k,l)$ represents the complex random variable for the l-th path of the CIR. Then the received signal in time domain can be written as $r(k,i) = s(k,i) * g(k,i)$ where $g(k,i)$ represents the channel response with ICI and $*$ denotes the time domain convolution.

3.5.1 Kalman Filtering based Channel Estimation

We present an adaptive frequency domain channel estimator for the equivalent channel matrix. The receiver operates in the training mode for P blocks including L_{pil} pilot symbols. Before the estimation, two equations, known as process equation and measurement equation, should be determined in order to set up the initialisation.

Process Equation

The process equation is used to stack the time domain channel impulse response vector based on one received signal frame, which can be expressed as

$$\mathbf{g} = \left\{ [\mathbf{g}(0)]^T, [\mathbf{g}(1)]^T, ..., [\mathbf{g}(P-1)]^T \right\}, \tag{3.10}$$

where $\mathbf{g}(i)$ denotes the i-th path block of the received frame. Since the equivalent CIR contains the ICI caused by Doppler spread, the process equation can be assumed and described as

$$\mathbf{g}(i+1) = \mathbf{A}\mathbf{g}(i) + \Lambda(i), \tag{3.11}$$

where $\mathbf{A}$ denotes the state transition matrix of size $L_{ch} \times L_{ch}$, and $\Lambda(i)$ represents a complex zero-mean AWGN vector of the i-th block with its covariance of $\mathbf{V}_P = \boldsymbol{E}[\Lambda(i)\Lambda^H(i)]$. With the estimated Doppler spread $\hat{\phi}_i$, the transition matrix can be expressed as $\mathbf{A} = e^{j\pi\Omega}\mathbf{Q}(i)$.

Measurement Equation

Define the $\tilde{\mathbf{F}}$ as the DFT operator matrix, and $\tilde{\mathbf{S}}$ is a matrix of size $N \times N$, whose m-th row is given by $\mathbf{e}_N(i) \circledast [\tilde{\mathbf{S}}^T(m,i), \tilde{\mathbf{S}}^{*T}(m,i)]^T$ with $\mathbf{e}_N(i)$ denoting a vector whose i-th element is 1, and all others are zeros. $\circledast$ denotes Kronecker product operator. Then

the received signal in frequency domain can be given by the following measurement equation as

$$\mathbf{R}(i) = \tilde{\mathbf{S}}(i)\tilde{\mathbf{F}}\mathbf{g}(i) + \mathbf{N}(i), \tag{3.12}$$

where the covariance of the AWGN $\mathbf{N}(i)$ can be expressed as $\mathbf{V}_m = \boldsymbol{E}[\mathbf{N}(i)\mathbf{N}^H(i)]$.

Channel Estimation

The frequency domain channel estimator operates in the training mode for L_{pil} blocks of pilot symbols. In the decision directed mode, hard decisions of data symbols are used in the following iteration. The recursion procedure can be used to obtain the tentative channel estimates block by block.

$$\tilde{\mathbf{g}}(i\|i-1) = \mathbf{A}\tilde{\mathbf{g}}(i\|i-1) \tag{3.13}$$

$$\mathbf{P}(i\|i-1) = \mathbf{A}\mathbf{P}(i-1\|i-1)\mathbf{A}^H + \mathbf{V}_P \tag{3.14}$$

$$\mathbf{K}(i) = \mathbf{P}(i\|i-1)\left[\tilde{\mathbf{S}}(i)\tilde{\mathbf{F}}\right]^H \cdot \left\{\tilde{\mathbf{S}}(i)\tilde{\mathbf{F}}\mathbf{P}(i\|i-1)\left[\tilde{\mathbf{S}}(i)\tilde{\mathbf{F}}\right]^H + \mathbf{V}_m\right\}^{-1} \tag{3.15}$$

$$\tilde{\mathbf{g}}(i\|i) = \mathbf{g}(i\|i-1)\mathbf{A} + \mathbf{K}(i)\left[\mathbf{R}(i) - \tilde{\mathbf{S}}(i)\tilde{\mathbf{F}}\tilde{\mathbf{g}}(i\|i-1)\right] \tag{3.16}$$

$$\mathbf{P}(i\|i) = \mathbf{P}(i\|i-1)\left[\mathbf{I}_{2L_{ch}} - \tilde{\mathbf{S}}(i)\tilde{\mathbf{F}}\mathbf{K}(i)\right]. \tag{3.17}$$

Equation (3.13) and (3.14) represent the Kalman filtering estimation process, where $\tilde{\mathbf{g}}(i\|l)$ $(l = i-1, i)$ denotes the estimate of $\mathbf{g}(i)$, $\mathbf{P}(i\|l) = E\left[\epsilon(i\|l)\epsilon^H(i\|l)\right]$ $(l = i-1, i)$ with $\epsilon(i\|l) = \tilde{\mathbf{g}}(i\|l) - \mathbf{g}(i)$ denoting the channel estimation error, and $\mathbf{K}(i)$ denotes the Kalman gain matrix. Equation (3.16) and (3.17) denote the update process of the channel estimation.

3.5.2 MMSE based Channel Equalisation

After obtaining the channel estimates of $\mathbf{g}(i)$ for each block in the received frame, the corresponding frequency responses $\mathbf{G}(i)$ can be derived by using DFT. From the equivalent channel model, the ICI has been gathered into the channel estimates and compensated through equalisation scheme. The MMSE based channel equalisation technique is applied in this chapter to recover the source in the received signals.

$$\hat{\mathbf{s}}(i) = \mathbf{W}(i)\mathbf{y}(i), \tag{3.18}$$

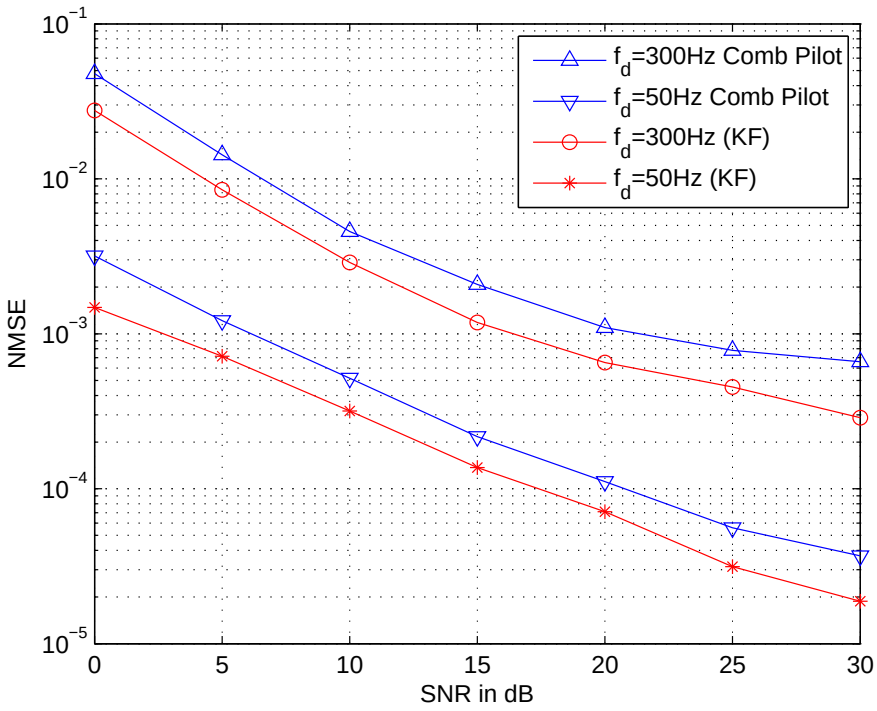

Figure 3.2: NMSE performance of the semi-blind Doppler spread Estimation in OFDM systems

where the MMSE based channel equaliser weight can be expressed as

$$\mathbf{W}(i) = \mathbf{G}^H(i) \left[\mathbf{G}(i)\mathbf{G}^H(i) + \sigma_{\mathbf{z}}^2 \mathbf{I}_N\right]^{-1}. \tag{3.19}$$

Finally, the equalised signals are operated through demodulation and hard estimates of the transmit signals.

3.6 Simulation Results

In this section, we use simulation results to evaluate the performance of the proposed semi-blind Doppler spread estimation and Kalman filtering based channel estimation approach, and the ICI compensation is incorporated with MMSE equalisation. We consider an OFDM system with $N = 128$ subcarriers, and each transmit frame consists of $P = 100$ blocks where the first 4 blocks are used as pilot, resulting in a training overhead of 4%. The Clarke's block fading channel model [1] is employed, where the exponential power delay profile is exploited with the RMS delay spread is $T_{RMS} = 1.4$ and is normalised to the sampling time interval. A CP of length $L_{cp} = 16$ is used. Two

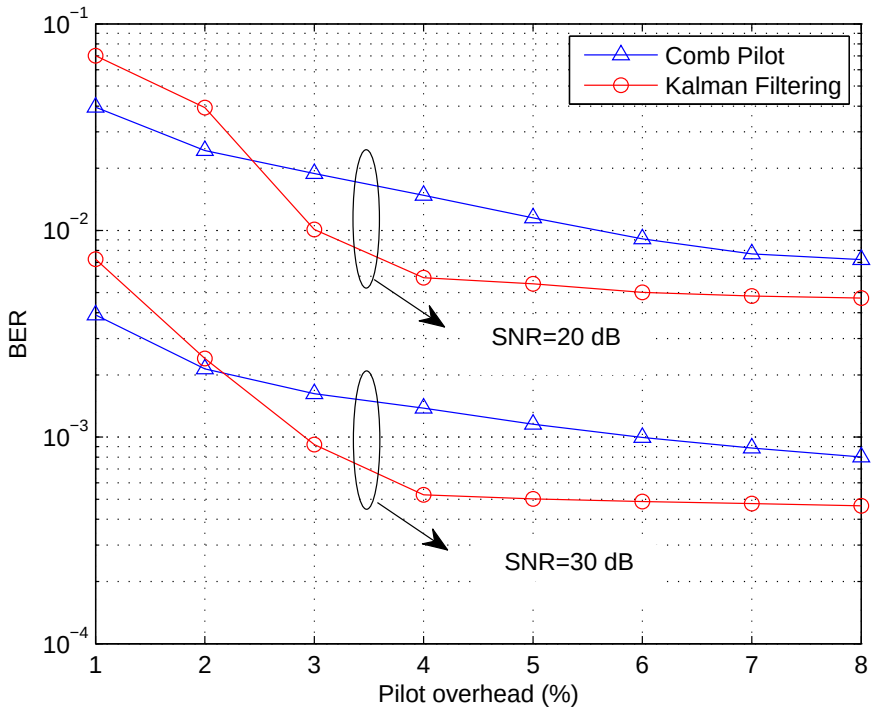

Figure 3.3: BER vs. Pilot overhead of the semi-blind Doppler spread tracking and Kalman filtering based channel estimation of OFDM systems

Doppler spread frequencies with $f_d = 50\ Hz$ and $f_d = 300\ Hz$ have been chosen to test the system performance.

Figure 3.2 shows the NMSE between the estimates of Doppler spread and the true values. The performance of the proposed semi-blind Doppler spread estimation method is shown in this figure, where another comb type pilot aided Doppler spread estimation scheme is employed for comparison. Under the two different Doppler spread $f_d = 50\ Hz$ and $f_d = 300\ Hz$, it can be obtained that the proposed semi-blind Doppler spread estimation can provide more accurate estimates than the referenced one with the same pilot overhead. In Figure 3.2, with the increasing of the SNR in dB, the NMSE of Doppler spread estimation is getting smaller, which mean the estimates are becoming more accurate. The gap between each two line with the same estimation method is almost parallel and fixed. The reason is that the SNR in dB is increasing constantly, and the Doppler spread is fixed as 50 Hz and 300 Hz. Therefore, the estimation is becoming easier, and the estimates is more accurate.

For comparison, a comb type pilot [77] aided Doppler spread estimation and ZF based equalisation scheme [78] is employed. In this referenced method, a sequences of pilot tones are applied and inserted to each transmit OFDM symbol. At the receiver side, these pilot symbols are used for Doppler spread tracking and channel estimation at pilot frequencies and then interpolating the channel frequency response. The estimation of the channel is based on LS, and The channel equalisation is realised by applying ZF, which are described in Chapter 2. In Figure 3.3, the pilot symbols overhead in each transmission data frame is simulated versus BER performance under two different SNR with 20 dB and 30 dB. It can be clearly obtained that with low pilot block overhead, such as lower than 2% to 3%, the comb type pilot method performs better than that of the proposed Kalman filtering based approach. Comb type pilot estimation employs pilots and inserts them evenly among the source data. With the increasing the number of pilot data, the estimation of Doppler spread is becoming more accurate, and as well as the recovery of source data. Therefore, the BER is linear and stably decreasing with the increasing of pilot overhead. However, if the pilot blocks overhead is larger than 3%, the proposed semi-blind Doppler spread tracking approach can outperform the referenced method and remain steadily better than the pilot aided ICA based scheme while the overhead is larger than 4%. While the proposed pilot based Doppler spread estimation approach is pre-pending the pilot blocks ahead to the source signal frame, the estimation of Doppler spread is not working very well since the pilot number is not enough, e.g., overhead is lower than $2\% \sim 3\%$. After the pilot overhead is larger than 4%, the BER tends to be saturated. The reason is that the number of pilot is enough to obtain the time variant channel information. With 4% pilot overhead, the Doppler spread can be estimated accurately.

The BER performance of the proposed semi-blind OFDM systems is given in Figure 3.4, which is also compared with the comb type pilot aided method. In addition, the MMSE based equalisation with perfect CSI is given for comparison. As it shown in this figure, the ICI caused by Doppler spread can be estimated and gathered into the equivalent system model and eliminated with the equalisation. With different Doppler spread 50 Hz and 300 Hz, the proposed approach can provide better BER performance

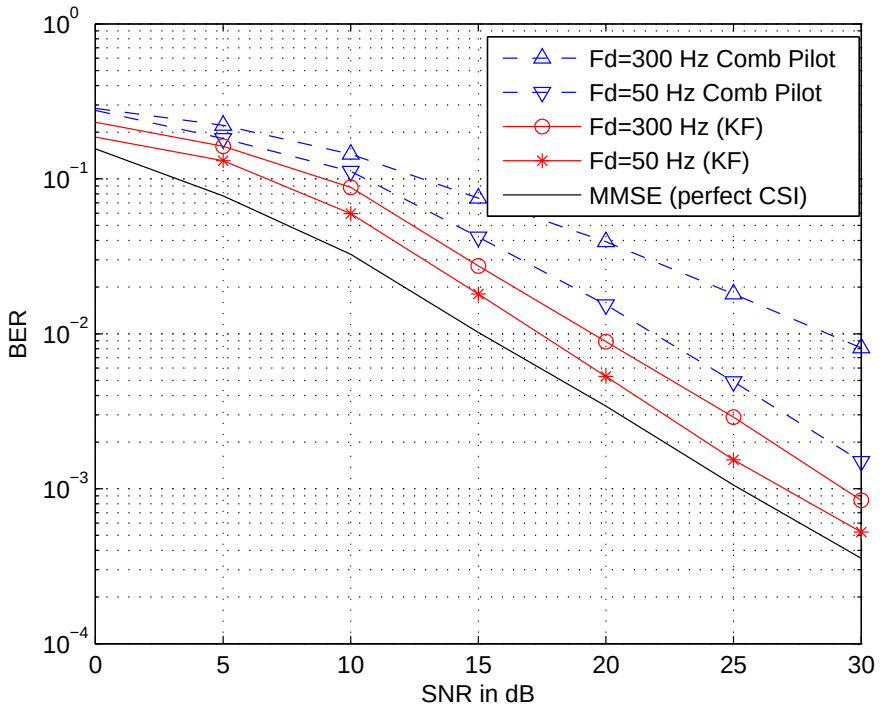

Figure 3.4: BER vs. SNR in dB performance of semi-blind Doppler spread tracking and Kalman filtering based channel estimation of OFDM systems

than the referenced one even with the increase of Doppler spread. Besides, with the same pilot overhead, the proposed approach can also reduce the system computational complexity.

3.7 Summary

In this chapter, a semi-blind Doppler spread tracking and Kalman filtering based channel estimation scheme for OFDM systems is proposed, where a short sequence of reference data are designed and employed as pilot blocks for the transmit data frame. After Doppler spread estimation and ICI compensation, the kalman filtering based method is applied to estimate the CSI.

A set of pilot data sequences are carefully designed and prefixed to the transmitting signal for the following use: it is employed to do Doppler spread estimation by doing cross-correlation between the original pilot and the received pilot blocks. Then the same pilot blocks are employed to initialise the Kalman filtering based channel estimation to

obtain the initial states of the channel estimates.

After the Doppler spread estimation, the ICI can be gathered into the equivalent system model. With the estimates of the channel response, MMSE based equalisation is applied to recover the source data, which can eliminate the ICI together with equalisation.

The simulation results show that the proposed semi-blind Doppler spread tracking and Kalman filtering based channel estimation approach has a high accuracy on the Doppler spread estimation in terms of NMSE. Furthermore, the BER performance of the proposed approach can perform better while the pilot blocks overhead is larger than 3%. Compared with the comb type pilot aided estimation method, the proposed approach can outperform it under different Doppler spread.

However, there are some limitation while employing Kalman filtering based channel estimation. It requires the noise or interference to be Gaussian. If not, a non-linear estimator can provide a better performance than the linear Kalman filtering based approach. The process of finding the best estimates from noisy data amounts to filtering out the noise. If the received signal is in deep fading or contains large ICI, Kalman filter may not clean up all of the interference among subcarriers.

Chapter 4

Precoding Aided Semi-Blind Doppler Spread Estimation and ICA Based Channel Equalisation for MIMO OFDM Systems

4.1 Introduction

MIMO and OFDM are two promising techniques for wireless communication systems, such as LTE. Thanks to the CP, OFDM systems can easily yield high spectral efficiency and mitigate the effects of ISI by making the block period much larger than the delay spread of the channel. Future wireless communication are expected to operate at high transmit frequency with high level of mobility, which suggests the MIMO OFDM systems designs should take into account the Doppler spread associated with time-varying channels. In an OFDM system, the orthogonality among subcarriers can be destroyed by Doppler spread resulting in an intercarrier interference (ICI) [12, 40]. ICI lead to a significant system performance degradation as the carrier frequency, vehicle velocity and block size increase.

A number of approaches have been proposed to eliminate the effect of ICI caused by Doppler spread in OFDM systems. Among the mitigation schemes, pilot-aided estimation methods [79, 80, 81] have been widely applied. However, pilot-aided estimation schemes not only have high computational complexity, but also consume extra transmit power and spectral resources which introduces high spectral overhead. The proposed estimation approach in [79] by applying channel interpolation. It requires two estima-

tion steps and inversion of a large matrix, which leads to a very high computational complexity. Its pilot symbols insertion rate is as high as 10%. In [80], a least-square estimation method based on the domain-transform process was proposed by estimating time-domain channel impulse response with pilot symbols. In [81], a channel estimation method based on distributed compressive sensing theory was proposed by taking advantage of the basis expansion model and the channel sparsity in the time-domain. However, the pilot symbol overhead of the systems in [80] and [81] are 7.1% and 23.4%, respectively.

In this chapter, we propose a semi-blind Doppler spread estimation approach with ICA based equalisation structure for MIMO OFDM systems, without introducing extra transmit power and spectral overhead. A number of reference data sequences, which are carefully designed offline and superimposed onto the source data via a non-redundant linear precoding process, are applied to estimate the Doppler spread and eliminate the phase and permutation ambiguity in ICA equalised signals. Our work is different in the following aspects.

- First, a pool of orthogonal data sequences are carefully designed as the whole reference data. A part of these sequences are selected from the pool to be superimposed onto the source data through precoding process. An optimal Doppler spread can be determined by minimising the summation of cross-correlation between the received signals with the trial normalised Doppler spread compensation and the rest orthogonal sequences of the pool.

- Second, with the same reference data sequences, the phase and permutation ambiguity in the ICA equalised signals can be eliminated by maximising the cross-correlation between the different reference data sequences from each transmit antenna.

- Simulation results show that the proposed semi-blind MIMO OFDM system, with a linear precoding Doppler spread estimation and ICA based equalisation approach, can achieve a BER performance close to the ideal case with perfect CSI. Besides, the proposed semi-blind Doppler spread estimation scheme out-

performs the training based estimation method in [41] without consuming extra transmit power and introducing any spectral overhead in terms of NMSE and BER performance.

In Section 4.2 and 4.3, the system model and precoding design are introduced, respectively. The linear precoding based Doppler spread estimation scheme is presented in Section 4.4. Section 4.5 describes the ICA based equalisation process. After presenting the simulation results in Section 4.6, Section 4.7 provides a summary of this chapter.

4.2 System Model

We consider an MIMO OFDM spatial multiplexing system with N subcarriers, K transmit antennas and M receive antennas. One transmit signal frame consists of P OFDM blocks, while the channel is assumed to remain constant within a block duration. The channel length is L between the k-th transmit antenna and the m-th receive antenna. The channel frequency response matrix is denoted as $\mathbf{H}_{m,k} = diag\{H_{m,k}(0), H_{m,k}(1), ..., H_{m,k}(N-1)\}$, where the entry $H_{m,k}(n)$ represents the channel frequency response element on the n-th subcarrier between the k-th transmit antenna and the m-th receive antenna. Before transmission, a CP with length L_{CP} is prepended to the beginning of each OFDM block, which will be removed at the receiver in order to avoid the ISI.

Let $s_k(n,i)$ denote the symbol on the n-th ($0 \leq n \leq N-1$) subcarrier in the i-th ($0 \leq i \leq P-1$) OFDM block transmitted by the k-th ($0 \leq k \leq K-1$) transmit antenna. Correspondingly, the signal vector in the i-th OFDM block and transmitted by the k-th transmit antenna can be denoted as $\mathbf{s}_k(i) = [s_k(0,i), s_k(1,i), ..., s_k(N-1,i)]^T$. Define an ICI matrix of size $N \times N$ as $\Phi(\phi_i)$ with the entries of $e^{j2\pi\phi_i(q^{'}-q)/N}$ and the normalized Doppler spread of the i-th block $\phi_i = \Delta f_i T_s$. Consequently, the received signal vector $\mathbf{y}_m(i) = [y_m(0,i), y_m(1,i), ..., y_m(N-1,i)]^T$ in the i-th OFDM block at the m-th receive antenna in the frequency domain after CP removal, including ICI, can

be given as

$$\mathbf{y}_m(i) = \sum_{k=0}^{K-1} \mathbf{H}_{m,k}\Phi(\phi_i)\mathbf{s}_k(i) + \mathbf{z}_m(i) \tag{4.1}$$

where $\mathbf{z}_m(i)$ is the AWGN vector whose entries are i.i.d. complex Gaussian random variables with zero mean and variance. Following [12, 41, 40], (4.1) can be written as

$$\mathbf{y}_m(i) = \sum_{k=0}^{K-1} \left[\mathbf{H}^U_{m,k}\mathbf{s}_k(i) + \mathbf{H}^I_{m,k}\mathbf{s}^I_k(i)\right] + \mathbf{z}_m(i) \tag{4.2}$$

where $\mathbf{H}^U_{m,k}$ is the corresponding diagonal channel frequency response matrix and $\mathbf{H}^I_{m,k}\mathbf{s}^I_k(i) = \sum_{q=0,q\neq q'}^{N-1} H^{\phi_i}_{m,k}(q-q')s_k(q-q',i)$ is the ICI term. It can be clearly obtained that the ICI occurs when $H^{\phi_i}_{m,k}(q-q') \neq 0$ for $q \neq q'$. The ICI term vanishes if the channel is assumed to be time-invariant during an OFDM block period.

It is obvious that the normalised Doppler spread ϕ_i introduces the ICI which destroys the orthogonality among subcarriers according to (4.1) and (4.2). In [41, 79, 80, 81], the pilot-aided Doppler spread estimation methods haven been applied. However, these schemes consume lots of transmit power and spectral resources.

4.3 Precoding Design

A number of reference data sequences are carefully designed through a linear precoding process before transmission, which is applied for Doppler spread estimation and ambiguity mitigation in the ICA equalised signals.

4.3.1 Precoding

A number of reference data sequences are superimposed onto the source data sequences through a non-redundant precoding process. Let $\mathbf{d}_k(i) = [d_k(0,i), d_k(1,i), ..., d_k(N-1,i)]^T$ denote the source data vector with length N in the i-th OFDM block transmitted by the k-th transmit antenna. Accordingly, the reference data vector can be written as $\mathbf{d}_{ref,k}(i) = [d_{ref,k}(0,i), d_{ref,k}(1,i), ..., d_{ref,k}(N-1,i)]^T$. The source data and the reference data sequences are assumed to be uncorrelated with each other, while both are supposed to have unit average power. The resulting transmit signal vector $\mathbf{s}_k(i)$ can be expressed as [69]

$$\mathbf{s}_k(i) = \frac{1}{\sqrt{1+a^2}}[\mathbf{d}_k(i) + a\mathbf{d}_{ref,k}(i)] \tag{4.3}$$

where a $(0 \leq a \leq 1)$ is the precoding weight constant which can give a trade off on the transmitted power allocation between source data vector $\mathbf{d}_k(i)$ and the reference data vector $\mathbf{d}_{ref,k}(i)$. A scaling factor $\frac{1}{\sqrt{1+a^2}}$ is employed to keep the signal with unchangeable transmit power.

4.3.2 Reference Data Design

Without requiring extra transmit power and extra bandwidth, the non-redundant reference data sequences are designed offline for two purposes, of which one purpose is to do Doppler spread estimation, and the other is to eliminate the ambiguity in ICA equalised signals. It is can be clearly obtained from Equation (4.3) that the reference data sequences play a significant role during the estimation and mitigation process. Denoting $\mathbf{D}_{ref,k} = [\mathbf{d}_{ref,k}(0), \mathbf{d}_{ref,k}(1), ..., \mathbf{d}_{ref,k}(P-1)]$ be the $N \times P$ reference matrix for the k-th transmit antenna. Let $\mathbf{Q}$ denote as the $U \times P$ projection operator matrix. The precoding based Doppler spread estimation is realised by minimising the sum cross-correlation between the reference data sequences $\mathbf{D}_{ref,k}$ and the projection operator $\mathbf{Q}$. Then the optimal ambiguity elimination in the ICA equalised signals can be realised by maximising the cross-correlation between the reference signals and the ICA equalised signals within different transmit antennas. Therefore, the optimal reference data design is to minimising the cost function, which can be written as

$$\mathbf{E} = \frac{1}{(N^2+NU)(K-1)K} \sum_{k=0}^{K-1} \sum_{l=0, l\neq k}^{L-1} \left(\left\| \mathbf{D}_{ref,k} \mathbf{Q}^H \right\|_F^2 + \left\| \mathbf{D}_{ref,k} \mathbf{D}_{ref,l}^H \right\|_F^2 \right). \quad (4.4)$$

In order to minimise Equation (4.4), the optimal solution is based on the set of reference data sequences that are orthogonal to each other and orthogonal to the projection operator $\mathbf{Q}$. Therefore, the cost function will be $\mathbf{E} = 0$ as $\mathbf{D}_{ref,k}\mathbf{Q}^H = 0$ as well as $\mathbf{D}_{ref,k}\mathbf{D}_{ref,l}^H$ when $(k \neq l)$.

A Hadamard matrix $\mathbf{M}_{had}$ [75, 76] can provide a solution to Equation (4.4), in which any two different rows are orthogonal to each other. A number of K different rows of $\mathbf{M}_{had}$ are randomly selected as the reference data sequences for K transmit antennas. For the k-th transmit antenna's reference data sequences design, the selected row in $\mathbf{M}_{had}$ is placed in each row of $\mathbf{D}_{ref,k}$. Therefore, according to the design of reference

data sequence and the projection operation, the correlation between the reference data sequences and the projection operator can be expressed as

$$\mathbf{D}_{ref,k}\mathbf{Q}^H = 0_{N\times U}, \tag{4.5}$$

and the correlation function between the reference data sequences of antennas k and l is given by

$$\mathbf{D}_{ref,k}\mathbf{D}_{ref,l}^H = \begin{cases} NI_N & \text{if} \quad k = l \\ 0_{N\times N} & \text{if} \quad k \neq l \end{cases} \tag{4.6}$$

From Equation (4.5), the different reference data sequences of K transmit antennas are orthogonal to the projection operator, which allows the Doppler spread estimation to be performed at the receiver. According to Equation (4.6), the reference data sequences of different transmit antennas are orthogonal to each other, which provides an optimal ambiguity elimination in the ICA equalised signals.

4.3.3 Precoding Constant

In Equation (4.3), the range of the precoding constant a varies from 0 to 1, which offers a power allocation trade off between the reference data and the source data. Besides, the variations of the precoding constant have significant impact on NMSE and BER performances. In order to obtain a good Doppler spread estimation in terms of NMSE, a large number of valued percoding constant is preferred, which can improve the reference data power, *i.e.* $|a| \rightarrow 1$. However, under this situation, the transmit power of the source data will decrease, resulting in a degradation of BER performance. If a good BER performance is desired by the system, a smaller value of the precoding consatant is preferred, *i.e.* $|a| \rightarrow 0$. However, this would lead to a worse Doppler spread estimation and ambiguity elimination in the ICA equalised signals, since the power for the reference data could not be preserved. Therefore, a precoding constant must be selected carefully to balance the power between the source data and the reference data, which leads to a good NMSE and BER performances.

In general, a larger sub-block length can provide a smaller optimal precoding constant. At a high SNR and with a properly chosen precoding constant, the unsolved quadrant and permutation ambiguity in the proposed structure has much less effect

than noise on the BER performance. Even the reference data for precoding are designed offline with very little complexity without consuming extra power and spectral resources, it requires power to process the ambiguity elimination at receiver side. However, as an optimal precoding constant a has been chosen to give a trade off of the power between the source data and reference data before transmission, the power consumption of processing at receiver side is reasonable.

4.4 Semi-Blind Doppler Spread Estimation

A semi-blind precoding aided Doppler spread estimation scheme is proposed for MIMO OFDM systems, where a number of carefully designed reference data sequences are superimposed to the source data without consuming extra transmit power. The Doppler spread estimation based on precoding process is realised by applying the cross-correlation between the trial values of normalised Doppler spread compensated received signals and the projection operator. The advantage of the proposed approach has high bandwidth efficiency, since the reference data sequences and the projection operator can be designed offline and known in advance at the receiver, which will not introduce additional training overhead.

With a normalised Doppler spread ϕ_i, the signal vector $\mathbf{s}_k^{\phi_i}(i)$ with the ICI in the i-th OFDM block can expressed as

$$\mathbf{s}_k^{\phi_i}(i) = \Phi(\phi_i)\mathbf{s}_k(i). \tag{4.7}$$

In order to tracking the Doppler spread, a trial value $\tilde{\phi}_i$ of normalised Doppler spread is given. Based on the Equation (4.1) and (4.7), the received signal vector $\tilde{\mathbf{y}}_m i$ can be also given as

$$\tilde{\mathbf{y}}_m(i) = \sum_{k=0}^{K-1} \mathbf{H}_{m,k}\mathbf{s}_k^{(\phi_i - \tilde{\phi}_i)} + \mathbf{z}_m(i). \tag{4.8}$$

Let $\boldsymbol{\beta}_m(i)$ denote as the cross-correlation between the projection operator $\mathbf{Q}$ and the received signal vector $\tilde{\mathbf{y}}_m(i)$ with ICI at the m-th receive antenna. It can be expressed as

$$\boldsymbol{\beta}_m(i) = \mathbf{Q}^H(i)\tilde{\mathbf{y}}_m(i). \tag{4.9}$$

Substituting Equation (4.8) into Equation (4.9) yields

$$\boldsymbol{\beta}_m(i) = \sum_{k=0}^{K-1} \left\{ \frac{\mathbf{H}_{m,k}}{\sqrt{1+a^2}} \left[\mathbf{Q}^H(i) \widetilde{\mathbf{d}}_k^{(\phi_i - \tilde{\phi}_i)}(i) + a\mathbf{Q}^H(i) \widetilde{\mathbf{d}}_{ref,k}^{(\phi_i - \tilde{\phi}_i)}(i) \right] \right\} + \mathbf{Q}^H(i)\mathbf{z}_m(i) \tag{4.10}$$

where the i-th vector of matrix $\mathbf{Q}$ is orthogonal to the reference data sequences in the received data. If the Doppler spread trial value is correctly estimated, the correlation function between the projection operator and the reference data sequences is zero, *i.e.*, $\mathbf{Q}^H(i)\widetilde{\mathbf{d}}_{ref,k}^{(\phi_i - \tilde{\phi}_i)}(i) = 0$. Therefore, the correlation $\boldsymbol{\beta}_m(i)$ between the projection operator and received signals are expressed as

$$\boldsymbol{\beta}_m(i) = \sum_{k=0}^{K-1} \left\{ \frac{\mathbf{H}_{m,k}}{\sqrt{1+a^2}} \left[\mathbf{Q}^H(i) \widetilde{\mathbf{d}}_k^{(\phi_i - \tilde{\phi}_i)}(i) \right] \right\} + \mathbf{Q}^H(i)\mathbf{z}_m(i). \tag{4.11}$$

It can be obtained that the correct normalised Doppler spread can result in a $\boldsymbol{\beta}_m(i)$ with the minimum energy. The high accuracy of the Doppler spread estimation can be performed by minimising the sum cross-correlations from all of the M receive antennas. However, the value of the precoding constant a should be taken into consideration. If a is too small, the energy of $\boldsymbol{\beta}_m(i)$ would be the same as the variations of the trial Doppler spread. In order to reduce this effect, we set a as small as it can be. Besides, a large size of matrix $\mathbf{Q}$ is required, which means that the projection operator should have sufficient data sequences. It can be derived that the correctly estimated $\hat{\phi}_i$ can be obtained by

$$\hat{\phi}_i = \underset{\tilde{\phi}_i \in [0,0.1]}{\arg\min} \left\| \sum_{m=0}^{M-1} \boldsymbol{\beta}_m(i) \right\|_F^2, \tag{4.12}$$

where $\|\cdot\|_F^2$ denotes the Frobenius norm. Since the proposed precoding based Doppler spread estimation approach only needs the information of the reference data sequences at the receiver which can be obtained offline, this scheme can provide higher spectral efficiency than other pilot based Doppler spread estimation methods.

4.5 ICA Based Channel Equalisation

After the Doppler spread estimation, the estimated value of Doppler spread $\hat{\phi}_i$ can be obtained, with which the ICI compensated received signals vector in the i-th block

$\hat{\mathbf{y}}_m(i) = [\hat{y}_m(0,i), \hat{y}_m(0,i), ..., \hat{y}_m(N-1,i)]^T$ can be written as

$$\hat{\mathbf{y}}_m(i) = \Phi^H(\hat{\phi}_i)\mathbf{y}_m(i). \tag{4.13}$$

Assuming perfect Doppler spread estimation and compensation, the received signals vector $\hat{\mathbf{y}}(n,i) = [\hat{y}_0(n,i), \hat{y}_1(n,i), , ..., \hat{y}_{M-1}(n,i)]^T$ in the i-th block on the n-th subcarrier can be given as

$$\hat{\mathbf{y}}(n,i) = \mathbf{H}(n)\mathbf{s}(n,i) + \hat{\mathbf{z}}(n,i), \tag{4.14}$$

where $\mathbf{H}(n) = \left[\mathbf{H}_0^T(n), \mathbf{H}_1^T(n), ..., \mathbf{H}_{K-1}^T(n)\right]^T$ with $\mathbf{H}_k(n) = [H_{0,k}, H_{1,k}, ..., H_{M-1,k}]^T$ is the $M \times K$ channel frequency response matrix between all K transmit antennas and M receive antennas on the n-th subcarrier, $\mathbf{s}(n,i) = [s_0(n,i), s_1(n,i), ..., s_{K-1}(n,i)]^T$ denotes the K transmit signal vector on the n-th subcarrier in the i-th block, and $\hat{\mathbf{z}}(n,i)$ is the noise vector.

4.5.1 JADE Algorithm for Equalisation

ICA [16] is an efficient HOS based BSS technique. It is employed to recover $\mathbf{s}(n,i)$ in Equation (4.14) by maximising the non-Gaussianity of the received signals. Among the ICA numerical algorithms, JADE algorithm [66] is an efficient one which requires shorter data sequences than others. It is applied in this chapter since the received signals are a linear mixture of the transmitted signals on each subcarrier as shown in Equation (4.14). However, there exists a major drawback of the ICA model. The signals equalised by ICA contains phase and permutation ambiguity, which can be resolved by maximising the correlation between the reference data and the ICA equalised data. Denoting $\theta(n) = [\theta_0(n), \theta_1(n), ..., \theta_{K-1}(n)]$ as the permuted order in the ICA separated signals on the n-th subcarrier. The ICA equalised signals vector $\tilde{\mathbf{s}}(n,i) = \left[\tilde{s}_{\theta_0(n)}(n,i), \tilde{s}_{\theta_1(n)}(n,i), ..., \tilde{s}_{\theta_{K-1}(n)}(n,i)\right]^T$ is given by

$$\tilde{\mathbf{s}}(n,i) = \mathbf{L}(n)\mathbf{P}(n)\mathbf{B}(n)\mathbf{s}(n,i) \tag{4.15}$$

where $\mathbf{L}(n)$ denotes the phase deviation matrix, $\mathbf{P}(n)$ is the permutation ambiguity matrix and $\mathbf{B}(n)$ is the phase ambiguity matrix.

4.5.2 Ambiguity Elimination

The phase deviation in $\tilde{\mathbf{s}}(n,i)$ can be resolved by de-rotating the phase of each data stream. Then the signal vector $\check{\mathbf{s}}(n,i) = \left[\check{s}_{\theta_0(n)}(n,i), \check{s}_{\theta_1(n)}(n,i), ..., \check{s}_{\theta_{K-1}(n)}(n,i)\right]^T$ can be obtained as

$$\check{\mathbf{s}}(n,i) = \mathbf{L}^{-1}(n)\tilde{\mathbf{s}}(n,i), \tag{4.16}$$

where $\mathbf{L}^{-1}(n) = diag\left\{\frac{\delta_{\theta_0(n)}(n)}{|\delta_{\theta_0(n)}(n)|}, \frac{\delta_{\theta_1(n)}(n)}{|\delta_{\theta_1(n)}(n)|}, ..., \frac{\delta_{\theta_{K-1}(n)}(n)}{|\delta_{\theta_{K-1}(n)}(n)|}\right\}$ denotes the de-rotation matrix, with the de-rotation factor for QPSK modulation $\delta_{\theta_k(n)}(n)$ being

$$\delta_{\theta_k(n)}(n) = \left\{\frac{1}{P}\sum_{i=0}^{P-1}\left[\tilde{s}_{\theta_k(n)}(n,i)\right]^4\right\}^{-\frac{1}{4}} e^{j\frac{\pi}{4}}, \tag{4.17}$$

where the de-rotation factor can be obtained from the statistics of the ICA equalised signals with the QPSK modulation [50, 69].

The cross-correlation between the reference data sequences and the $\theta_k(n)$-th ICA separated substream on the n-th subcarrier of the k-th transmit antenna over a number of P block can be defined as

$$\rho_{\theta_k(n),k}(n) = \frac{1}{P}\sum_{i=0}^{P-1}\check{\mathbf{s}}_{\theta_k(n)}(n,i)\mathbf{d}^*_{ref,k}(n,i). \tag{4.18}$$

Based on the design of the reference data sequences, the cross-correlation between different reference data sequences of K transmit antennas is minimised, to make sure that the different reference data sequences are orthogonal to each other. This design provides an optimal solution to tracking the correct order $\theta_k^{cor}(n)$ by maximising the correlation $\rho_{\theta_k(n),k}(n)$ between the ICA equalised signals and the reference signals on the n-th subcarrier as

$$\theta_k^{cor}(n) = \arg\max_{\theta_k(n)}\left|\rho_{\theta_k(n),k}(n)\right|. \tag{4.19}$$

After reordering, the correlation $\rho_{\theta_k(n),k}(n)$ can be applied again to eliminate the phase ambiguity in the equalised signals. Therefore, the estimate of the transmitted signals can be expressed as

$$\bar{\mathbf{s}}(n,i) = [\mathbf{B}(n)]^{-1}[\mathbf{s}_{\theta_0^{cor}(n)}(n,i), ..., \mathbf{s}_{\theta_{K-1}^{cor}(n)}(n,i)]^T, \tag{4.20}$$

where $\mathbf{B}(n)$ denotes the diagonal phase ambiguity matrix, with the entry $b_{\theta_k^{cor}(n)}(n)$ for QPSK modulation being as

$$b_{\theta_k^{cor}(n)}(n) = \left[e^{-j\frac{\pi}{4}} sign\left(\frac{\rho_{\theta_k(n),k}(n)}{\left|\rho_{\theta_k(n),k}(n)\right|} e^{j\frac{\pi}{4}} \right) \right]^{-1}. \tag{4.21}$$

4.6 Simulation Results

The performance of the proposed semi-blind precoding aided Doppler spread estiation scheme and ICA based equalisation structure for MIMO OFDM systems is demonstrated by the simulation results. We apply $N = 64$ subcarriers, $K = 2$ transmit antennas and $M = 2$ receive antennas. A CP of length $L_{CP} = 16$ is applied to each OFDM symbol. The Clarke's block fading channel model [1] is employed, where the CSI remains constant during one block. Each transmit signal frame consists of $P = 256$ OFDM blocks with QPSK modulation. The precoding constant is set as $a = 0.3$. The carrier frequency is $f_c = 2.4\ GHz$. A number of $U = 64$ sequences are selected from the Hadamard matrix to form the projection operator $\mathbf{Q}$. Two Doppler spread frequencies with $f_d = 50\ Hz$ and $f_d = 300\ Hz$ have been chosen to test the system performance.

Figure 4.1 shows the NMSE between the true and estimated Doppler spread, which can be defined as

$$NMSE = \frac{1}{P} E\left\{ \sum_{i=1}^{P} \frac{\left\| \hat{\phi}_i - \phi_i \right\|^2}{\left\| \phi_i \right\|^2} \right\}, \tag{4.22}$$

where $E\{\cdot\}$ denotes the expectation. The performance of the proposed semi-blind Doppler spread estimation method is shown in this figure, where a training based estimation scheme [41] is employed for comparison. Under the two different Doppler spread $f_d = 50\ Hz$ and $f_d = 300\ Hz$, it can be clearly obtained that the the precoding based Doppler spread estimation can provide better NMSE performance than the training based method, especially at large Doppler shift at high mobility.

The BER performance of the proposed semi-blind MIMO OFDM systems is given in Figure 4.2, which is also compared with the training based estimation scheme in [41]. In addition, the MMSE based equalisation with perfect CSI is given for comparison. As it shown in this figure, the ICI caused by Doppler spread degrades the systems per-

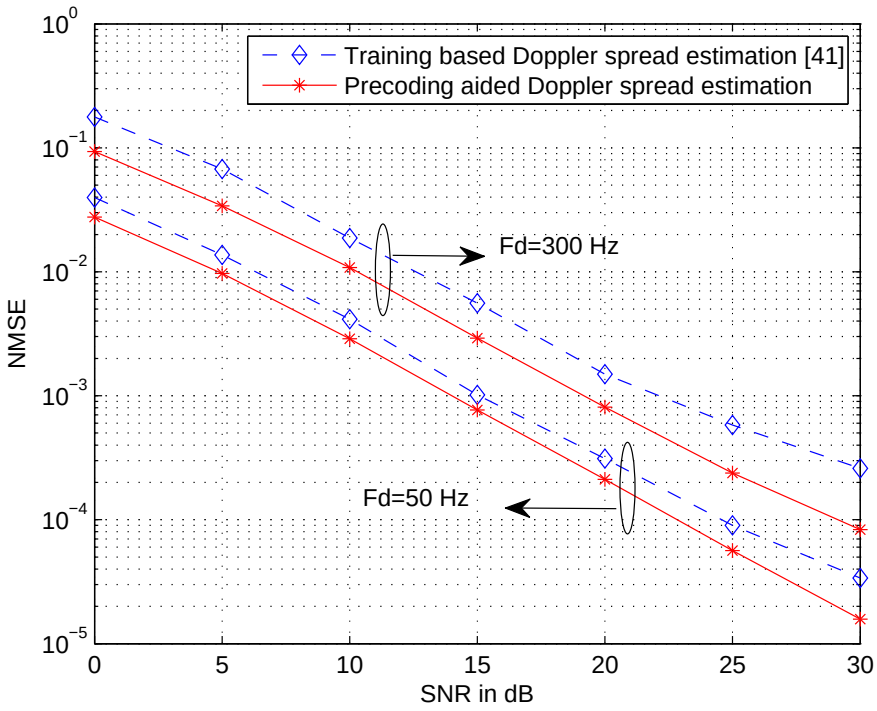

Figure 4.1: NMSE performance of the proposed semi-blind Doppler spread estimation in MIMO OFDM systems

formance severely if it is not compensated properly. The space between two subcarriers is 1.5 KHz, which results in an bandwidth of 96 KHz. Therefore, a Doppler spread of (300 Hz) can affect the subcarriers with ignorable interference, which lead to an error floor. If not be compensated, the system performance is bad, which is demonstrated as the ICA-only lines in the figure. Under low mobility with Doppler spread is 50 Hz, the proposed compensation approach can provide a BER performance which is close to the perfect case of MMSE equalisation and better than that of the referenced pilot-aided compensation method. With the increasing of the Doppler spread (300 Hz), the ICI becomes worse and the orthogonality among subcarriers is destroyed severely. The proposed precoding compensation approach can also outperform than the referenced method in [41] by obtaining much better BER. The proposed semi-blind Doppler spread estimation and ICA based equalisation approach has a high efficiency without introducing extra transmit power and consuming extra spectral resources, while the training based method requires a number of pilot symbol with an overhead of 4.4%.

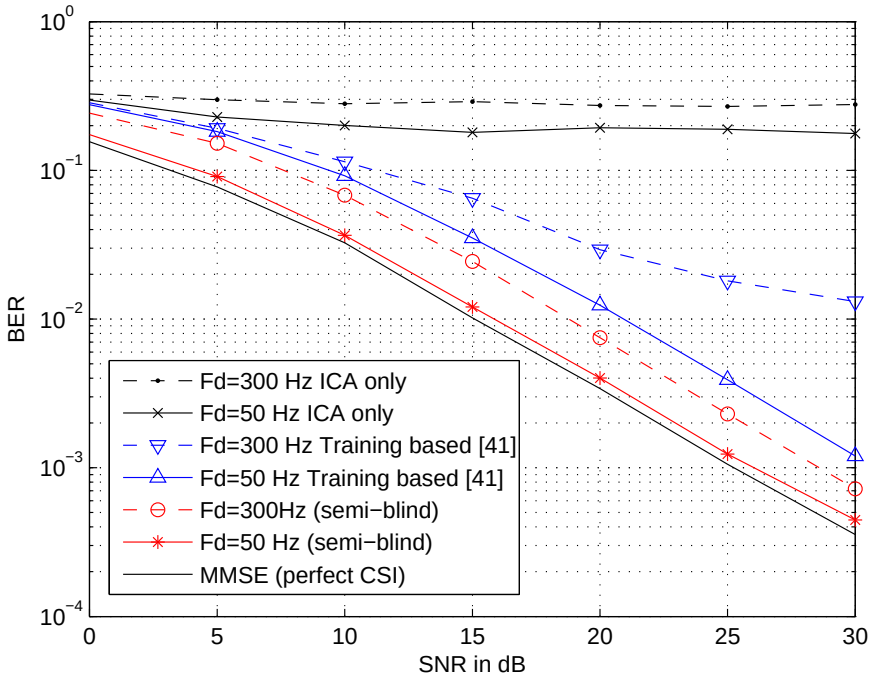

Figure 4.2: BER vs. SNR in dB performance of semi-blind Doppler spread estimation and ICA based equalization of MIMO OFDM systems

4.7 Summary

In this chapter, a semi-blind Doppler spread estimation and ICA based equalisation method for MIMO OFDM systems is proposed, where a number of reference data sequences are designed offline and superimposed into the source data sequences through a non-redundant linear precoding process before transmission, without additional transmit power and spectral resources consumption. The receiver only requires the knowledge of the reference data sequences, which can be process offline.

The reference data sequences are carefully designed offline for two purposes: Doppler spread estimation and ambiguity elimination in the ICA equalised signals. A cost function is formed for the referenced data sequences and the projection operator, which can be obtained from the Hadamard matrix by minimising the cost function. Then, the precoding constant introduced in the precoding process is discussed, while it can give a power trade-off between the source data and the reference data without introducing additional transmit power.

At the receiver, the Doppler spread estimation can be realised by the sum of cross-correlation between the reference data sequences and the projection operator. The projection operator is formed by a number of data sequences which are selected from the reference data. In the traditional Doppler estimation and ICI elimination methods, such as [79, 80, 81], which require high complexity as well as high pilot symbol overhead, the proposed semi-blind precoding based Doppler spread estimation method requires only the reference data sequences which are designed offline. Therefore, it can ensure a lower complexity and higher power efficiency.

After Doppler spread estimation and ICI compensation, ICA equalisation is employed at the receiver on each subcarrier. However, there exit permutation and phase ambiguity in the ICA equalised signals. By applying the offline designed reference data sequences, the cross-correlation between different reference sequences of transmit antennas is minimised so that the different sequences are orthogonal to each other. Then the optimal solution to eliminate the permutation and ambiguity is realised by maximising the correlation between the ICA equalised signals and the reference signals. Besides, the correlation can also be employed on each subcarrier for phase ambiguity elimination.

Chapter 5

Verification of Semi-Blind OFDM Receiver Structures over the Air

In order to investigate the OFDM wireless communication systems and verify different receiver structures performance in real-time, a wireless communication test-bed is developed and implemented on the Agilent wireless vector signal generator and vector signal analyser with a pair of antennas. Several equalisation approaches are tested through this platform under different wireless environments including Reverberation chamber and room. Two efficient receiver structures are applied and validated through this real-time test-bed.

5.1 Wireless Communication Testbed

5.1.1 System Requirement

In this subsection, the system requirement of the platform will be presented, including the introduction of the equipments. It is established to realise the connection between computer and the two instruments which are Vector Signal Generator (VSG) and Vector Signal Analyser (VSA). VSG is wireless signal transmitter while VSA is the wireless signal receiver. The computer can control the instruments through the controlling software so that the communication (sending and receiving data) between computer and the instruments can be performed.

I. Hardware

- RF Vector Signal Generator: Keighley® 2920/Agilent

As the wireless signal transmitter, the model type of the RF VSG is Keithley 2920/Agilent (V2920A RF). It is designed as a mid-performance measurement and test instrument for Research & Development. It is also regarded as a valuable modern RF communications devices and equipment. In order to generate excellent repeatable and high accurate RF test signals, this next-generation equipment is aided with digital signal processing (DSP) and state-of-the-art RF technology. It can be switched on frequencies, amplitude and modulation types with rapid transfer function speed. Furthermore, V2920A can also make it simple to test the wireless communication devices, such as mobile phones, economically by generating data sequences compatible with a series of communication standards. With the increasing number of applications in the mobile phones, the connection between mobile phones and other equipments is becoming a common phenomenon. Therefore, it is quite necessary to integrate more wireless standards into the device.

The signal generation accuracy is over a wide ranges. The frequency and output power ranges from 10 MHz to 6 GHz and -125 dBm to $+13$ dBm, respectively. It also has a broad operating flexibility with 80 MHz bandwidth and 100 megasample Arbitrary waveform. The waveforms will be first downloaded and then processed with the high speed DSP in the arbitrary waveform generator memory. By employing this approach, the RF signal can be defined by the software in terms of I-Q data of the waveform. The ARB is considered as a larger memory which can store multiple waveforms. Finally, V2920A can be switched between different waveforms by rapid DSP.

- Vector Signal Analyser: Keighley 2820/Agilent.

  As the wireless signal receiver, the model type of the RF VSA is Keithley 2820/Agilent (V2820A RF). The Model of 2820ss digital signal processing based software defined radio (SDR) architecture and 40 MHz bandwidth to make sure that it has the capability to measure signals and also the flexibility to handle signals in the future. The VSA has a superior performance with 40 MHz to 6 GHz frequency

range while the measurement input power can be ranged from $-146\ dBm$ to $+35\ GHz$. In order to have a high accuracy, the absolute amplitude is $\pm 0.6\ dB$. It also has 650 MHz/s at 1 kHz bandwidth characteristic spectrum analysis sweep update rate and 30 ms characteristic signal analysis personality switching time.

The VSA has three powerful operating modes which are spectrum analyser mode, vector signal analysis mode and signal capture mode. For the mode of signal analysis, the VSA is designed to be combined with a number of personality options on signal analysis for testing to the common wireless standards, such as 802.16e mobile-WiMAX, 802.11 WLAN, W-CDMA FDD, EDGE and GSM. While capturing the signal, the VSA can receive RF signals of up to 40 MHz bandwidth and store them in its 32 megasample waveform memory as I-Q data pairs. A record of waveform with time duration up to 30 sec. can be captured at a one ms/sec sampling rate. Besides, the I-Q data can be uploaded to a PC through the USB or LAN interfaces for analysis or to playback with an RF VSA. The signal waveform can be analysed with PC-based software such as MATLAB. Under the spectrum analyser mode, the VSA has four multiple-purpose spectrum analysis functions for measuring the most common signal parameters of RF signals, which will be discussed in the following in detail.

1. The function of spectrum analysis can display the RF power vs. frequency of all signals within a user-defined frequency span. The signal spectrum features can be analysed under this mode by selecting the filter types and bandwidth resolution. Furthermore, the RF signal characteristics and parameters can be measured by employing the traditional markers functions.
2. The ACPR (Adjacent Channel Power Ratio) function can measure the channel power of the primary signal along with that of the next two adjacent channels. The adjacent channels, test limits, channel bandwidth and channel frequency are user-definable. Each channel power and spectral parameters of frequency is measured separately with a high accuracy.

3. The channel power list function allows setting up a pre-defined list of frequencies, measurement times and measurement bandwidths.

4. By utilising the zero span function, the analyser can be used and considered as a fixed-turned receiver to capture and analyse signals up to 40 MHz bandwidth at a fixed carrier frequency. The RF signal is demodulated and the signal power vs. time is displayed. A wide range of selection on filter types and bandwidth are available. An assortment of triggers, which is easily applied, could also be utilised to capture the wireless data sequences.

- A pair of wireless antennas with central frequency at 2.4 GHz.

  A pair of antennas operating at 2.4 GHz central frequency are applied in this program. The antennas are designed with a dual-feed Planar Inverted-F [82] for wireless communication systems at 2.4 GHz. The design of this pair of antennas has innovation that it contains only one radiating plate with a pair of matched and isolated port in order to reduce the mutual coupling and achieving a good isolation.

  If the two ports of the antenna elements are strongly enough coupled then the transmitted signal of one port will not be radiated and most of the signal will be absorbed by the second port. So for the two ports to radiate efficiently, they should be highly isolated and mutual coupling should be reduced to enable the two ports to radiate efficiently. The pair of antennas [82] employed in this thesis have two ports that are noticeably coupled through the ground plane in order to decrease the mutual coupling between the two ports and to enhance the isolation. This pair of antennas can cover 2.45 GHz WLAN band from 2.35 GHz to 2.55 GHz and can be utilised in mobile communication systems.

- A computer to which the instruments to be linked and controlled from.

  A computer or PC is needed with the driving and control software inside. In order to connect and control the communication and process the wireless data in the system, all of the software should be installed into the PC. Also, the initialisation and parameters setting before transmission is done through PC based on these

Figure 5.1: The real-time wireless communication systems test-bed

software platform.

- An Ethernet/LAN box having at least three sockets.

  An ethernet router is required in order to physically connect the PC, VSG and VSA. The PC can detect both of the transmitter and receiver through IP address while communication.

- Three Ethernet/LAN cables that can connect PC and the two instruments through the ethernet router.

II. Software

- Two software are required to be download from the equipment official website under the section of "Shared Component". The software names are "IviShared-Components" and "IviVisaSharedComponents". The respective software can be downloaded based on the 32-bit or 64-bit systems. Here in our system, we selected

the later version since the PC is a 64-bit control system. Another requirement should be noticed that these two software need to be installed before the installation of MATLAB and IVI instrument drivers which should be installed on the well developed platform. A user guide can also be downloaded from this wevsite with the title of "Using IVI with MATLAB" in which the introduction and guidance can be found.

- MATLAB® software with the version of 2009 or newer is required in order to apply it with IVI instruments drivers.

- IVI instrument driver of the specific instrument is to be downloaded from its respective website or from CD of the instrument. Here we have downloaded the IVI instrument drivers from the Agilent official website.

- The latest version of "Agilent IO Libraries Suit" to be downloaded from Agilent official website. The version that has been applying in this project is updated.

5.1.2 System Setup

1. The software of "IviSharedComponents" and "IviVisaSharedComponents" are installed on the PC. Then the IVI instrument drivers of the VSG and VSA are installed on the PC. After that, the MATLAB of version 2011 is installed on the PC. The MATLAB must contain the instrument control toolbox which is used to connect and control the instruments through software. Finally, the "Agilent IO Libraries Suite" is installed on the PC.

2. The 2.4 GHz antennas are connected to VSG and VSA, respectively with cables. Then they are fixed with two separate stable station in order to get steady signal while transmitting and receiving data.

3. The two instruments, VSG and VSA, should be physically connected to the PC through the Ethernet/LAN router with cables. Turn on all of the instruments. Then detecting the instruments through PC. Opening the Agilent IO window, the two instruments, VSG and VSA, can be detected through TCPIP address

and added into the IO control window. If these two instruments are connected to the PC well, then connection should be done and smoothly.

4. This step is to connect/interface the instrument to MATLAB through the PC so that the instruments may be controlled from MATLAB. Then the device and interface objects should be created. The instruments can be connected to the MATLAB by utilising either of these objects. However, the interface objects are used to send the data from the MATLAB to the instrument or to receive the data in MATLAB from the instrument whereas the device objects are used to change different properties of the instrument and perform different functions in the instruments through MATLAB.

5. The final real-time wireless communication system test-bed is shown in Figure 5.1.

Communication between PC and Instruments

In this subsection, the communication method between MATLAB in the PC and the instruments is described, which is used as the main communicating method of this project.

The TCP interface objects of both instruments VSG and VSA are firstly required and created. The creation of the TCP interface objects command can be expressed as

$$tcpobj = tcpip(\text{`}192.168.0.101', 5025), \tag{5.1}$$

where 'tcpobj' is the variable name of the TCP interface object, '192.168.0.101' is the TCP address of the instrument V2920A taken from "Agilent Connection Expert" and '5025' is the socket no of the instrument. The instrument can be connected and disconnected to the MATLAB using this interface object with the following commands in the command window

$$fopen(tcpobj);\ fclose(tcpobj). \tag{5.2}$$

From now onward, The communication can be processed directly between MATLAB and the instruments through the LAN interface.

Sending IQ data using MATLAB

- A MATLAB script named "SenData.m" is used for this purpose. The inputs are the IQ data sequences with the sample rate in Mega-sample-per-second (Msps).
- The IQ data is a vector of numbers according to the desired modulation scheme. If BPSK is used, then IQ data is a real vector while it is a complex vector if QPSK or QAM is applied. The IQ data is a time based description of the data which should have an even amount of numbers. If not, an error message occurs in the VSG while transmitting data. Before sending the data to the VSG, the data has to be ready up-sampled, pulse shaped, IFFT if it is OFDM. The IQ data sequence is the final data exactly how the VSG transmit in the time domain.
- The "samplerate" in the sending IQ data command is in Mega-sample per second (Msps) which is specified for the signal Miester® software. There are specific values that can be taken. If an arbitrary sample rate is imputed, it will be automatically allocated to the nearest allowed value. However, this mechanism is not very beneficial since the data would be up-sampled by the machine and might not be able to down-sampled accordingly after the IQ data extraction. In order to obtain an real-time accurate communication on this platform, a sample rate should be selected carefully.

Extracting IQ data using MATLAB

- Another script named "GetData.m" is used to extract the IQ data from the VSA. The input variables are the output data from VSG convoluted with wireless channel which added with Gaussian Noise.
- The variable is used to tune the extraction parameters, so that the appropriate part of the IQ data can be extracted appropriately.
- The extracting process is based the received time-domain IQ data sequence. It might be oversampled since the VSA extracts data at a minimum of $\frac{5}{4}$ of its input. However, if the setting is carefully modified, the extracted data would be the same

Figure 5.2: The Reverberation chamber at the University of Liverpool

rate as was in-putted. The approach that has been taken is to oversample the data manually before transmitting with VSG; then a filter bandwidth is setted to $\frac{4}{5}$ times the value of the input sample rate data. Under this way, the extracted data is the same rate as the data that was transmitted.

- Another parameter called out-sample-rate is applied by the VSA to extract the received data. It can be used to determine the down-sampling ratio if the technique in the preceding point is used used.

- This getting data script is well commented and is easy to follow. When a large amount of IQ data is being extracted, the value of the pause has to be increased to allow the data to settle in the VSA.

5.1.3 Experimental Environments

- Reverberation Chamber

  Reverberation chambers (RC) was originally introduced environment for electro-

magnetic compatibility measurements and other electromagnetic investigations [83, 84]. The RC is designed as a screened room with minimum of absorption of electromagnetic energy. One or more rotational stirrers are employed to reduce the inhomogeneity. The RC at the University of Liverpool as showed in Figure 5.2 is a large metal chamber with size of $(5.8 \times 3.6 \times 4)\ m^3$, where two metal stirrers are setted inside it.

- Office Area

  Another measurement environment to verify the receiver structure in this thesis is normal office area. The lab of our working placing is chosen as the measurement place.

5.2 Verification of Precoding Aided ICA Based Equalisation

In this section, the precoding aided ICA based equalisation approach is verified in real-time wireless communication channels by applying a testbed which consists of a pair of Keithley signal generator and signal receiver connected to a pair of antennas. First, We evaluate the system performance in practical environment and compare the measured results with simulated results. Second, the reference data sequences formed by constant amplitude zero autocorrelation (CAZAC) sequences for time synchronisation in order to compensate the transmit and receive time mismatch. It shows that this semi-blind ICA based equalisation scheme can perform well with the measurement results close to the simulated results. Since there is only one signal transmitter and one receiver, the system can be performed through SISO systems.

5.2.1 Measurement Setup

The transmit antenna of V2920A transmits one signal frame each transmission time span. Before transmission, a CAZAC sequence data is pre-fixed ahead to the each frame, which will help to do the time synchronisation at the receiver through cross-correlation between the CAZAC sequence data and received data with time delay. By searching for the maximum value of the correlation results, the starting point of the

received frame can be determined. The system model of precoding aided ICA based channel equalisation approach can be found in Chapter 4. Since the measurement is processed in the real-time wireless communication environment, the channel cannot designed in advance.

After synchronisation detection, the initial start point of the received frame can be determined. The next step is doing semi-blind ICA based equalisation. The process and function equations are as same as in the previous section while there is only one transmit antenna and one receive antenna.

We employ the real-time wireless communication test-bed to realise the semi-blind precoding aided ICA based equalisation approach in room environment. We apply $N = 512$ subcarriers and CP of length $L_{CP} = 64$. Each transmit signal frame consists of $P = 256$ OFDM blocks with QPSK modulation. The carrier frequency is $f_c = 2.4\,GHz$.

5.2.2 Measurement Results

Since the measurement is implemented in real-time, the condition indoors especially the multipath channel is always changing, which can lead to some parameters variable. So the precoding constant a is tested in a range of $(0 \leq a \leq 0.5)$ in order to find out the optimal trade off between the source data and reference data sequences. The room temperature is 17°C, and the transmit power is set as 0 dBm (1 mW). Then the calculated SNR in dB can be obtained [2] approximately as 30 dB. The measurement result is shown in Figure 5.3 which provides a BER performance which is close to the optimal case with simulated one. Under the measurement parameters at that time, the optimal precoding constant $a = 0.36$ is determined.

In Figure 5.4, the BER performance with increasing SNR in dB was provided from the measurement. The precoding constant is set as $a = 0.36$. By comparing the measured result and simulated result with ZF and MMSE equalisation, we can obtain that the precoding aided ICA based equalisation approach can provide similar BER with that of ZF, which is better than the training data aided scheme. Therefore, the ICA based equalisation can provide a good trade off between system complexity and bandwidth efficiency.

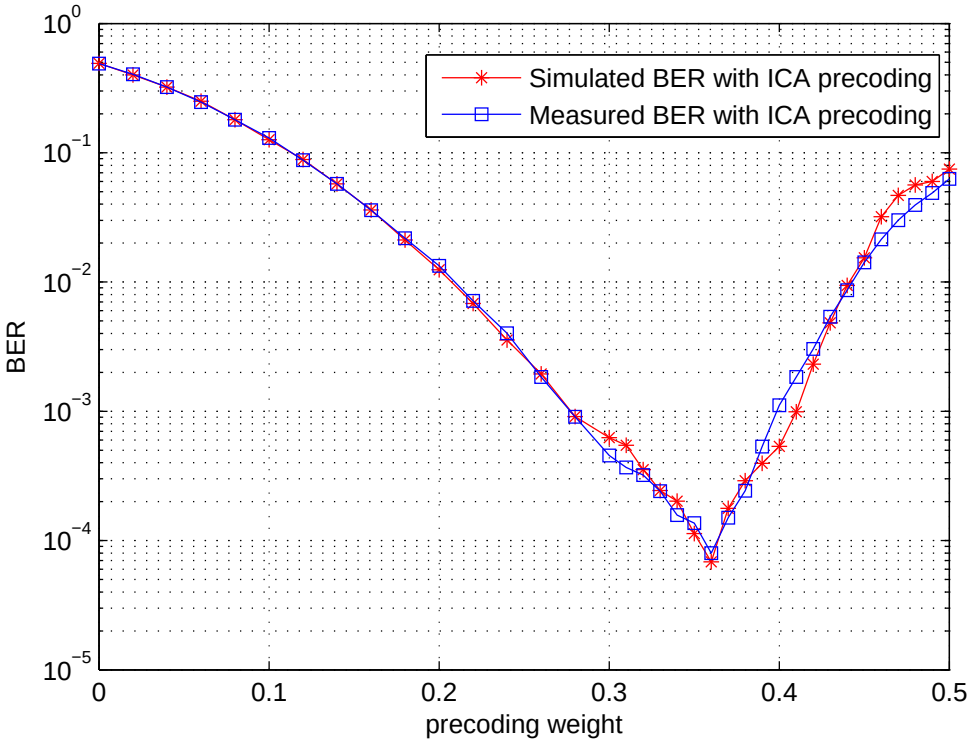

Figure 5.3: BER vs. precoding constant in room with SNR (dB)=30 dB

Besides the precoding constant a, the frame length is another parameter which can affect the ICA based equalisation performance. Figure 5.5 demonstrates the measured BER performance with different frame length. It can be obtained that with longer frame length, the precoding aided ICA based equalisation approach can provide better performance in terms of BER. If the frame size is larger than 128, the effect from the different frame lengths will become stable. As it discussed in the previous chapter, a larger frame size requires a smaller precoding constant a, which leads to a higher power allocation on the source data and lower power allocation on the reference data. A higher SNR can provide a lower BER performance of the system. While the frame size is larger than 128, the recovery of source after equalisation is reaching to the optimised point. That is why the BER performance tends to be saturated when the frame length is larger than 128.

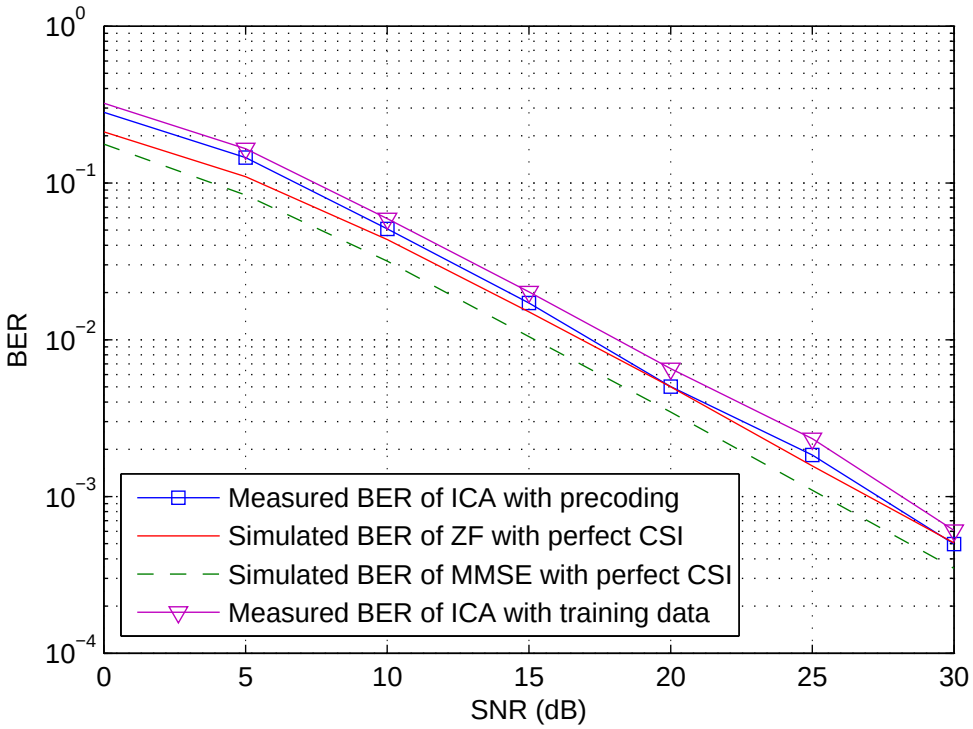

Figure 5.4: BER vs. SNR (dB) in room area with precoding constant $a = 0.36$

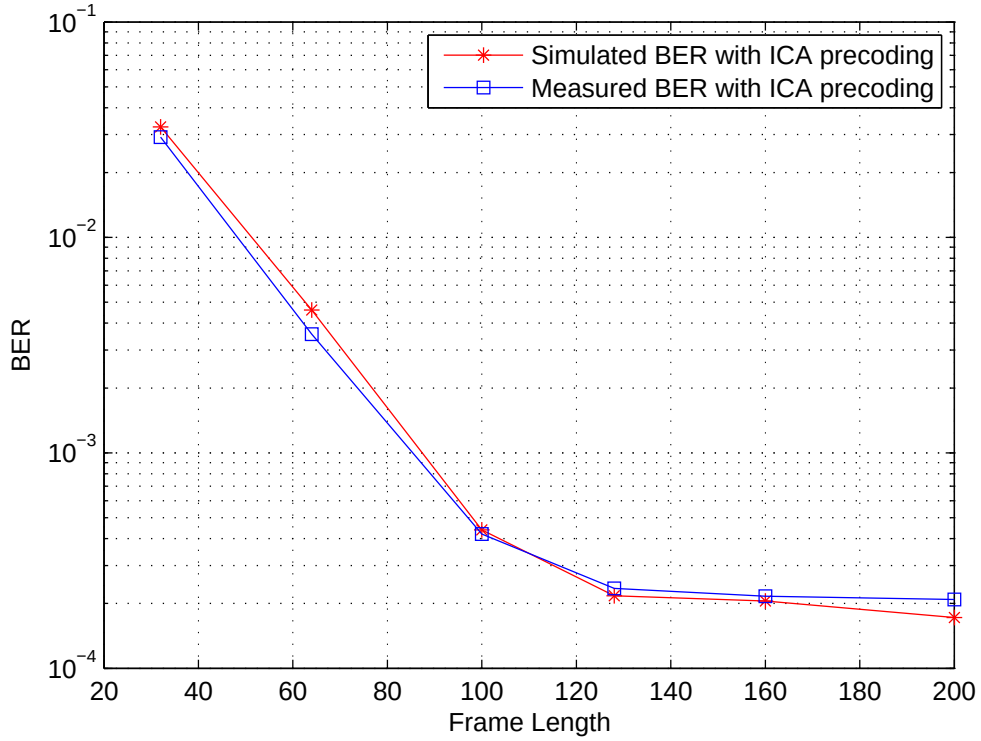

Figure 5.5: BER vs. frame length in room area with $a = 0.36$, SNR (dB)=30 dB

5.3 Verification of Semi-Blind Doppler Spread Estimation and Kalman Filtering Based Channel Estimation

In this section, the semi-blind Doppler spread tracking and Kalman filtering based channel estimation approach is verified through the developed real-time wireless communication platform. A short sequences of reference data is carefully designed and employed as the pilot blocks of the transmit data frame for multiple use: time synchronisation, Doppler spread estimation and Kalman filtering channel estimation initialisation. A electrical fan with different rotational speed is used to modulate a time varying channel. The signal analyser (V2820A) is employed to obtained the received signal spectrum and frequency shift range. The results from the direct measurement with the equipments are compared with the simulate-measurement results. Two measurement environments are applied, which are room and Reverberation chamber.

5.3.1 Measurement Setup

Before transmission, a sequence of pilot signals are prefixed ahead to the information signal blocks. At the receive side, a sample of time domain received frame structure can be given as it shown in Figure 5.6. Because the real time wireless communication systems platform is totally based on the two equipments, the received signal frame may contain some redundant head and tails. In the received frame frame, block D and T means multipath delay and received redundant tails samples, respectively.

The Vector Signal Generator (VSG) V2920A and Vector Signal Analyser (VSA) V2820A are applied as the transmit and receive instrument, respectively. Accompanied with a pair of antennas on the central frequency at 2.4 GHz, the system can be operated and monitored through PC with the control panel software on it.

5.3.2 Measurement Results

In this subsection, some measurement results are used to demonstrate the performance of the proposed pilot based Kalman filtering channel estimation and MMSE equalisation scheme for OFDM systems.

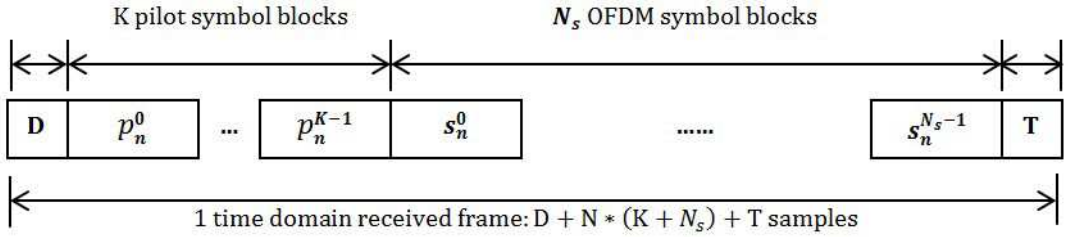

Figure 5.6: Time domain received signal frame structure

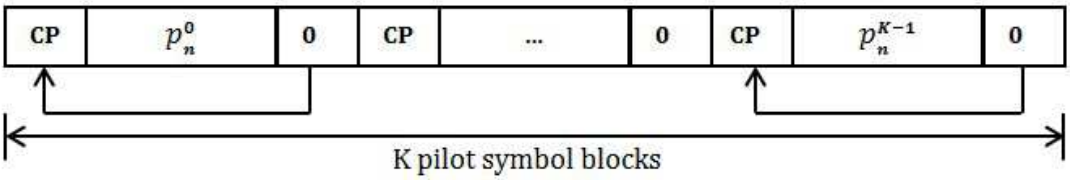

Figure 5.7: Proposed pilot structure with nulled CP

Time Synchronisation

A pilot sequence with length of K is designed for each frame that to be transmitted. In this program, the pilot is applied to do time synchronisation, determine Doppler shift under specific Fan speed and the initialisation of the channel estimation with Kalman filtering method. With a reasonable low overhead ($3.5\% - 5\%$) of the pilot blocks among the transmitted signal frame, it can be multi-used. In order to avoid the interference (ICI) between frequency bins, which is caused by CFO that leads to phase shift of CP, all of the CP in pilot blocks are nulled to zero as well as the last L_{CP} symbols of each block. The structure of pilot with length of K blocks is shown as in Figure 5.7. The pilot design scheme can be found in Chapter 3.

After receiving the signal sequence, the first step is to do time domain synchronisation in order to find out the initial point by doing cross-correlation between pilot blocks and the front-end or half-front-end frame (larger than the pilot overhead rate among the frame length) in order to find out the maximum value. After comparison, the sample point with index would be the determined start of the actual frame, which can eliminate the multipath delayed sequence.

After time synchronisation, the initial sample point of the received frame is determined; also the redundant received tailing samples are eliminated. Then the received

Figure 5.8: Electrical fan speed test with different speed

pilot blocks are used to obtain the Doppler spectrum which will determine the exact Doppler shift under different relevant speed between the transmitter and receiver. From the spectrum, the Doppler shift frequency f_d under specific speed will be determined when an appropriate threshold is chosen.

Electrical Fan Speed Measurement

The Doppler shift can be modelled by applying an electrical fan and determined through the received signal spectrum in frequency domain. We set a LED light at the outer edge of the fan, and put it in a dark room while rotating it. The outer edge angle speed of the fan can be measured by setting the camera shutter duration as a certain value and taking picture in order to track the light radian during this shutter period.

Based on the general analytical maximum Doppler shift with the outer edge of the electrical fan was calculated as follows

$$v = 2\pi r \frac{\alpha}{360}, \tag{5.3}$$

where r is the rotational radium of the fan, and α is the angle speed of the electrical fan which is measured by the camera. Then the maximum linear Doppler shift can be determined by Equation (2.10), where c is the wave speed with equals to $3 \times 10^8\ m/s$, and f_c is the carrier frequency of the wave which is $2.4\ GHz$. Three measured rotational fan pictures with different speed are shown in Figure 5.8.

In order to determine the wireless channel characteristic, the coherence time should be calculated can compared with the transmitted signal period. Two major calculating

Table 5.1: Electrical Fan Speed Measurement Results and Coherence Time Calculation

Speed	Speed 1 (Low)	Speed 2 (Medium)	Speed 3 (Fast)
Measured Angle 1 (Degree)	215.5	242.0	304.5
Measured Angle 2 (Degree)	213.5	243.0	308.5
Measured Angle 3 (Degree)	213.5	242.5	313.0
Averaged Angle (Degree)	214.2	242.7	308.8
Fan Radius (m)	0.2		
Shutter Speed (sec)	0.05		
Linear Speed (m/s)	15.0	17.0	21.5
Calculated Doppler Shift (Hz)	119.6	135.5	172.5
Coherence Time-Rapp. (ms)	3.5	3.1	2.5
Coherence Time-Clks. (ms)	1.5	1.3	1.0

model of the coherence time have been widely used. Both of the two schemes can be expressed as the following equations.

- Rappaport Model

$$T_c = \frac{1}{f_d}\sqrt{\frac{9}{16\pi}} = \frac{0.423}{f_d} \tag{5.4}$$

- Clarke's Model

  Clarke's model assumes that paths of equal average amplitude and random phases arrive at the mobile from random directions in a azimuth, then the 50% coherence time can be defined as

$$T_c = \frac{9}{16\pi f_d} = \frac{0.179}{f_d} \tag{5.5}$$

By setting the camera shutter duration as 1/20s and then taking pictures, the fan rotation speed can be tracked with the LED light fixed at the edge of the fan. With the averaged measured angle speed, the linear speeds under different rotation speeds can be calculated. Accordingly, the Doppler shift can be obtained. Based on the two coherence time calculating schemes, the coherence time of the wireless channel will be determined. All of the parameters and results are shown in Table 5.1.

Doppler Spectrum

A continuous time domain sine wave is transmitted Q times. In this section, the Rappaport coherence time calculation scheme is utilised. By averaging the received signal sequences, the spectrum can be obtained with doing correlation function.

Table 5.2: Software Measured Doppler Spread under Different Fan Speed

Electrical Fan Speed	0 m/s	15 m/s	17 m/s	22 m/s
Calculated Doppler Spread	0 Hz	119.6 Hz	135.5 Hz	172.5 Hz
Room f_d (Software Test)	1 Hz	109.5 Hz	134.0 Hz	163.5 Hz
Room f_d (Equipment Test)	6 Hz	108.0 Hz	131 Hz	167 Hz
Reverb. Chamber f_d (Software Test)	8.5 Hz	124.5 Hz	157.0 Hz	209.5 Hz
Reverb. Chamber f_d (Equipment Test)	12 Hz	129.0 Hz	155.0 Hz	216.0 Hz

Figure 5.9 and 5.14 show the Doppler spread spectrum in room and Reverberation chamber environments by using VSG and VSA, respectively. A reasonable threshold is chosen as $-70\ dBm$, then the measured Doppler shift can be easily obtained from the spectrum under different fan rotational speed. The reason why $-70\ dBm$ is chosen as the threshold is because that the signal might be dramatically affected by the noise below this threshold line. Therefore, the Doppler shift measurement based on transmitted signal and the equipment can be obviously marked from Figure 5.9 and 5.14. Then the exact Doppler shift values can be seen in Table 5.2.

Based on the receiver equipment VSA V2820A, the received signal can be displayed on the screen while switching the VSA to the spectrum mode. Since we are using the antennas with 2.4 GHz, the centre of the spectrum will be automatically focused onto 2.4 GHz. As one of the example shown in Figure 5.10, a pulse shape wave is appeared on the screen. Under the default mode, the transmitter will continuously transmit the same sine wave through the real-time wireless channel while the receiver is capturing the new signal sequence. Thus, the spectrum will be changing with time and any interference that can affect the signal. In order to get a stable and reasonable result, we choose "HOLD" mode, which makes the receiver keep receiving signal sequences and overlap them to the temporary storage to get average spectrum. This will realised by setting an average number which will lead to an more accurate spectrum while increasing it. Then the frequency span should be selected and narrowed. Since the default spectrum span is 50 MHz and is too wide to see the Doppler shift changing affected by the outer interference. Here in this section, a spectrum span with band of 1500 Hz and 2000 Hz are chosen as the display band. The next step is to set the resolution bandwidth. The smaller of the resolution value, the more accurate of the

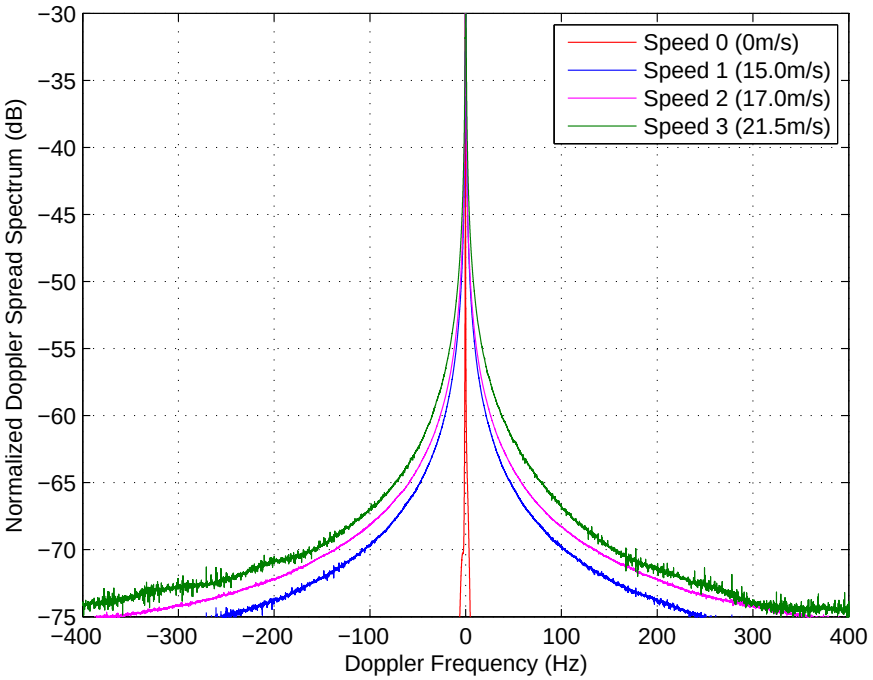

Figure 5.9: Doppler spread spectrum in room with electrical fan

spectrum displayed. In this section, 1 Hz is setted as the resolution so that a high accurate spectrum span will be obtained.

After finish setting the parameters on the VSA, the electrical fan is switched on with three different speed. The spectrum displayed on the VSA screen will spread and become wide. A threshold with 70 dBm is also selected to measure the Doppler shift. Figure 5.10-5.13 show the Doppler shift spectrum under different electrical fan speed in room environment while Figure 5.15-5.18 are the results in Reverberation Chamber. The measured Doppler shift values based on VSA can be found in Table 5.2. For the room environment measurement, the Doppler shift is supposed to be 0 Hz when there is no relevant movement between the transmitter and receiver,

BER Performance

The BER vs. SNR in dB results in room and Reverberation chamber environment are used to demonstrate the system performance of the proposed pilot aided Kalman filtering based channel estimation and MMSE equalisation scheme in time varying wireless circumstance. We also utilised Pilot aided and ICA based channel equalisation

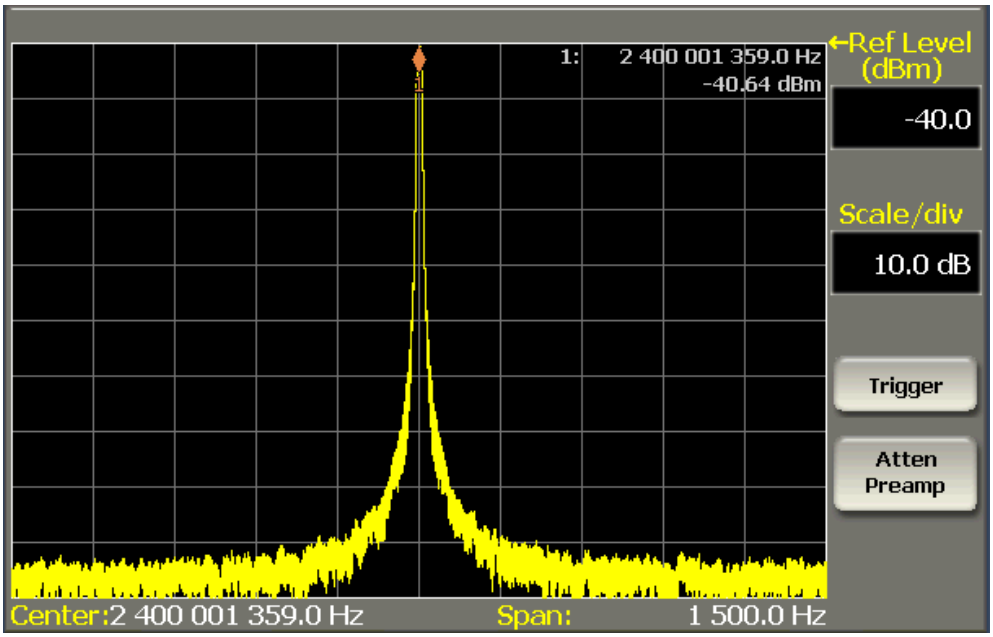

Figure 5.10: Measurement of Doppler spread spectrum in room with electrical fan speed 0 (0 m/s)

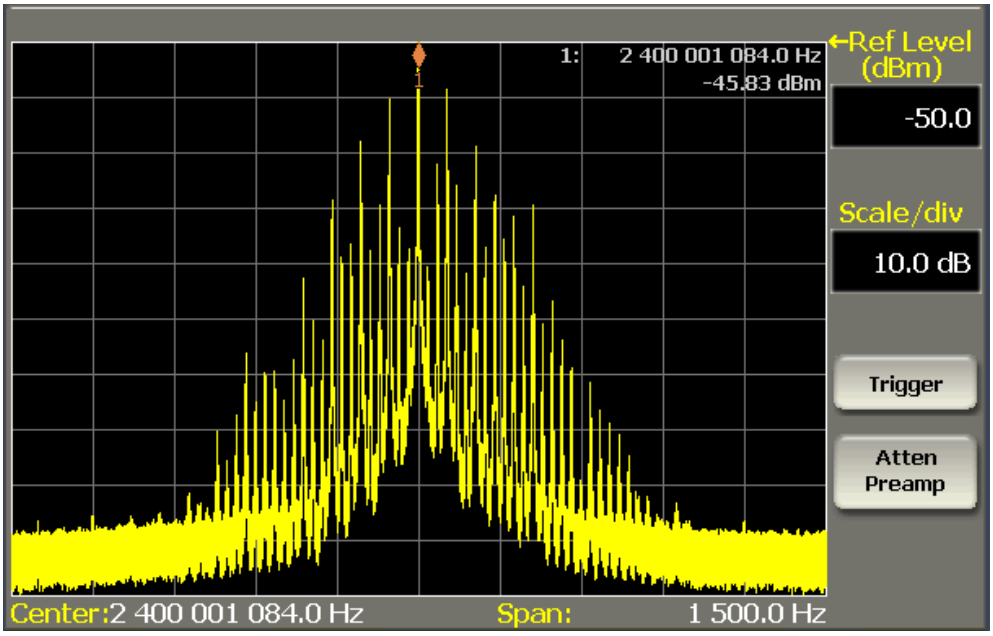

Figure 5.11: Measurement of Doppler spread spectrum in room with electrical fan speed 1 (15.0 m/s)

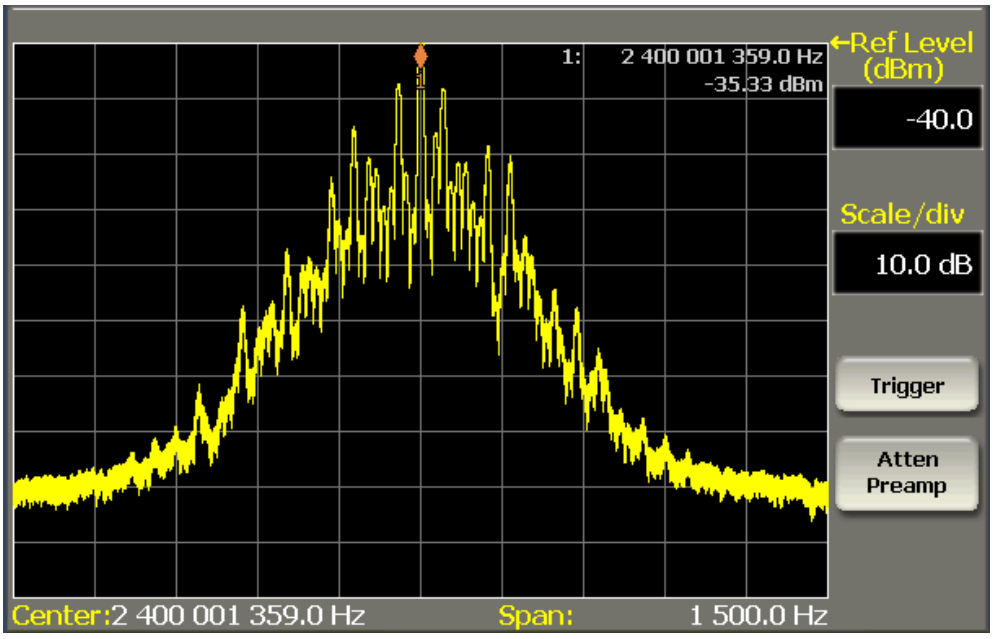

Figure 5.12: Measurement of Doppler spread spectrum in room with electrical fan speed 2 (17.0 m/s)

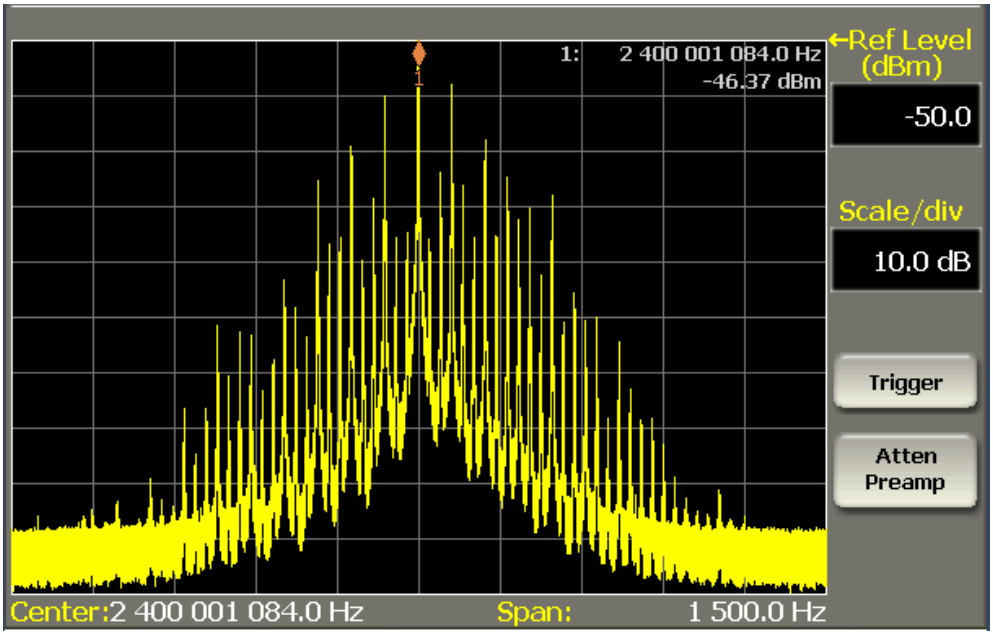

Figure 5.13: Measurement of Doppler spread spectrum in room with electrical fan speed 3 (21.5 m/s)

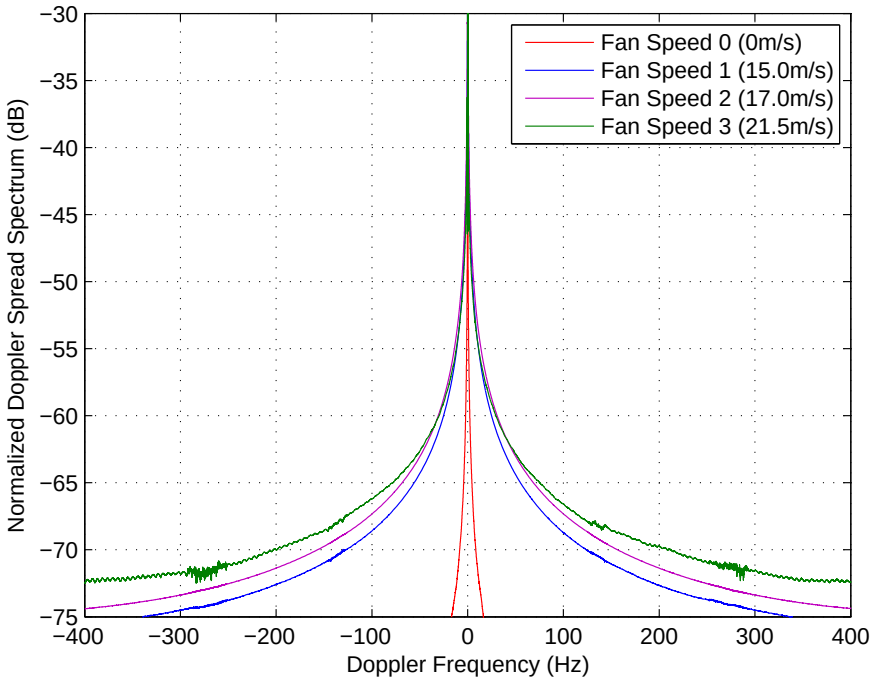

Figure 5.14: Doppler spread spectrum in Reverberation Chamber with electrical fan

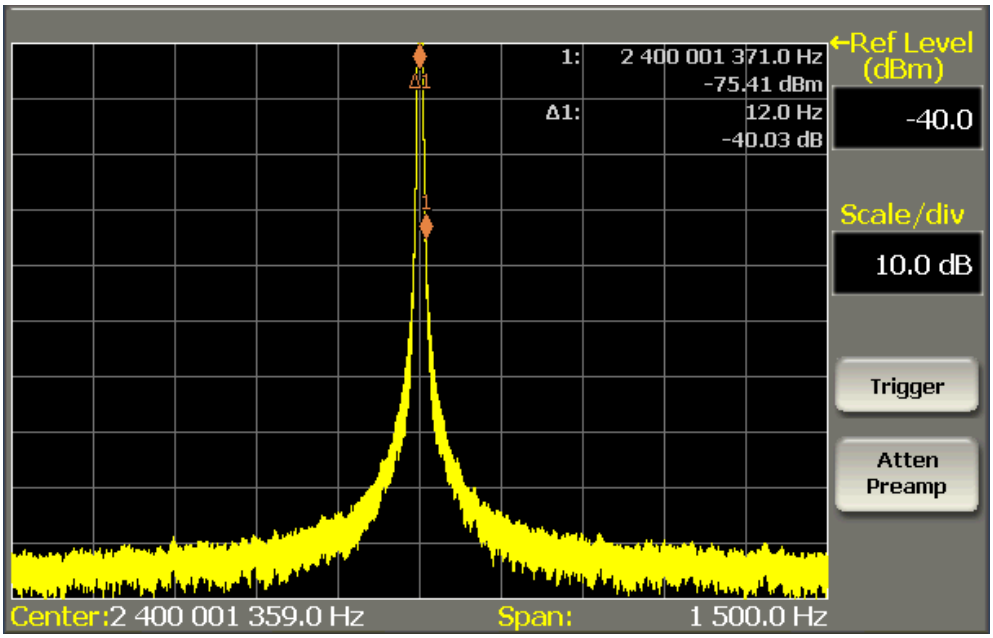

Figure 5.15: Measurement of Doppler spread spectrum in Reverberation Chamber with electrical fan speed 0 (0 m/s)

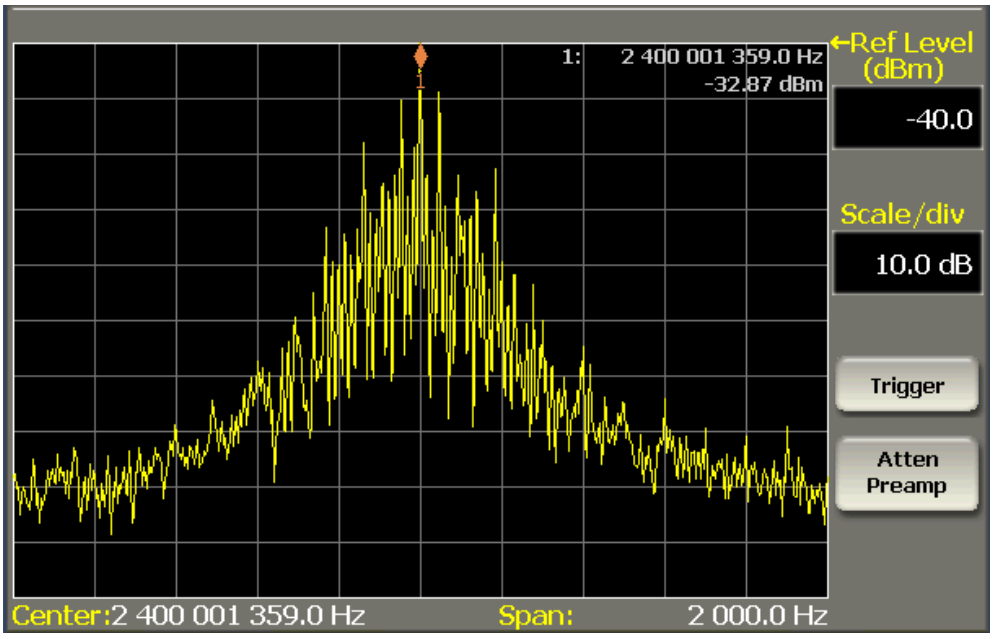

Figure 5.16: Measurement of Doppler spread spectrum in Reverberation Chamber with electrical fan speed 1 (15.0 m/s)

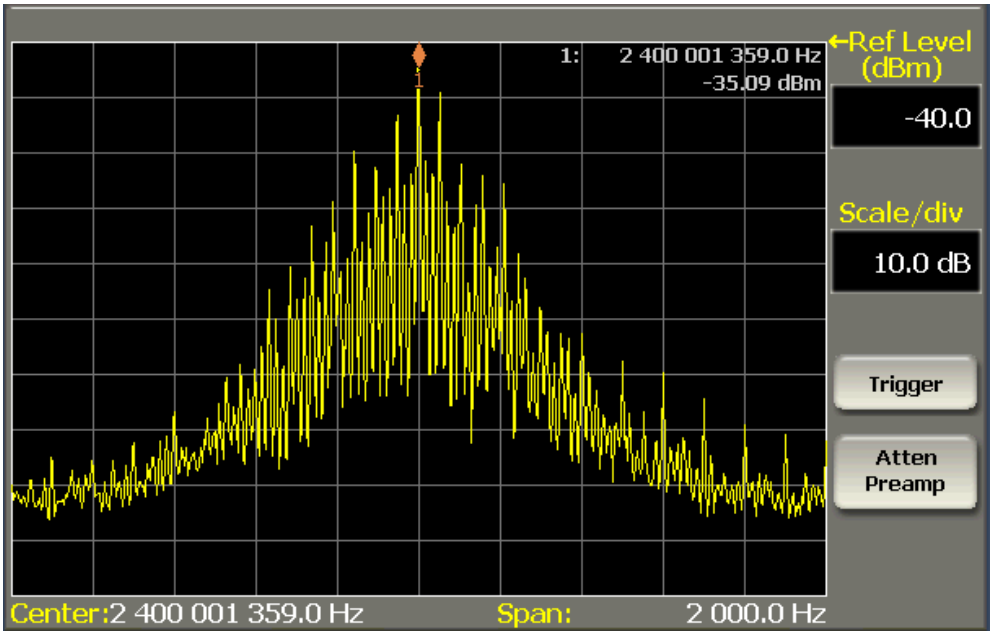

Figure 5.17: Measurement of Doppler spread spectrum in Reverberation Chamber with electrical fan speed 2 (17.0 m/s)

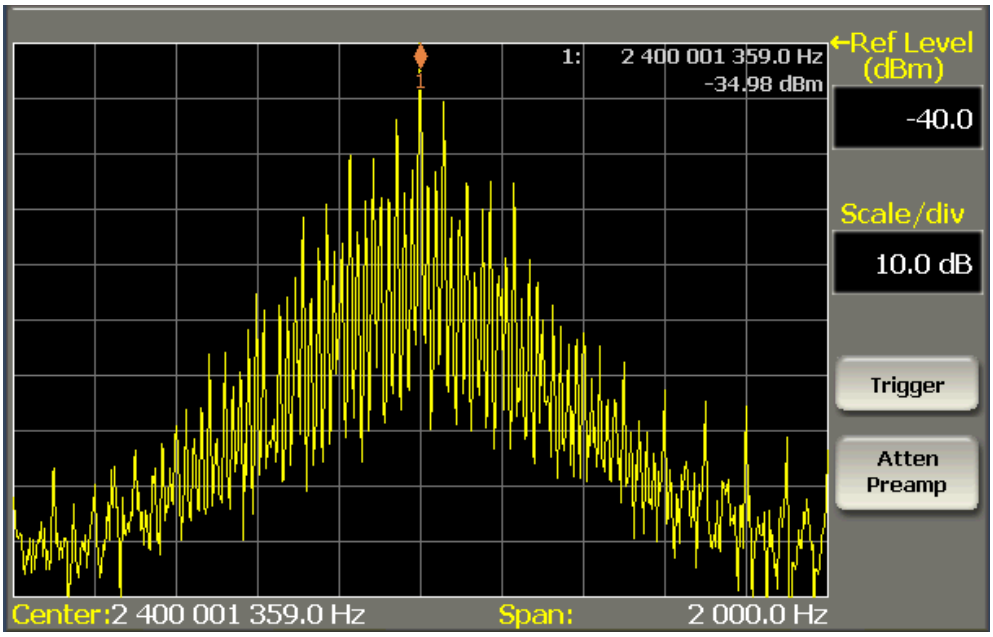

Figure 5.18: Measurement of Doppler spread spectrum in Reverberation Chamber with electrical fan speed 3 (21.5 m/s)

method for comparison. In both measurement circumstances, we applied two different electrical fan linear speeds of 15 m/s and 22 m/s. The results can be seen in Figure 5.19 and 5.20. It is obvious that, under the same fan speed, the proposed Kalman filtering based approach has a stronger ability to compensate the Doppler effect in time varying wireless channel than that of pilot ICA scheme in a region of high SNR. When the SNR in dB is low while the noise in the received signal data is in dominant, e.g., less than 15 dB, pilot aided ICA based equalisation method performs better than that of Kalman filtering based method. It is because that the Kalman filter estimation scheme is a recursive approach, it can estimate the current channel information by applying the previous status information. The accuracy is becoming better while the power on the source signal is getting larger. Pilot aided ICA based equalisation approach mainly depending on the pilot overhead among the signal frame. That is why the Kalman filtering based channel estimation approach can outperform the ICA based method when the SNR in dB is increasing.

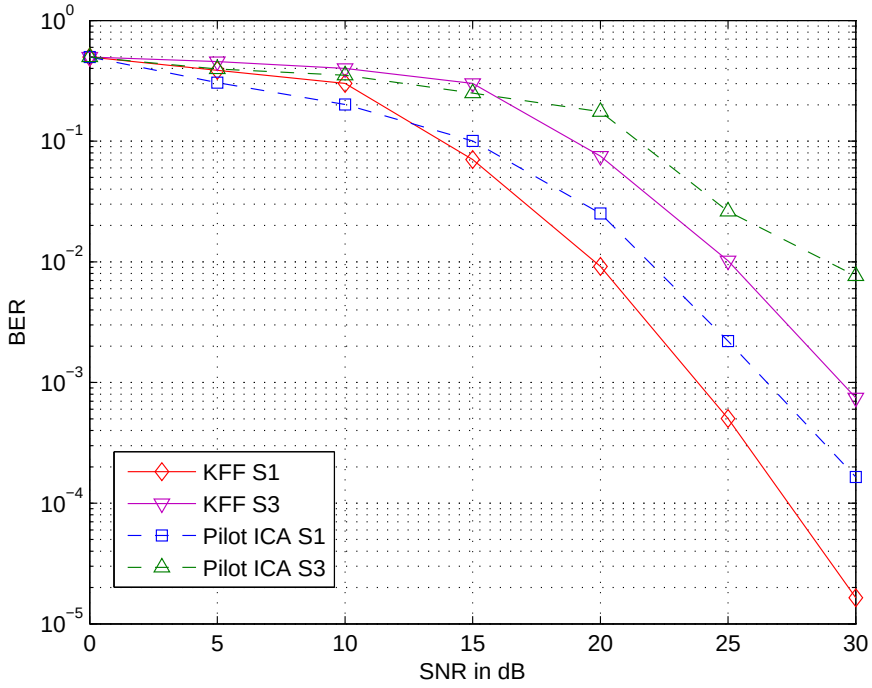

Figure 5.19: BER vs. SNR in dB for Kalman filtering channel estimation approach in room

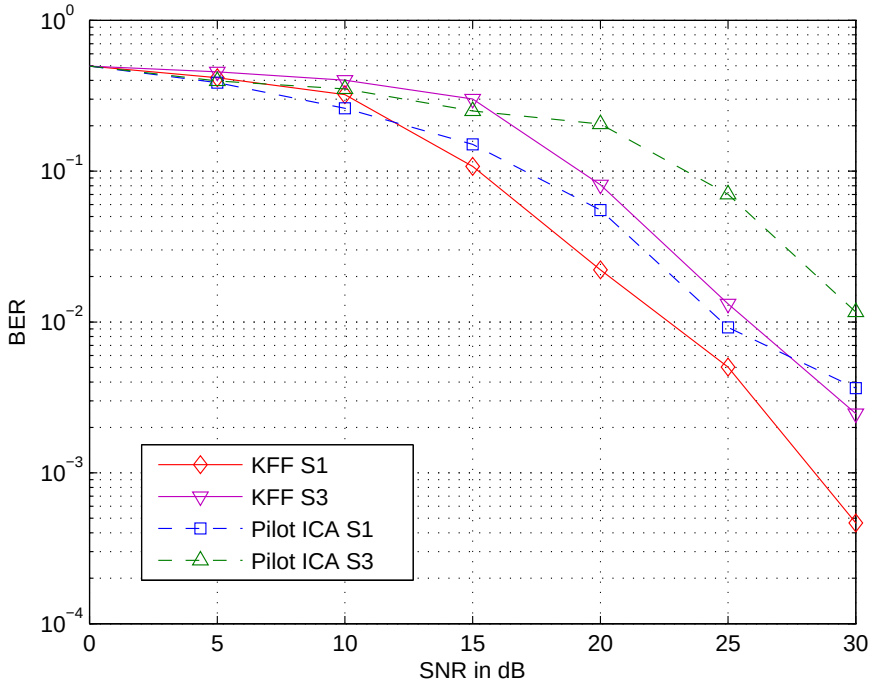

Figure 5.20: BER vs. SNR in dB for Kalman filtering channel estimation approach in Reverberation Chamber

5.4 Summary

The semi-blind precoding aided ICA based equalisation approach is verified by applying the real-time test-bed composed of the Keithley signal generator and signal receiver. The reference data sequences for precoding are also designed offline, which is as same process as it in the simulation. The optimal precoding constant a is tested in office room, and the best performance value range is between $[0.3, 0.4]$. A frame size with no less than 128 OFDM blocks can provide a good steady-state system performance.

The reason why Doppler spread in the Reverberation chamber is stronger than that in room environment under the same fan speed and situation is that room is an open area so that some wireless wave will scatter and never be reflected back to the receiver. Also, the power will missed on some frequency.

The pilot aided ICA based channel equalisation method cannot efficiently compensate the ICI effect caused by Doppler spread due to rotational fan even with large number of pilot ahead prefixed onto the transmitted signal sequences. Kalman filtering based estimation approach accompanied with MMSE channel equalisation has a better performance while compensating the ICI effect, especially at high SNR. With a reasonable length of overhead, pilot blocks are multi-utilised for time synchronisation, Doppler spectrum determination and initialisation of the Kalman filtering estimation, the ICI can be dramatically reduced while being gathered into the equivalent channel model, which also degrades the computational complexity of the whole system. The BER performance within the measurement shows that this method can obtain a quite well result.

Chapter 6

Conclusions and Future Work

6.1 Conclusions

Several semi-blind energy efficient receiver structures for broadband wireless communication systems are proposed in this thesis. A pilot-aided semi-blind Doppler spread tracking scheme is proposed in a Kalman filtering based channel estimation system. Then the statistical tool of ICA is applied to perform semi-blind equalisation in the first system which employed a number of reference data sequences for Doppler spread estimation. Both receiver structure approaches are verified through the developed real-time wireless communication platform based on a signal generator, a signal analyser connected and a pair of antennas.

In Chapter 3, a low complexity semi-blind OFDM system is presented, with pilot-aided Doppler spread estimation and Kalman filtering based channel estimation scheme. A short pilot data is designed for two uses: simultaneous low complexity Doppler spread estimation and Channel estimation initialisation based on Kalman filter. A cost function is formed for the design of these pilot symbols. The Doppler spread can be estimated by maximising the cost function. A number of pilots are designed to be orthogonal to each other, then the Doppler spread can be determined when the maximum value of cross-correlation function between the pilot and received pilot blocks. Then the estimates of ICI caused by Doppler spread is gathered into the equivalent system model. The following channel estimation is based on a recursive Kalman filtering operator, which applies the pilot data to estimate the initial CSI. After obtaining the estimates of CSI which contains the ICI, MMSE equalisation method

is applied to recover the source data by compensate the multipath channel and ICI. Simulation results show that the proposed method can estimate the Doppler spread accurately, and it can achieve better BER performance than the comb type pilot-aided receiver structure.

In Chapter 4, a semi-blind precoding aided Doppler spread estimation approach and ICA based equalisation structure are proposed for MIMO OFDM systems. A number of reference data sequences are superimposed into the source data via a linear precoding process, without introducing additional transmit power or real-time spectral overhead. The reference data sequences are carefully designed offline, which can be employed for Doppler spread estimation and ambiguity elimination. A cost function is formed for the reference data sequences and the projection operator. By minimising the cost function, the optimal reference data sequences and the projection operator can be designed, and obtained from a pool of orthogonal sequences in the Hadamard matrix. The precdoing constant is then discussed, which can provide a power trade-off between the source data and the reference data. The precoding aided Doppler spread estimation is performed by minimising the sum cross-correlations between the reference data sequences and the rest of orthogonal sequences in the pool. After the Doppler spread estimation and compensation, ICA is employed for equalisation at the receiver on each subcarrier. However, the permutation and phase ambiguities are introduced into the output signals by ICA equalisation. According to the reference data sequences design, the cross-correlation between different reference data sequences of transmit antennas is minimised in order to make sure that the different reference data sequences are orthogonal to each other. This can provide an optimal solution to eliminate the permutation ambiguity by maximising the cross-correlation between the ICA equalised signals and the reference signals. Then the correlation is employed again on each subcarrier for phase ambiguity elimination. Simulation results show that the proposed semi-blind Doppler spread estimation and ICA based equalisation approach in MIMO OFDM systems can achieve a BER performance close to the ideal case with perfect CSI.

In Chapter 5, a verification real-time testbed is developed based on a signal gener-

ator, a signal receiver connected and a pair of antennas in order to verify the proposed two energy-efficient receiver structures for broadband wireless communication systems. A vector signal generator (V2920A) and a vector signal analyser (V2820A) are applied as real-time data transmitter and receiver with the antennas at 2.4 GHz. The real-time data can be generated by computer through software and passed to the transmitter. After passing through the wireless environments, office area and Reverberation chamber, the data frame can be received by the signal analyser and send back to computer for further process. The previous proposed two receiver structures, semi-blind ICA equalisation and Kalman filtering based channel estimation, are realised on the real-time communication platform. The measurement results show that both receiver structures can perform very well in the practical wireless communication environments. The reasonable BER performance can be achieved after process through computer process.

6.2 Drawbacks of the Proposed Receiver Structures

The proposed receiver structures perform very good in the simulation as well as the verification on the testbed. They can outperform other referenced methods. However, there are some drawback existing in the proposed semi-blind receiver structures.

- In Chapter 3, the proposed semi-blind Kalman filtering based channel estimation still need a sequence of pilot data to do estimation, which may consume extra resource. Besides, with the frame length increasing, larger number of pilot will be required to estimate the Doppler spread. Furthermore, longer frame will be easier suffer from the ICI caused by Doppler spread. Finally, it requires the noise or interference to be Gaussian. If not, a non-linear estimator can provide a better performance than the linear Kalman filtering based approach. The process of finding the best estimates from noisy data amounts to filtering out the noise. If the received signal is in deep fading or contains large ICI, Kalman filter may not clean up all of the interference among subcarriers.

- For the semi-blind precoding aided ICA based equalisation method in Chapter 4, the precoding constant a provides a power trade off between the source data

and the reference data sequences. The reference data sequences are designed offline and superimposed onto the source data without introduce extra transmit power, but they are allocated part of the transmit power from the source data, which results in a power degradation on the source data. Even the optimal value of a is found out to make sure the system can perform and lead to good BER, the whole system might be affected by this precoding process before transmission. Furthermore, the ICA equalised signal contains phase and permutation ambiguity that is needed to be eliminated after equalisation. This ambiguity mitigation process also increase the numerical complexity at the receiver side. Finally, due to the nature of the ICA algorithm, large number of symbols in a frame is needed. ICA can not work very well at deep fading frequencies.

- In Chapter 5, first, the electrical fan speed is tested and measured with a camera by setting the shutter speed. However, this is not very accurate since the camera shutter is also a mechanical scheme which has delay. Therefore, the electrical fan speed measurement in this Chapter is an approximate measurement. Secondly, in the pilot based Kalman filtering based channel estimation approach, the pilot block consumes a part of the frame, which degrades the system efficiency. Thirdly, the spectrum measured by the vector signal analyser has high fluctuation even with average process, which makes the measurement of Doppler spread values change while the outside environment changes.

6.3 Future Work

Further to the proposed approaches and verification in this thesis, a list of possible continuous work can be given as:

- For the semi-blind precoding aided ICA based equalisation verification in Chapter 5, Doppler spread estimations would be taken into consideration within time varying channel in real-time. The ICA based equalisation scheme has been validated through the testbed and performed very well. Furthermore, the precoding aided Doppler spread estimation is proposed and simulated with good perfor-

mance. This approach is considered as an energy-efficient receiver structure with the offline designed reference sequences without consuming extra transmit power and spectral resources. The Doppler spread compensation performance need to be verified under Reverberation chamber and office area environments with electrical fan.

- The parameters, which can affect the receiver structures performance, would be exploiting in the future, such as training data block length, frame length, number of subcarriers and so on. Since these parameters play significant roles while verifying the receiver structures in real-time, it is necessary to measure how these parameters would affect on the system performance. For precoding aided ICA based equalisation approach, longer frame length will lead to a better BER performance. However, longer frame length would suffer more interference from outside, such as Doppler spread, CFO and IQ imbalance. Therefore, the optimal values of these parameters need to be verified and found out through the test.

- The real-time communication system platform would be extended to MIMO system by introducing extra signal generators and signal analysers. As MIMO and OFDM become the two promising techniques and widely used in modern wireless communication systems, a MIMO OFDM wireless communication system need be to developed with the real-time instruments.

- Other test environments would be considered to make the measurement more practical, such as outdoors, in and out buildings, on mobile vehicles and so on.

Bibliography

[1] A. Goldsmith, *Wireless Communications*. N. Y., USA: Cambridge university press, 2005.

[2] T. S. Rappaport, *Wireless Communications Principles and Practice*, 2nd ed. Upper Saddle River, N. J., USA: Prentice Hall, 2002.

[3] G. J. Foschini, "Layered space-time architecture for wireless communication in a fading environment when using multi-element antennas," *Bell labs technical journal*, vol. 1, no. 2, pp. 41–59, 1996.

[4] S. Weinstein and P. Ebert, "Data transmission by frequency-division multiplexing using the discrete fourier transform," *IEEE Transactions on Communication Technology*, vol. 19, no. 5, pp. 628–634, Oct. 1971.

[5] M. Rumney, *LTE and Evolution to 4G Wireless: Design and Measurement Challenges*, 2nd ed. N. Y., USA: John Wiley & Sons, 2008.

[6] D. Tse and P. Viswanath, *Fundamentals of wireless communication*. Cambridge university press, 2005.

[7] L. Tong and S. Perreau, "Multichannel blind identification: From subspace to maximum likelihood methods," *Proceedings of the IEEE*, vol. 86, no. 10, pp. 1951–1968, Oct. 1998.

[8] W. C. Jakes, *Microwave Mobile Communications*. N. Y., USA: John Wiley, 1974.

[9] R. Steele, *Mobile Radio Communications*. IEEE Press, 1994.

[10] J. Ahn and H. S. Lee, "Frequency domain equalisation of OFDM signals over frequency nonselective Rayleigh fading channels," *Electronics letters*, vol. 29, no. 16, pp. 1476–1477, Aug. 1993.

[11] Y. Li and L. J. Cimini, "Bounds on the interchannel interference of OFDM in time-varying impairments," *IEEE Transactions on Communications*, vol. 49, no. 3, pp. 401–404, 2001.

[12] M. Russell and G. Stuber, "Interchannel interference analysis of OFDM in a mobile environment," *IEEE 45th Vehicular Technology Conference*, vol. 2, pp. 820–824, 1995.

[13] R. E. Kalman, "A new approach to linear filtering and prediction problems," *Journal of Fluids Engineering*, vol. 82, no. 1, pp. 35–45, 1960.

[14] T. Y. Al-Naffouri, "An EM-based forward-backward kalman filter for the estimation of time-variant channels in OFDM," *IEEE Transactions on Signal Processing*, vol. 55, no. 7, pp. 3924–3930, 2007.

[15] S. Song, A. C. Singer, and K. M. Sung, "Soft input channel estimation for turbo equalization," *IEEE Transactions on Signal Processing*, vol. 52, no. 10, pp. 2885–2894, Oct. 2004.

[16] A. Hyvärinen, J. Karhunen, and E. Oja, *Independent component analysis*. N. Y., USA: John Wiley & Sons, 2004.

[17] L. Tong, G. Xu, and T. Kailath, "A new approach to blind identification and equalization of multipath channels," pp. 856–860, Nov. 1991.

[18] B. Muquet and M. Courville, "Blind and semi-blind channel identification methods using second order statistics for ofdm systems," in *1999 IEEE International Conference on Acoustics, Speech, and Signal Processing*, vol. 5. IEEE, 1999, pp. 2745–2748.

[19] K. Pahlavan and P. Krishnamurthy, *Principles of Wireless Networks: A Unified Approach*, 2nd ed. Englewood Cliffs, N. J., USA: Prentice-Hall, 2002.

[20] V. K. Garg and J. E. Wilkes, *Principles and Applications of GSM.* Upper Saddle River, N. J., USA: Prentice-Hall, 1999.

[21] R. Attar, R. Ghosh, C. Lott, M. X. Fan, P. Black, R. Rezaiifar, and P. Agashe, "Evolution of cdma2000 cellular networks: multicarrier EV-DO," *IEEE Commun. Mag.*, vol. 44, no. 3, pp. 46–53, Mar. 2006.

[22] J. Bergman, M. Ericson, D. Gerstenberger, B. Göransson, J. Persa, and S. Wager, "HSPA evolution - boosting the performance of mobile broadband access," *Ericsson Review*, vol. vol. 85, no. 1, pp. 32–37, 2008.

[23] N. Boudriga, M. Obaidat, and F. Zarai, "Intelligent network functionalities in wireless 4G networks: Integration scheme and simulation analysis," *Computer Communications*, vol. 31, no. 16, pp. 3752–3759, Oct. 2008.

[24] S. Haykin and M. Moher, *Modern Wireless Communications.* Upper Saddle River, N. J., USA: Pearson Prentice Hall, 2005.

[25] R. W. Chang, "Synthesis of band-limited orthogonal signals for multichannel data transmission," *Bell Syst. Tech. Journal*, vol. 45, no. 10, pp. 1775–1796, 1966.

[26] L. J. Cimini, "Analysis and simulation of a digital mobile channel using orthogonal frequency division multiplexing," *IEEE Trans. on Commun.*, vol. 33, no. 7, pp. 665–675, 1985.

[27] I. W. Group *et al.*, "IEEE standard for information technology–telecommunications and information exchange between systems–local and metropolitan area networks–specific requirements-part 11: Wireless lan medium access control (MAC) and physical layer (PHY) specifications amendment 6: Wireless access in vehicular environments," *IEEE Std.*, vol. 802, no. 7, p. 11p, 2010.

[28] K. Fazel and S. Kaiser, *Multi-carrier and spread spectrum systems: from OFDM and MC-CDMA to LTE and WiMAX*, 2nd ed. N. Y., USA: John Wiley & Sons, 2008.

[29] C. J. Hansen, "WiGiG: Multi-gigabit wireless communications in the 60 GHz band," *IEEE Wireless Commun*, vol. 18, no. 6, pp. 6–7, 2011.

[30] P. Demestichas, A. Georgakopoulos, D. Karvounas, K. Tsagkaris, V. Stavroulaki, J. Lu, C. Xiong, and J. Yao, "5G on the horizon: Key challenges for the radio-access network," *IEEE Vehi. Tech. Mag.*, vol. 8, no. 3, 2013.

[31] C. Edwards, "5G searches for formula to shake off shannon," *Eng. & Tech.*, vol. 8, no. 8, pp. 82–85, 2013.

[32] R. Schober and S. Pasupathy, "Noncoherent space-time equalization," *IEEE Transactions on Wireless Communications*, vol. 2, no. 3, pp. 537–548, 2003.

[33] L. Sarperi, X. Zhu, and A. K. Nandi, "Reduced complexity blind layered space-time equalization for MIMO OFDM systems," vol. 1. IEEE, 2005, pp. 236–240.

[34] X. Zhu and R. D. Murch, "Layered space-time equalization for wireless MIMO systems," *IEEE Transactions on Wireless Communications*, vol. 2, no. 6, pp. 1189–1203, 2003.

[35] A. Paulraj, R. Nabar, and D. Gore, *Introduction to space-time wireless communications*. Cambridge university press, 2003.

[36] J. Akhtman, *MIMO-OFDM for LTE, WiFi and WiMAX: Coherent versus non-coherent and cooperative turbo transceivers*. John Wiley & Sons, 2010, vol. 9.

[37] M. Rumney, *LTE and the evolution to 4G wireless: Design and measurement challenges*. John Wiley & Sons, 2013.

[38] C. D. Meyer, *Matrix analysis and applied linear algebra*. Siam, 2000.

[39] S. Orfanidis, *Introduction to Signal Procesing*. Beijing: Tsinghua University Publishing House, 1998.

[40] J. Armstrong, "Analysis of new and existing methods of reducing intercarrier interference due to carrier frequency offset in OFDM," *IEEE Transactions on Communications*, vol. 47, no. 3, pp. 365–369, 1999.

[41] W. G. Jeon, K. H. Chang, and Y. S. Cho, "An equalization technique for orthogonal frequency-division multiplexing systems in time-variant multipath channels," *IEEE Transactions on Communications*, vol. 47, no. 1, pp. 27–32, Jan. 1999.

[42] M. Morelli and U. Mengali, "Carrier-frequency estimation for transmissions over selective channels," *IEEE Transactions on Communications*, vol. 48, no. 9, pp. 1580–1589, 2000.

[43] M. Sabbaghian and D. Falconer, "Joint turbo frequency domain equalization and carrier synchronization," *IEEE Transactions on Wireless Communications*, vol. 7, no. 1, pp. 204–212, 2008.

[44] B. Razavi, "Design considerations for direct-conversion receivers," *IEEE Transactions on Circuits and Systems II: Analog and Digital Signal Processing*, vol. 44, no. 6, pp. 428–435, 1997.

[45] A. Tarighat and A. H. Sayed, "Joint compensation of transmitter and receiver impairments in OFDM systems," *IEEE Transactions on Wireless Communications*, vol. 6, no. 1, pp. 240–247, 2007.

[46] G. Xing, M. Shen, and H. Liu, "Frequency offset and I/Q imbalance compensation for direct-conversion receivers," *IEEE Transactions on Wireless Communications*, vol. 4, no. 2, pp. 673–680, 2005.

[47] J. G. Proakis and M. Salehi, *Digital Communications*, 5th ed. N. Y., USA: McGraw-Hill, 2008.

[48] S. Coleri, M. Ergen, A. Puri, and A. Bahai, "Channel estimation techniques based on pilot arrangement in OFDM systems," *IEEE Transactions on Broadcasting*, vol. 48, no. 3, pp. 223–229, 2002.

[49] Y. S. Cho, J. Kim, W. Y. Yang, and C. G. Kang, *MIMO-OFDM wireless communications with MATLAB*. John Wiley & Sons, 2010.

[50] L. Sarperi, X. Zhu, and A. K. Nandi, "Blind OFDM receiver based on independent component analysis for multiple-input multiple-output systems," *IEEE Transactions on Wireless Communications*, vol. 6, no. 11, pp. 4079–4089, Nov. 2007.

[51] M. Shin, H. Lee, and C. Lee, "Enhanced channel-estimation technique for MIMO-OFDM systems," *IEEE Transactions on Vehicular Technology*, vol. 53, no. 1, pp. 261–265, 2004.

[52] S. M. Kay, "Fundamentals of statistical signal processing: estimation theory," 1993.

[53] O. Edfors, M. Sandell, J. V. de Beek, S. Wilson, and P. Borjesson, "OFDM channel estimation by singular value decomposition," *IEEE Transactions on Communications*, vol. 46, no. 7, pp. 931–939, 1998.

[54] A. Petropulu, R. Zhang, and R. Lin, "Blind OFDM channel estimation through simple linear precoding," *IEEE Transactions on Wireless Communications*, vol. 54, no. 3, pp. 647–655, Mar. 2004.

[55] R. Lin and A. Petropulu, "Linear precoding assisted blind channel estimation for OFDM systems," *IEEE Transactions on Vehicular Technology*, vol. 54, no. 3, pp. 983–995, May 2005.

[56] F. Gao and A. Nallanathan, "Blind channel estimation for OFDM systems via a generalized precoding," *IEEE Transactions on Vehicular Technology*, vol. 56, no. 3, pp. 1155–1164, Jan. 2007.

[57] ——, "Blind channel estimation for MIMO OFDM systems via nonredundant linear precoding," *IEEE Transactions on Signal Processing*, vol. 55, no. 2, pp. 784–789, Jan. 2007.

[58] A. Cichocki and S. Amari, *Adaptive blind signal and image processing.* Chichester, U.K.: John Wiley & Sons, 2003.

[59] J. Treichler and B. Agee, "A new approach to multipath correction of constant modulus signals," *IEEE Transactions on Acoustics, Speech and Signal Processing*, vol. 31, no. 2, pp. 459–472, Apr. 1983.

[60] S. Zhou and G. B. Giannakis, "Finite-alphabet based channel estimation for OFDM and related multicarrier systems," *IEEE Transactions on Communications*, vol. 49, no. 8, pp. 1402–1414, Aug. 2001.

[61] L. Rota, V. Zarzoso, and P. Comon, "Parallel deflation with alphabet-based criteria for blind source extraction," pp. 751–756, Jul. 2005.

[62] L. Castedo, C. J. Escudero, and A. Dapena, "A blind signal separation method for multiuser communications," *IEEE Transactions on Signal Processing*, vol. 45, no. 5, pp. 1343–1348, May 1997.

[63] A. K. Nandi, *Blind estimation using higher-order statistics*. Amsterdam, Netherland: Kluwer Academic Publisher, 1999.

[64] A. J. Bell and T. J. Sejnowski, "An information-maximization approach to blind separation and blind deconvolution," *Neural computation*, vol. 7, no. 6, pp. 1129–1159, Feb. 1995.

[65] A. Hyvarinen, "Fast and robust fixed-point algorithms for independent component analysis," *IEEE Transactions on Neural Networks*, vol. 10, no. 3, pp. 626–634, May 1999.

[66] J. F. Cardoso, "High-order contrasts for independent component analysis," *Neural computation*, vol. 11, no. 1, pp. 157–192, 1999.

[67] ——, "Blind signal separation: statistical principles," *Proceedings of the IEEE*, vol. 86, no. 10, pp. 2009–2025, Oct. 1998.

[68] D. Obradovic, N. Madhu, A. Szabo, and C. S. Wong, "Independent component analysis for semi-blind signal separation in MIMO mobile frequency selective communication channels," in *IEEE International Joint Conference on Neural Networks (ICNN)*. IEEE, Jul. 2004.

[69] J. Gao, X. Zhu, and A. K. Nandi, "Non-redundant precoding and PAPR reduction in MIMO OFDM systems with ICA based blind equalization," *IEEE Transactions on Wireless Communications*, vol. 8, no. 6, pp. 3038–3049, Jun. 2009.

[70] D. Falconer, S. L. Ariyavisitakul, A. Benyamin-Seeyar, and B. Eidson, "Frequency domain equalization for single-carrier broadband wireless systems," *IEEE Communications Magazine*, vol. 40, no. 4, pp. 58–66, 2002.

[71] B. Yang, K. B. Letaief, R. S. Cheng, and Z. Cao, "Channel estimation for OFDM transmission in multipath fading channels based on parametric channel modeling," *IEEE Transactions on Communications*, vol. 49, no. 3, pp. 467–479, 2001.

[72] H. C. Wu and X. Huang, "Joint phase/amplitude estimation and symbol detection for wireless ICI self-cancellation coded ofdm systems," *IEEE Transactions on Broadcasting*, vol. 50, no. 1, pp. 49–55, 2004.

[73] H. Wu, X. Huang, Y. Wu, and X. Wang, "Theoretical studies and efficient algorithm of semi-blind ICI equalization for OFDM," *IEEE Transactions on Wireless Communications*, vol. 7, no. 10, pp. 3791–3798, 2008.

[74] M. Huang, X. Chen, L. Xiao, S. Zhou, and J. Wang, "Kalman-filter-based channel estimation for orthogonal frequency-division multiplexing systems in time-varying channels," *IET Communications*, vol. 1, no. 4, pp. 795–801, 2007.

[75] Q. K. Trinh and P. Z. Fan, "Construction of multilevel hadamard matrices with small alphabet," *Electronics Letters*, vol. 44, no. 21, pp. 1250–1252, 2008.

[76] A. C. Iossifides, "Complex orthogonal coded binary transmission with amicable Hadamard matrices over Rayleigh fading channels." IEEE, 2011, pp. 335–340.

[77] M. Hsieh and C. Wei, "Channel estimation for ofdm systems based on comb-type pilot arrangement in frequency selective fading channels," *IEEE Transactions on Consumer Electronics*, vol. 44, no. 1, pp. 217–225, 1998.

[78] H. H. Hijazi and L. Ros, "Polynomial estimation of time-varying multipath gains with intercarrier interference mitigation in ofdm systems," *IEEE Transactions on Vehicular Technology*, vol. 58, no. 1, pp. 140–151, 2009.

[79] W.-G. Song and J.-T. Lim, "Pilot-symbol aided channel estimation for OFDM with fast fading channels," *IEEE Transactions on Broadcasting*, vol. 49, no. 4, pp. 398–402, 2003.

[80] M. Yu and P. Sadeghi, "A study of pilot-assisted OFDM channel estimation methods with improvements for DVB-T2," *IEEE Transactions on Vehicular Technology*, vol. 61, no. 5, pp. 2400–2405, 2012.

[81] P. Cheng, Z. Chen, Y. Rui, Y. Guo, L. Gui, M. Tao, and Q. Zhang, "Channel estimation for OFDM systems over doubly selective channels: a distributed compressive sensing based approach," *IEEE Transactions on Communications*, vol. 61, no. 10, pp. 4173–4185, 2013.

[82] H. T. Chattha, Y. Huang, X. Zhu, and Y. Lu, "A dual feed PIFA diversity antenna for MIMO systems," in *2010 International Workshop on Antenna Technology (iWAT)*. IEEE, 2010, pp. 1–4.

[83] J. G. Kostas and B. Boverie, "Statistical model for a mode-stirred chamber," *IEEE Transactions on Electromagnetic Compatibility*, vol. 33, no. 4, pp. 366–370, 1991.

[84] K. Rosengren and P. Kildal, "Study of distributions of modes and plane waves in reverberation chambers for the characterization of antennas in a multipath environment," *Microwave and Optical Technology Letters*, vol. 30, no. 6, pp. 386–391, 2001.